ISSN: 1224-7626

ANALELE UNIVERSITĂŢII DIN ORADEA

Fascicula CHIMIE
XXX (30) 2023

EDITURA UNIVERSITĂŢII DIN ORADEA

2023

Editorial Adress
University of Oradea, Chemistry Departament
Str. Universitatii, nr.1, 410087, Oradea, Bihor, România
General Information
ISSN: 1224-7626
Place of publishing: Oradea, Romania
Year of the first issue: 1995
Releasing frequency: 1 issue / year
Language: English
Abstracting/Indexing:

Chemical Abstracts Service-CAS Source Index (CASSI)

Academic Research Index- ResearchBiB

TABLE OF CONTENTS

Analele Universităţii din Oradea-Fascicula Chimie, Vol. XXX (30), p.5-10, 2023

THE STUDY COMPLEXATION OF β-CYCLODEXTRIN WITH SALICYLIC ACID

Mioara SEBEŞAN[1], Horea SEBEŞAN[1], Gabriela Elena BADEA[1], Radu SEBEŞAN[2], Sorin HODIŞAN[1]

[1]University of Oradea, Faculty of Informatics and Sciences, Universitatii 1st., RO-410087, Oradea, Romania
[2]University of Oradea, Faculty of Electrical Engineering and Information Technology, Universitatii 1st., RO-410087, Oradea,Romania
E-Mail: msebesan@uoradea.ro

Abstract: This paper presents a study of the process of formation of inclusion complexes between salicylic acid and *beta*-cyclodextrine (β-CD). Three inclusion compounds, resulting from complexation of salicylic acid and beta-cyclodextrin, were studied. The inclusion complexes have been prepared in different ratio of β-CD/ salicylic acid. The bioactive nanoparticles of complexes included different concentrations of salicylic acid. The inclusion complexes resulting were analysis, using UV-VIS spectrophotometry.

Keywords: *beta*-cyclodextrin, UV-VIS spectrophotometry, inclusion compounds.

INTRODUCTION

Cyclodextrins are chemical compounds, from the class of oligosaccharides, which have a cyclic structure. 3 types of natural cyclodextrins are known, α-cyclodextrin, β-cyclodextrin and γ-cyclodextrin, the difference between them being the number of linked glycosidic cycles. These compounds are obtained naturally from starch, by fermentation, in the presence of cultures of bacteria and fungi, [1].
The cyclic structure of cyclodextrins allows the formation of an internal cavity, in which a foreign molecule can enter, thus forming a new chemical compound. The obtained chemical compound is characterized by the physical interaction of two components: the "host" reactant, which is cyclodextrin, and the "guest" reactant, represented by the molecule that embeds itself inside the cyclodextrin cavity, [2].

In order for this process to take place, certain conditions need to be met: the "guest" molecules must have suitable dimensions to be embedded; to have a low solubility in water; the complexation method used have to give a good yield and lead to a stable inclusion complex over time.

So, due to the shape that cyclodextrins have, they are able to form inclusion complexes. The process is characterized by the mobilization of an external molecule, inside the non-polar cavity of the cyclodextrin. This molecule must be of the right size so that it can penetrate inside the cyclodextrin, have a low solubility in water and allow the formation of a stable complex, [3].

Through the reaction of β-cyclodextrin and salicylic acid (o-hydroxybenzoic acid), a complex is formed, which has different physical and chemical properties compared to the reagents. Obtaining the complex can be done by several techniques: in solution, in suspension, by mixing or by melting. The choice of one of the techniques is made according to the "guest" molecule, so that the yield of the reaction is as high as possible and

a large amount of complex is obtained.

Obtaining the complexes in solution is done by mixing an aqueous solution of β-cyclodextrin with the solution of a guest molecule. After mixing the two solutions, shake the contents and refrigerate for several hours. The formation of the complex can be seen by observing the formation of a turbidity of the obtained solution, [4].

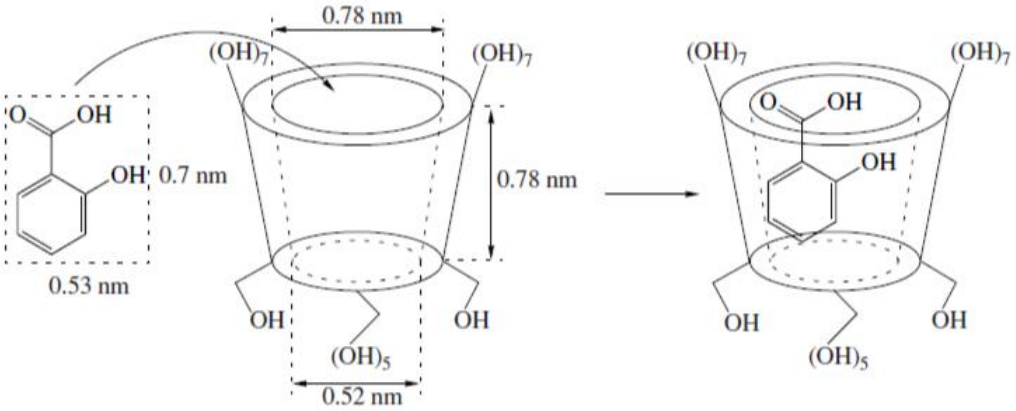

Figure 1. Schematic of the complexation between β-cyclodextrin and salicylic acid, [5]

The advantage of this method is the short reaction time, it only requires mixing the two reactant solutions, and then keeping cold for a few hours or days to let the complex precipitate. The reaction in this phase occurs in good yield, and the remaining uncomplexed compounds can be determined instrumentally or chromatographically.

EXPERIMENTAL PART

Due to the abilities of salicylic acid to be complexed by β-cyclodextrin, the method for chose for the preparation of inclusion complexes is that in solution because it is a method often used to obtain complexes, it is a method that have rezults and a good yield the ability to complex β-cyclodextrins can be calculating, [6].

The complexes were prepared in 3 samples, well determined amounts, both of β-cyclodextrin and of salicylic acid, to establish the optimal conditions of the process, i.e. when the complexation proceeded with a better yield and when a greater amount of complex obtained. Quantities used were determined based on stoichiometric calculations, [7-9].

Guest molecules of salicylic acid dissolved in ethanol are added to the solution of β-CD. The balance is achieved by intense agitation and then cooled for several hours. The reagents to use were of analytical purity and chromatographic use. Preparation of β-CD/ salicylic acid inclusion complexes was made in three ways , obtaining 3 samples, as following:

1) 0.5675 g of β-CD was dissolved in 6 ml of distilled water at 55 ° C, to hot solution was added an ethanol solution of salicylic acid, namely, 0.2072 g salicylic acid in 3 ml of ethanol. The molar ratio: β-CD and salicylic acid is 1:3, in sample **1**.

2) 0.5675 g of β-CD was dissolved in 4 ml ethanol and 2 ml of distilled water at 50 ° C, to hot solution was added an ethanol solution of salicylic acid, namely, 0.1035 g salicylic acid in 1 ml of ethanol. The molar ratio: β-cyclodextrin / salicylic acid is 1:1.5, in sample **2**.

3) 0.5675 g of β-cyclodextrin was dissolved in 3 ml of ethanol and 3 ml of distilled water at 50 ° C, to hot solution was added an ethanol solution of salicylic acid, namely 0,1381 g salicylic acid in 2 ml of ethanol. The molar ratio: β-cyclodextrin / salicylic acid is 1:2, in sample **3**.

The three samples were kept under stirring for 20 minutes, at 50 ºC in a round-bottomed flask equipped with condenser upward. After maintaining the samples at 22°C for 5 hours for slow cooling, they were cooled in a refrigerator at 5°C for 36 hours.

The complexes of β-ciclodextrin / salicylic acid that were formed in the three samples were filtered.

RESULTS AND DISCUSSIONS

Results from UV-VIS spectrophotometric analysis, the absorption spectra of salicylic acid, β-cyclodextrin, and of the three inclusion complexes are shown in figure 2, 3 and 4.

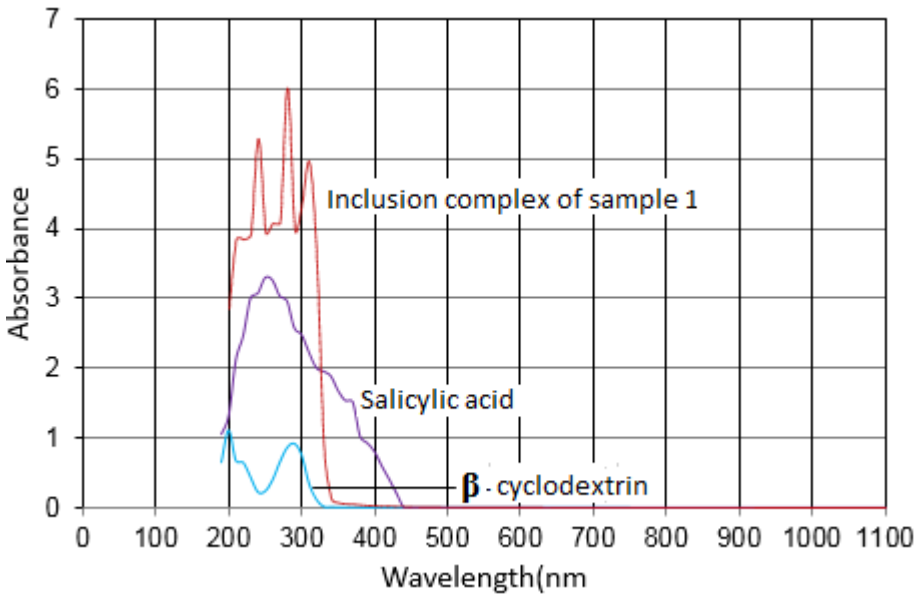

Figure 2. UV-VIS absorption spectra for: inclusion complex of samples 1- red, β-cyclodextrin (β-CD)-blue and salicylic acid - mauve.

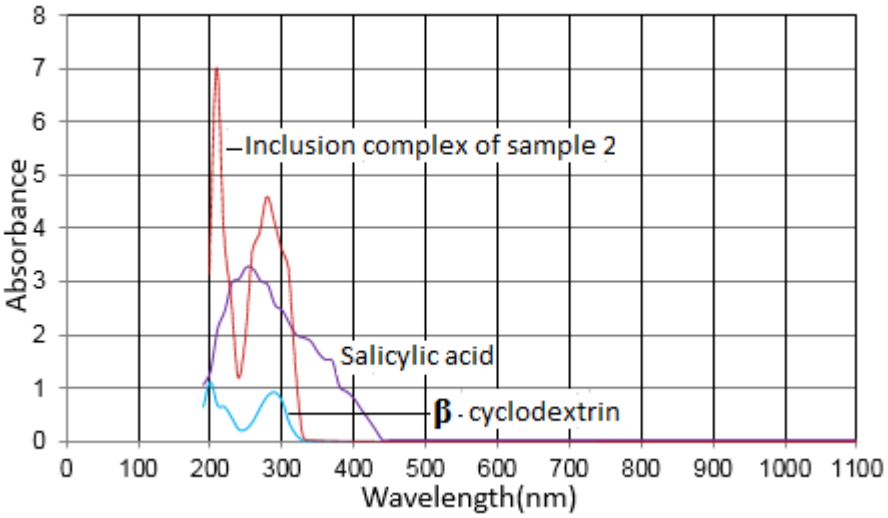

Figure 3. UV-VIS absorption spectra for: inclusion complex of samples 2- red, β-cyclodextrin (β-CD)-blue and salicylic acid - mauve.

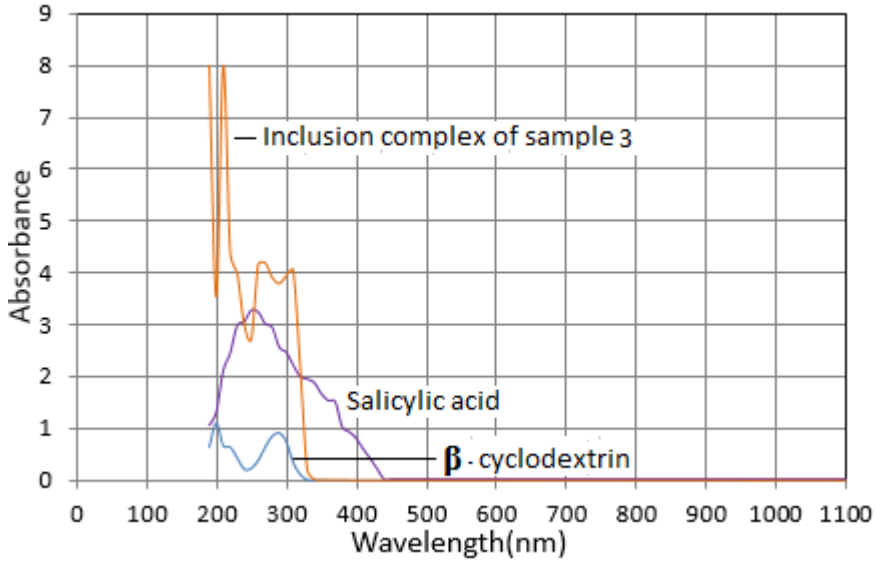

Figure 4. UV-VIS absorption spectra for: inclusion complex of samples 3- red, β-cyclodextrin (β-CD)-blue and salicylic acid - mauve.

The study of Ultraviolet-Visible Absorbtion (figures 2, 3 and 4) revealed that the salicylic acid shows an maximum absorption at around 262 nm, β-CD has two maximum absorption, the second one is sharper, around 300 nm.

Inclusion complex that it is formed in sample 1, exhibits maximums between 200 and 370 nm, the highest being 280 nm and the last around in 360 nm. We found that, after complexation with salicylic acid, the absorption spectrum of β-CD is modified. By adding β-cyclodextrin the absorbance of the inclusion complex, increases significantly compared with salicylic acid. Similar results are also obtained and by examining figures 3 and 4.

The absorption peaks of the inclusion complexes between β-CD/

salicylic acid are located far above those of β-CD. Inclusion compound between β-ciclodextrin and salicylic acid formed in sample 2 has an absorption peak between 200 and 300 nm, the highest being at 200 nm and the most well defined maximum is around 300 nm, the above the β-cyclodextrin.

In sample 3 we obtained a peak for inclusion compound by salicylic acid with β-ciclodextrină at about 220 nm and two absorption peaks for the inclusion complex, in the spectral absorption area of the β-cyclodextrin at 270-320 nm.

CONCLUSIONS

The study of inclusion complexes of cyclodextrins is one of the most important processes for the synthesis of compounds with new uses.

This study is based on the formation of a new compound, starting from two reactants, cyclodextrin and a "target" molecule, which will have new properties, [10-12].

What is specific to this process is the fact that it is not a chemical process, there is no chemical reaction between the reactants, but they physically interact and form the complex.

The interaction takes place by embedding the "guest" molecule in that of the cyclodextrin, being dependent on the structure, dimensions, polarity and solubility of the "guest" molecule.

Inclusion complexes are characterized by a stability constant, therefore the choice of the formation process must be aimed at obtaining a stable complex, a complex inert to the action of the surrounding environment and have properties protected against the reactant molecule, [13,14].

Synthesis of the inclusion complex of β-cyclodextrin with salicylic acid led to the discovery that it is a compound with uses in the pharmaceutical industry.

When forming the complex, the most practical method of synthesis is chosen, the path with the highest yield and the one in which the stability of the complex is as good as possible.

Following the formation of the complex in solution, it can be seen that the formation of the complex occurs rapidly, occurs in good yield, and that the process does not involve a complicated and expensive process. In all 3 cases realized, the complex was obtained, its formation being identified by UV-VIS spectrophotometry.

Obtaining and identifying the obtained complex, under the conditions carried out in the experimental part, indicates that upon the interaction of a salicylic acid solution with a β-cyclodextrin solution, based on a physical complexation process, a new compound with new properties is obtained, in a state of solid aggregation and which is both physically and chemically different from the two reactants.

The tests carried out were done in the same way, but the amounts of reactants are different, to see in which case, the complexation occurred better. From the results obtained, in sample 1, when the β-cyclodextrin:salicylic acid ratio was 1:3, the reaction yield was the best, the amount of complexed salicylic acid being the highest.

In this sense, we can say that the inclusion process depends a lot on the amount of "guest" molecule

introduced, on the reaction conditions, on the solubility and polarity of the molecule, the resulting chemical complex having new physical and chemical properties.

REFRENCES

[1] A. Liptak, P. Fügedi, Z. Szurmai, J, Imre, P. Nanasi and J. Szejtli (1982). *The chemistry of cyclodextrin derivates*. I. Int. Symp. on Cyclodetrins Budapest, D. Reidel Publishing, Dordrecht, 275-287.
[2] J. Szejtli (1982). *Cyclodextrins and their Inclusion Complexes*. Akademiai Kiado, Budapest, 115–122.
[3] Marcel Dekker, Inc.,(1996) *Microencapsulation. Methods and Industrial Applications*, Benita, S. (ed.) New York - Basel - Hong Kong, 3.
[4] W. Saenger (1984). *Structural aspects of cyclodextrins and their inclusion complexes*. *Inclusion compounds*. Academic Press, London, vol.2, 231-259.
[5] D. Duchêne (1987). *Cyclodextrins and their industrial uses.* Editions de Santé, Paris.
[6] Janisse Crestani de Miranda, Tércio Elyan Azevedo Martins, Francisco Veiga, Humberto Gomes Ferraz (2011). *Cyclodextrins and ternary complexes: technology to improve solubility of poorly soluble drugs*. Brazilian Journal of Pharmaceutical Sciences, vol. 47, n. 4, 665-681
[7] J. Bergsma, P.M. Bruinenberg, H. Hokse and J.B.M. Meiberg (1988). *Cyclodextrins from potato starch, recent developments*. Proceeding of the fourth international symposium on cyclodextrins, Dordrecht, 41-46.
[8] Tablet C., Dumitrache L., Minea L., Hillebrand M, (2012). *Inclusion complexes of 3-carboxy- and 7-diethylamino-3-carboxy-coumarin with α-cyclodextrin: spectral study and molecular modeling*, Revue Roumaine de Chimie, 57(7-8), 665-673.
[9] M. Vikmon (1982). *Rapid and simple spectrophotometric method for determination of micro-amounts of cyclodextrins*. I. Int. Symp. on Cyclodetrins Budapest, D. Reidel Publishing, Dordrecht, 69-74.
[10] H. Hokse (1983). *Colorimetric analysis of cyclomalto-octaose (γ-cyclodextrin)*. Carbohydrate Res., 114, 303-305.
[11] M. Mäkelä, T. Korpela and S. Laakso (1987). *Colorimetric determination of β-cyclodextrin: two assay modifications based on molecular complexation of phenolphtalein*. J. Biochem. Biophys. Meth., 14, 85-92.
[12] Horia Iustin Naşcu și Lorentz Jäntschi (2006). *Chimie analitică şi instrumentală.* Academic Pres, Cluj-Napoca, 114.
[13] Sanjoy Kumar Das, Rajan Rajabalaya, Sheba David, Nasimul Gani, Jasmina Khanam, and Arunabha Nanda (2013). *Research Journal of Pharmaceutical, Biological and Chemical Sciences Cyclodextrins*. RJPBCS, Volume 4, Issue 2, 1694.
[14] Hadaruga N.G., Hadaruga D.I, Paunescu V., Tatu C., Ordodi V.L., Bandur G., Lupea A.X., (2006). Thermal stability of the linoleic acid/α- and β -cyclodextrin complexes, Food Chemistry, 99, pg.500–508.

SPECTROPHOTOMETRIC DETERMINATION OF PARACETAMOL IN PHARMACEUTICAL PRODUCTS

Alexandrina FODOR[1], Mirabela-Maria VAŢLAVIC[2], Claudia Mona MORGOVAN[1]

[1]University of Oradea, Informatics and Science Faculty, Chemistry Department, Oradea, University Street no. 1, Romania, afodor@uoradea.ro
[2]University of Oradea, Informatics and Science Faculty, Structural and Applicative Chemistry, student I year of study, mirabelavatlavic@yahoo.com

Abstract: *In this work, the UV-VIS spectrophotometric method was used for the quantitative determination of paracetamol in different pharmaceutical products. This method of determination was chosen as it is easier to put into practice, not requiring complex equipment, expensive reagents and complex work methodology (like the chromatographic methods), thus being within the reach of more modest laboratories. It was chosen to use $FeCl_3$ as a colour reagent.*
Key words: *UV-VIS Spectrophotometric method, Paracetamol, pharmaceutic products*

INTRODUCTION

In the pharmaceutical world, paracetamol, also known as acetaminophen, has established itself as one of the most recognized and used compounds, providing rapid and effective relief of mild to moderate pain and fever [1]. Over time, research has confirmed its effectiveness and elucidated some aspects of its mode of action in the body. However, it should be noted that although paracetamol is available without a prescription, it is important to strictly follow the recommended doses and consult a medical professional before use, especially for children, pregnant women or people with pre-existing medical conditions [2,3].

Being available in various forms such as tablets, syrups, effervescent powders and suppositories, paracetamol adapts to the individual needs of patients of all ages [4]. However, despite its benefits, the use of paracetamol is not without potential risks. Overdose can lead to serious liver damage, which emphasizes the importance of following recommended doses and avoiding combination with other drugs containing the same active ingredient[5-8].

In this work, the UV-VIS spectrophotometric method was used for the quantitative determination of paracetamol in various pharmaceutical products.

The spectrophotometric method of determination was chosen due to its ease of implementation, not requiring complex equipment, expensive reagents and complex working methodology (as well as chromatographic methods), thus being within the reach of more modestly equipped laboratories. It was chosen to use $FeCl_3$ as a colour reagent.

ANALYZED PRODUCTS

The following pharmaceutical products, in the form of tablets, both with a single active component and with several components, were analysed: Paracetamol 500 mg Zentiva, Paracetamol 500 mg Terapia, Fasconal Gedeon Richter Romania, Coldrex Sinus Extra tablets, Antinevralgic P tablets Sanofi.

Paracetamol 500 mg Zentiva

Composition according to the leaflet [9]:
- The active substance is paracetamol. Each tablet contains 500 mg paracetamol, in the form of paracetamol DC 555.55 mg.
- The other components are: povidone K 30, corn starch, pregelatinized corn starch, sodium starch glycolate, stearic acid, propylhydroxybenzoate (E216), ethylhydroxybenzoate (E214).

Paracetamol 500 mg Terapia

Ingredients according to the leaflet [10]:
Each tablet contains 500 mg paracetamol.
The other components are corn starch, pregelatinized starch, povidone, carboxymethylsodium starch, stearic acid.

Fasconal Gedeon Richter România

Composition, according to the leaflet [11]:
- The active substances are: acetylsalicylic acid, paracetamol, caffeine and codeine. Each tablet contains acetylsalicylic acid 200 mg, paracetamol 200 mg, caffeine anhydrous 25 mg and codeine phosphate hemihydrate 10 mg.
- The other components are: corn starch, microcrystalline cellulose type 101, anhydrous colloidal silicon dioxide, pregelatinized starch, talc, sodium stearyl fumarate.

Coldrex sinus Extra comprimate

Composition, according to the leaflet [12]:
- The active substances are: paracetamol, chlorpheniramine maleate and pseudoephedrine hydrochloride. Each tablet of Coldrex Sinus Extra contains paracetamol 500 mg, chlorpheniramine maleate 3 mg and pseudoephedrine hydrochloride 50 mg
- The other components are: pregelatinized starch, povidone and stearic acid.

Antinevralgic P comprimate Sanofi

Composition, according to the leaflet [13]:- The active substances are acetylsalicylic acid, paracetamol and anhydrous caffeine. One tablet contains acetylsalicylic acid 250 mg, paracetamol 150 mg and caffeine anhydrous 20 mg.- The other components are: lactose monohydrate, povidone K 30, sodium starch glycolate, stearic acid, corn starch, microcrystalline cellulose (E 460), colloidal anhydrous silicon dioxide, pregelatinized starch, propyl p-

hydroxybenzoate (E 216), Ethyl p-hydroxybenzoate (E 214).

Principle of the spectrophotometric analysis method of Paracetamol [14].

Paracetamol, also called acetaminophen or (N-4 - hydroxyphenyl acetamide) dissolved in H_2SO_4 0.05 mol/L has an absorption maximum in UV at the wavelength λ=243 nm and can be spectrophotometrically dosed from different samples (biological fluids, pharmaceutical products) in the UV range [23].**Necessary reagents:** 0.1 N NaOH solution, 1% $FeCl_3$ alcoholic solution

Coloured reaction [17]: Adding a few drops of 1% $FeCl_3$ alcoholic solution to 1-2 ml of paracetamol alcoholic solution (5% methanolic) the appearance of a pale green colour is observed[24]. The appearance of the colour is due to the reaction:

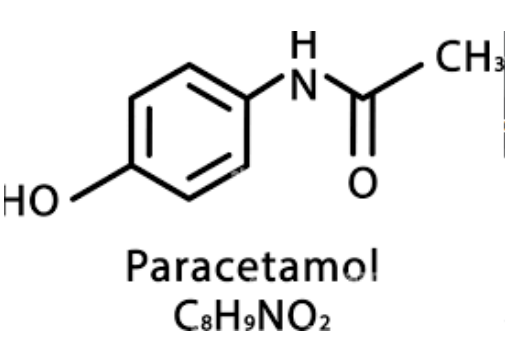

Paracetamol Struucture[15]

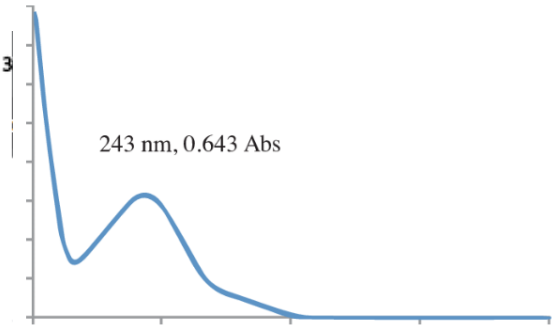

Paracetamol UV Spectrum [16]

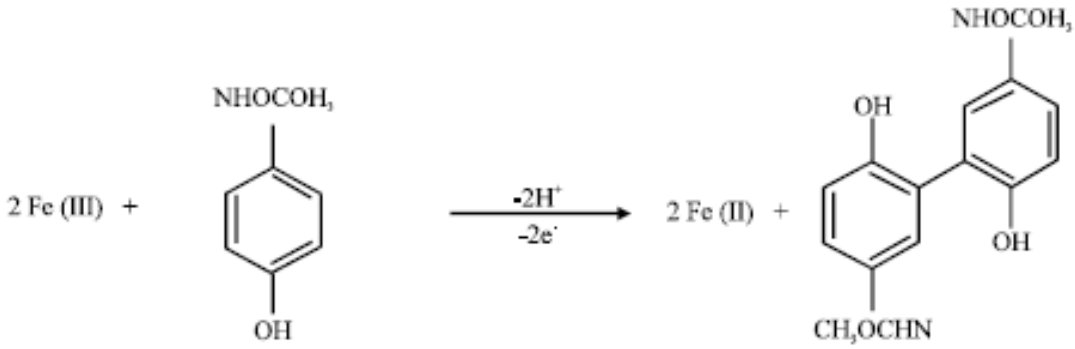

Procedure [18]

- Preparation of the solution A: 50 mg paracetamol powder were dissolve in 10 ml 0.1 N NaOH with vigorous stirring in a 100 ml volumetric flask, then make up to 100 ml with distilled water
- Preparation of the solution B: 5 ml of solution A was diluted with 5 ml of 0.1 N NaOH and bring to the mark in a 50 ml volumetric flask with distilled water.
- Series of solutions for the calibration curve were prepared diluting individually: 1, 2, 3 and respectively 4 ml of solution B with distilled water in four 25 ml volumetric flasks and bring to the mark
- Two drops of 1% $FeCl_3$ alcoholic solution was added to 1-2 ml of paracetamol alcoholic solution (5% methanolic).
-The absorbance at 257 nm A_{257} was measured for each of the standard solutions using a UV-VIS spectrophotometer.

Calculus:

Solution. A concentration is:
50mg/100 i.e. 0.05g/100ml or = 0.05 %.

Solution B concentration is:
$C_A \times V_A = C_B \times V_B$
$C_B = (C_A \times V_A)/V_B = (0.05 \times 5) / 50 = 0.005$ %

Solution 1:are concentration is $C_B \times V_B = C_1 \times V_1$
$C_1 = (C_B \times V_B)/V_1 = (0.005 \times 1) / 25 = (0.005 / 25) = (1/5) \times 10^3 = 2 \times 10^4$ %

Calibration curve data:

Solution no.	**Paracetamol concentration** $\times 10^4$ %	**Absorbance measured at 257 nm** A_{257}
1	2	0,12
2	4	0,17
3	6	0,22
4	8	0,28

Using the calibration curve, by interpolation, the concentrations of paracetamol in the aqueous solutions of the analysed pharmaceutical products are determined.

Preparation of the solutions to be analysed from the pharmaceutical products [14]:

- 50 mg of powder obtained by mortaring the analysed pills was dissolved in 10 ml of 0.1 N NaOH with vigorous stirring in a 100 ml volumetric flask, then make up to 100 ml with distilled water. The obtained solutions were filtered.
- 5 ml of the solution prepared by dissolving the pills and filtering was diluted with 5 ml of 0.1 N NaOH solution and bring to the mark in a 50 ml volumetric flask with distilled water.
- Two drops of 1% $FeCl_3$ alcoholic solution to 1-2 ml of paracetamol alcoholic solution (5% methanolic) was added

Each tablet is weighed before mortaring and dissolution so that calculations can be made to express the concentration of paracetamol as presented by the manufacturers (mg paracetamol/tablet).

RESULTS

The results of the analyses performed after weighing the tablets, mortaring, passing into the solution according to the procedure, adding the colour reagent ($FeCl_3$), measuring the absorbance, determining the concentration of Paracetamol in the solution ($C \times 10^4$ (%) by interpolating on the calibration curve and performing the calculations for express the amount of Paracetamol mg/tablet, are presented in table 1.

Table 1. The results of the determination of paracetamol in the investigated pharmaceutical products expressed in mg paracetamol/tablet

Pharmaceutical product	**Paracetamol determinate concentration PDC mg/tablet**	**Paracetamol concentration mentioned by the producer PMP mg/tablet**	**Difference between the PC and PMP %**
Paracetamol 500 mg Zentiva	495,47	500	0,906
Paracetamol 500 mg Terapia	491,53	500	1,694
Fasconal Gedeon Richter România	197,97	200	1,015
Coldrex sinus Extra comprimate	494,96	500	1,008
Antinevralgic P comprimate Sanofi	246,76	250	1,296

CONCLUSION

The spectrophotometric method for determining paracetamol from tablets pharmaceutical products using $FeCl_3$ as a colour reagent proved to be a reliable method, the % difference of the determined concentration compared to that mentioned by the manufacturer being 0.906-1.296 %.

REFERENCES

[1] Buzoianu, A.D. (2017), Farmacologie, Vol.II, Ed. Medicala Universitară I. Haţieganu, Cluj Napoca
[2] https://ro.scribd.com/doc/252639099/Paracetamol/ , 14.04.2023
[3] https://www.sfatulmedicului.ro/medicamente/paracetamol_9651/ , 16.04.2023
[4] https://www.medicover.ro/medicamente/paracetamol,34,n,1153#Cum%20sa%20luati%20
[5] https://www.doc.ro/sanatate/intoxicatia-cu-paracetamol-acetaminofen-semne-simptome-si-tratament/, 17.05.2023
[6] https://www.romedic.ro/toxicitatea-hepatica-a-paracetamolului/ , 20.05.2023
[7]https://www.drmax.ro/articole/acetaminofenul-paracetamolul-si-riscul-de-supradoza-tot-ce-trebuie-sa-stii/, 10.05.2023
[8]https://www.revistagalenus.ro/toxicologie/intoxicatia-cu-paracetamol-metabolizare supradozaj/ 20.05.2023
[9] https://www.anm.ro/_/_PRO/pro_12881_31.12.19.pdf
[10] https://www.anm.ro/_/_PRO/pro_13157_16.04.20.pdf
[11]https://www.gedeonrichter.com/ro/-/media/sites/ro/documents/produse/prospect/pil_fasconal_pro.pdf?rev=28e125dac144457d9f07a654408f8ff7
[12] https://www.anm.ro/_/_PRO/PRO_11391_31.01.19.pdf

[13] https://www.antinevralgic.ro/pages/prospecte/antinevralgic-p-prospect.html
[14]https://www.studocu.com/ro/document/universitatea-de-medicina-si-farmacie-gr-t-popa/chimie-organica/chimie-analitica-lp-14-experimental-analytical-chemistry/13884025 , ,16.07.2023
[15] https://www.alamy.com/paracetamol-molecular-structure-acetaminophen-skeletal-chemical-formula-chemical-molecular-formula-vector-illustration-image451274084.html
[16]https://www.researchgate.net/figure/UV-spectrum-of-paracetamol-in-the-basic-medium_fig1_322076506
[17] Dorneanu, V., Stan, M. (2007). Metode Chimice şi Instrumentale de Analiză, Ediţia a II-A Revizuită, Editura Universităţii de Medicină şi Farmacie "Gr.T.Popa", Iaşi, pp. 236-332
[18] Dorneanu, V., Stan, M. (2000). Chimie Analitică – lucrări practice, Editura Universităţii de Medicină şi Farmacie "Gr.T.Popa", Iaşi, pp. 224-322

COMPARATIVE STUDY OF Ca CONTENT FROM ALMOND, CHIA AND SESAME SEEDS

Alexandrina FODOR, Anda Ioana Graţiela PETREHELE
University of Oradea, Informatics and Science Faculty, Chemistry Department, Oradea, University Street no. 1, Romania, afodor@uoradea.ro

Abstract*: Different volumetric methods were developed for the comparative study of Calcium content in vegetal dietary Ca sources as the almonds, chia and sesame seeds. In the quantitative analysis of calcium ion, two volumetric methods were applied: redox (Clark-Collip Method) and complexometric. Volumetric methods were chosen for the study because these methods are quick, cheap, easy to put into practice, are not requiring complex equipment and also are prove to be reliable methods for performing macroelements dosages.*
Key words: *Ca, complexometric method, redox Clark-Collip method, Almond, Chia, Sesame, Seeds*

INTRODUCTION

Calcium is indispensable for maintaining the solidity of bones in the body, but also for the functioning of nervous system and optimal muscle cells functioning. This macroelement intervenes also in the reception of hormonal messages by the cells and in the activation of enzymes. In addition, it is involved in blood clotting. This is why it is important to have a balanced diet that brings us calcium intake [1].

Calcium deficiency is manifested by: involuntary muscle contractions (cramps), osteoporosis, heart rhythm disorders, numbness and tingling in the limbs, menstrual cycle irregularities, insomnia, palpitations, intense headaches, menopausal disorders, depression, rickets and growth disorders [2].

Important sources of dietary Ca are milk and derived products as well as fish meat but also vegetables, such as seeds which have high bioavailable calcium [3]. These vegetal resources of calcium are very important for people who cannot tolerate lactose or milk proteins.

In this paper different volumetric methods were applied to comparatively study of the Ca content of almond, chia and sesame seeds. Volumetric methods were chosen for the study because these methods are quick, cheap, easy to put into practice, not requiring complex equipment and also are prove to be reliable methods for performing macroelements dosages [4].

EXPERIMENTAL

Analyzed samples

Raw seeds of: chia, sesame and almonds purchased online from Sanovita (a highly advanced research development, and production company of natural minerals, plant extracts, amino and humic acids for sustainable agriculture [5]) were analysed. The analysed products were purchased online from the manufacturing company

.

Figure 1. Analysed products: raw seeds of chia, sesame and almonds, purchased online from Sanovita

Processing of samples

About 100 g of each investigated seeds were taken and ground into a powder. 1 g of the obtained powder was weighed on the analytical balance and then transfer into a conical flask. An aliquots, 20 mL of acid mixture of HCl and HNO_3 in the molar ratio of 3:1, was added. The sample was digested by heating gently on a hot plate until the sample became clear. The obtained solution was cooled and then vacuum filtered. The concentration of Ca^{+2} was determined using the filtrate [6].

Determination of Ca^{+2} using complexometric titration with EDTA [7,8]

Preparation of solutions

To prepare 1 liter of Titriplex III $5 \cdot 10^{-2}$ M, 18.607 g of EDTA ($C_{10}H_{16}N_2O_8$)weigh on an analytical balance was bring to the mark in a 1L volumetric flask with distilled water. EDTA was purchased from Sigma-Aldrich.

The preparation of the Murexide indicator was done by mortaring 200 mg Murexid with 100 g NaCl. Murexid was purchased from Sigma-Aldrich.

Procedure

10 ml of the sample to be analysed was dilute to 50 mL with distilled water, alkalinize with 5 ml NaOH 1N to pH = 11-12. A tip of the murexide indicator spatula is added to the solution and quickly titrated (to avoid the calcium precipitation due to the carbonating reaction) with Titriplex III $5 \cdot 10^{-2}$ M solution until the colour turns from pink to purple.

Calculation of results (mg Ca^{2+}/100g seed sample) were done taking into account the volume (mL) of solution Titriplex III $5 \cdot 10^{-2}$ M used for the titration process, the stoichiometry of the reaction and the dilution of the sample: from the analysed solution.

$$gCa^{2+} = \frac{2{,}0040 \cdot V \cdot T}{18{,}6070}$$

V- volume (mL) of complexon III 5·10-2 M solution used for titration

T-Titer of the solution used for titration

Three titrations were performed for each sample and then the arithmetic mean of the results obtained was calculated.

Determination of Ca^{2+} using redox titration with Potassium Permanganate (Clark-Collip Method) [9,10]

Preparation of solutions

0.1 N solutions are prepared: Oxalic acid $(HCOO)_2$ (9.003 g/1L water); Potassium Permanganate $KMnO_4$ (15.8034 g/1L water). Both reagents were purchased from Sigma-Aldrich.

Procedure

10 mL of the analysed solutions were taken and dilute to 50 ml with distilled water into a conical flask. 10 ml of 0.1 N Oxalic acid solution was added. The formed precipitate is vacuum filtered and then dissolved with 10% sulfuric acid.

The obtained oxalic solution is diluted up to 15 ml with distilled water and then titrated with Potassium Permanganate until persistent pink.

The reactions that take place are:

- $CaCl_2 + (NH_4COO)_2 = 2NH_4Cl + Ca(COO)_2$;
- $Ca(COO)_2 + H_2SO_4 = (HCOO)_2 + CaSO_4$;
- $2KMnO_4 + 5(HCOO)_2 + 3H_2SO_4 = 2MnSO_4 + K_2SO_4 + 10CO_2 + 8H_2O$.

Calculation of results (mg Ca^{2+}/100g seed sample) were done taking into account the volume (mL) of solution $KMnO_4$ 0,1N used for the titration process, the stoichiometry of the reaction and the dilution of the sample: from the analysed solution.
Three titrations were performed for each sample and then the arithmetic mean of the results obtained was calculated.

EXPERIMENTAL RESULTS

The results obtained from the different volumetric analyses of the samples obtained from chia, sesame and almond seeds are presented in the table 1. In order to evaluate the obtained results, they were compared with the data from the specialized literature [11]. Both methods used for the Ca^{2+} content in the investigated seeds prove to be reliable (the results are in good correspondence with those presented in the literature [11]). In the case of the redox method, the amount of determined calcium was slightly lower (4.32-4.58%) than that determined by the complexometric method (table 2).

Table1. Complexometric and redox (Clark-Collip method) titration of the samples prepared from chia, sesame and almond seeds for the determination of Ca^{2+}

Sample	Complexometric method mg/100g	Redox Clark-Collip method mg/100g	Ca^{2+} content mentioned in the literature [11] mg/100g
Chia seeds	625	598	673
Sesame seeds	109	98	116
Almond seeds	254	241	264

Table 2. The amount of the differences between the results obtained in the complexometric and redox titration of the samples prepared from chia, sesame and almond seeds for the determination of Ca^{2+}

Sample	Complexometric method mg/100g	Redox Clark-Collip method mg/100g	Ca^{2+} content mentioned in the literature [11] mg/100g
Chia seeds	625	598	4,32
Sesame seeds	109	104	4,58
Almond seeds	254	243	4,33

These values express the soluble calcium from the solution obtained when dissolving the powders prepared from the analysed seeds in aqua regia (acid mixture of HCl and HNO_3 in the molar ratio of 3:1)

CONCLUSIONS

Calcium content in vegetal dietary Calcium sources as the seeds of almonds, chia and sesame analysed using volumetric methods obtained results are in good respect with the literature data.

The complexometric method proved to be quick, cheap, easy to put into practice, not requiring complex equipment and also reliable for performing Calcium dosages as macroelement in the analysed seeds samples.

In the case of the redox volumetric method (Clark-Collip method), the amount of determined calcium was slightly lower (4.32-4.58%) than that determined by the complexometric method, probably due to the losses recorded in the stages of precipitation / filtration / dissolution of oxalate.

REFERENCES

[1]Harris, E.D. (2014) Minerals in food, Nutrition, metabolism, Bioactivity, DEStech

[2]Crăciun, A.M., Bridişcă, I. (2018) Biochimie clinică, Ed. Medicală Universitară I. Haţieganu

[3] Ross,A.C., Taylor,C.L., Yaktine,A.L. et al (2011) Dietary Referenec Intakes for Calcium and Vitamin D, National Academies Press (US)/ https://www.ncbi.nlm.nih.gov/books/NBK56060/, 10.06.2023

[4] McPherson P.A.C (2014) Practical Volumetric Analysis, 1st edition, Royal Society of Chemistry

[5] https://sanovita.ro/

[6]Akpata,E.I., Ezeanyika, L.U.S., Nwodo,O.F.C., Ezugwu,A.L. (2014), Variation in the Calcium and Magnezium Content of Selected Nigerian Leafy Vegetables and Seeds of Legumes, Gourd and Friuts, IOSR Journal of Pharmacy and Biological Science, Vol.9 (6), pp.5-9

[7] Dulman, V., Onofrei, T., Simion, C., Bârsănescu, A., Buhăceanu, R. Irimia,G., Ţarălungă, M. (1996) Analitică Calitativă - manual de lucrari practice, Ed. Univ. "Al.I.Cuza", Iaşi;

[8] Donald, J., Pietrzyk, C. W, Frank, F. (1989). Chimie analitică, EdituraTehnică, Bucureşti

[9]Vlădescu, L. (2003). Echilibre omogene în chimia analitică, Editura didactică şi pedagogică, Bucureşti

[10] http://medical-dictionary.thefreedictionary.com/Clark-Collip+method

[11]National Institutes of health, Office of Dietary Supplements, „Calcium": https://ods.od.nih.gov/factsheets/Calcium-Consumer/

Analele Universităţii din Oradea-Fascicula Chimie, Vol. XXX (30), p.21-25, 2023

IDENTIFICATION AND SEPARATION OF SOME FLAVONOIDS FROM BLUEBERRY LEAVES BY CHROMATOGRAPHIC SEPARATION

Sorin HODIȘAN[1], Rares Mihnea HODIȘAN [2], Mioara SEBEȘAN[1] , Csaba Nandor PELLE[3]
[1] University of Oradea, Faculty of Informatics and Sciences, Romania
[2] Iuliu Hateganu University of Medicine and Pharmacy, Cluj-Napoca, Romania
[3] Masterand CSA II, University of Oradea, Faculty of Informatics and Sciences, Romania

Abstract:*Flavonoids are phenolic pigments that contain in their molecule a pyranic or furanic heterocycle condensed with a benzene ring. Another benzene ring is attached to the heterocycle. The rings have hydroxyl groups, which determines the phenolic character of these pigments.*
Flavonoid deficiency can be very common today and in today's society because people don't eat enough fresh fruits and vegetables, eat more on the run, or prefer fast food. Also, overcooking food is a major contributing factor to the flavonoid deficiency that many of us experience.
Key words: Flavonoids,pyranic or furanic heterocycle , phenolic character, pigments, fruits and vegetables

1. INTRODUCTION

Flavonoids are plant pigments that predominate in higher plants. They are found in flowers, fruits, leaves, stems, roots, tree bark, etc. Small amounts are found in some algae, microorganisms and some insects (flavones). Most flavonoids are colored and largely contribute to the formation of the color of flowers and fruits. They are found in nature in a free state, but mostly in the form of glycosides. From a chemical point of view, flavonoid pigments are phenolic glycosides, soluble in water. They are found in vacuolar juice and chromoplasts. There are 6 types of flavonoids: flavans, anthocyanidins, flavones, flavanones, chalcones and aurones. These groups differ from each other by the type of heterocycle and by the number and position of the hydroxyl and methoxyl groups, connected to the benzene rings.[1-2]
Flavan (2-phenyl-benzopyran or 2-phenyl-chroman) and isoflavan (3-phenyl-benzopyran) are the skeletons best represented among flavonoid compounds.

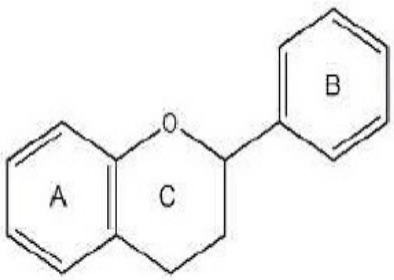

Flavan

There are 6 types of flavonoids:

1. Flavans
2. Anthocyanidin
3. Flavones
4. Flavanones
5. Chalcones
6. Aurones

Flavans (chromans) are pigments derived from flavan (2-phenyl-benzopyran, chroman). They have a benzopyranic ring in the molecule. They have a tendency to polymerize and form catechins that are included in the constitution of catechinic tannins.[2]

Anthocyanidins and anthocyanins. Anthocyanidins are pigments derived from 2-phenyl¬benzopyrene (2-phenyl-chromene). They are the main pigments that give the red and blue color to flowers and fruits. They are found in nature usually in the form of glycosides, which are called anthocyanins. The most important anthocyanids are: pelargonidin, cyanidin and delphinidin, which differ from each other by the number and position of the hydroxyl groups on the benzene ring C.[5]

Anthocyanins are found in flowers alone and especially mixed with other pigments, forming a wide variety of colors. Pink, red, bright red flowers predominantly contain pelargonidin, purple and cherry flowers contain cyanidin. Anthocyanins are soluble in water and alcohol, hardly soluble in ether, benzene and chloroform. They are extracted with water or alcohol in hydrochloric acid medium. From the extract obtained, if ether is added, anthocyanin chloride precipitates. With mineral acids, anthocyanins form red salts, stable when diluted (unlike flavones). Anthocyanidins with neighboring hydroxyl groups form with metals (Al, Fe) blue complexes. Anthocyanins change color depending on pH, which is why they are used as acid-base indicators.[3]

Flavones are crystalline substances, yellow in color, soluble in alcohol. In an alkaline medium, the pyran ring opens and diketones are formed. Flavones have absorption maxima between 335-350 nm, and flavanols between 360-380 nm. With metals, flavones form complexes. It dissolves in concentrated sulfuric acid giving yellow solutions, due to the formation of flavyl salts. Flavones show two or three characteristic absorption bands in the ultraviolet. They protect the oxidation of vitamin C and adrenaline in the body. They absorb ultraviolet radiation and protect the cytoplasm and chlorophyll from this radiation.[4]

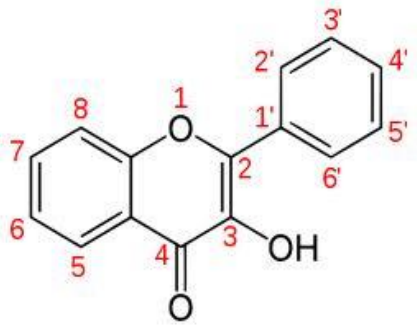

3 – hidroxi – flavona, Flavonol

Chalcones and aurones also have hydroxyl groups on rings A, C and even on the heterocycle. They are found in nature usually in the form of glycosides. Aurones and chalcones usually occur in flowers, and flavanones in flowers, leaves, wood, etc. In addition to the property of easily isomerizing into flavanones, chalcones also have the important property of easily oxidizing into 2-benzylidene-coumaranone compounds, called aurones:

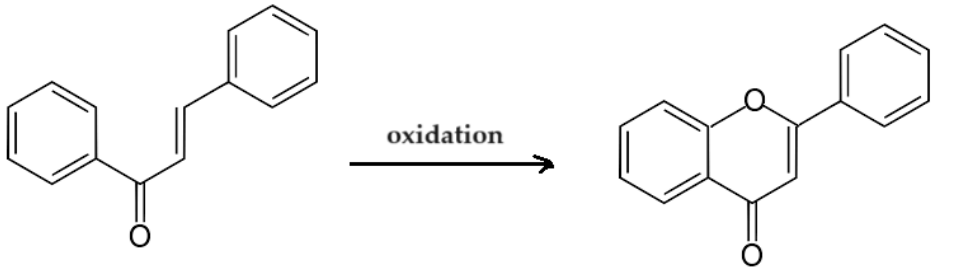

chalcona aurone (2-benziliden cumarone)

2. EXPERIMENTAL

The separation and identification of the main flavonoids from an extract of blueberry leaves (*Vaccinium myrtillus*) was studied. This was done by thin layer chromatography (TLC). The main work stages were:

a) extraction

b) separation and identification of flavonoids

The blueberry leaves were left to dry for several days at room temperature (the temperature must be constant, between 20 - 23 0 C), in the dark, until it reached about 55 - 60% of the initial mass. In order to be able to extract the flavonoids from the analysed plant, the dry leaves were placed in a mortar and with the help of a pestle we mixed until a fine powder was formed. Accurately weigh a quantity of 10 grams of *Vaccinium myrtillus* plant product, which will be subjected to the extraction of flavonols (the class of compounds that include quercetin, apigerin, luteolin and rutin) with 100 ml of ethyl alcohol each, using a type installation Soxhlet. After exhausting the plant material, when the solvent no longer turns straw-yellow, the obtained extracts are evaporated to a smaller volume, using a rotary evaporator. The obtained extracts are used for carrying out identification reactions and for the separation of flavonoids compounds on a thin layer of cellulose.

3. RESULTS AND DISCUSSIONS

Separation of quercetin, luteolin, apigerin and rutin on a thin layer of cellulose:

In order to identify the flavones from blueberry leaves, I did the reaction with NH_4 OH 3%, in which I took 2 ml extractive solution and treated it with a few drops of HN_4OH 3% solution. A yellow-green color is obtained, characteristic of flavonols.

In order to separate quercetin, apigerin, luteolin and rutin (the four main flavonoids present in blueberry leaves), 10 X 20 cm plates covered with a cellulose adsorbent layer, with a layer thickness of 0 .3 mm. Before

being used, the plates are activated for about 60 minutes at 120°C. At a distance of 5 cm from one of the ends of the plate, samples from the extracts of the plant under analysis can be applied with a micropipette. The chromatographic plate, on which the extracts were applied, was inserted into a vat, which contains, as developer (mobile phase), the solvent system: ethyl acetate – formic acid – water = 60 : 10 : 20 (v/v/v).

Reference solutions:

1. Metalonic extract of Vaccinium myrtillus
2. Quercetin standard solution 3 mg / 7 ml methanol
3. Routine ethanol solution 3 mg / 7ml methanol
4. Luteolin standard solution 3 mg / 7 ml methanol
5. Apigerin standard solution 3 mg / 7 ml methanol

After the migration of the developer, the plate is dried in a stream of warm air, it is sprayed with a mixture of 20 ml of the 3% boric acid solution and 7 ml of the 10% oxalic acid solution, then it is studied in UV light at λ = 366 nm, the existence of spots . The spots of flavonic derivatives show yellow-greenish fluorescence, before spraying with the revealing solution, and yellow, after spraying.

In the table below we have the Rf values of the four flavonoids present in blueberry leaves depending on the mobile and stationary phase :

Representation of experimental data:

:

Nr.	**flavonoids**	**R_f**
1	quercitin	0.785
2	rutin	0.568
3	apigerin	0,654
4	luteolin	0,579

The R_f value of a substance is the numerical value of the ratio between the distance traveled by an area of the substance and the distance traveled by the developer; the measurement is made in millimeters or centimeters, from the start to the center of the stain, respectively to the front of the developer. The retention factor R_f has values between 0 and 1. The retention factors depend on the temperature, the thickness of the layer, the degree of saturation with the solvent in the separation chamber, the size of the sample, the type of mobile and stationary phase.

The chromatogram obtained by thin layer chromatography (TLC) for the separation of the main flavonoids from *Vaccinium myrtillus* leaves has the following form:

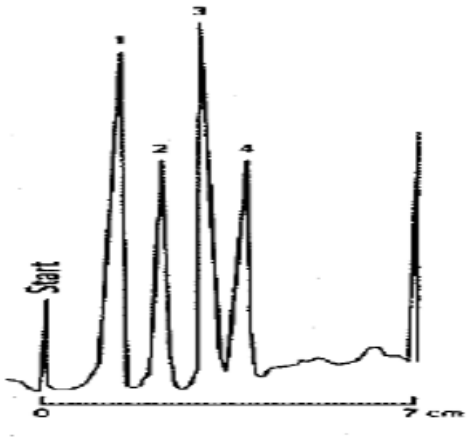

CSS chromatogram of the total extract.

The identified flavonoids are: 1- apigerin; 2- quercitin;3- luteolin;4- rutin

4.CONCLUSIONS

The aim of this work was to find a simple extraction method, coupled with an effective separation and identification method of the main flavonoids from blueberry leaf extract, used in the pharmaceutical, cosmetic, etc. industry. Based on the results obtained by thin-layer chromatography, it is possible to evaluate the quantitative and qualitative composition of flavonoids from the plant extract of *Vaccinium myrtillus.* Thin layer chromatography offers some significant advantages compared to other conventional chromatographic methods, namely: it is simple, relatively fast, sufficiently sensitive and can be used without special treatment of the sample.

5. REFERENCES

[1] Kirchner, J. G. *Thin Layer Cromatography, In: Tehnique of Organic Chemistry, vol. XII*, editor Weissberger A. New York, Interscience, 1987.
[2] E. Atanasiu, „*În lumea plantelor de leac",* Editura Ceres, Bucureşti, 1998,
[3] Kirchner, J. G. *Thin Layer Cromatography, In: Tehnique of Organic Chemistry, vol. XII*,
[4] Ciulei, I., Grigorescu, E şi Stănescu, U., „Plante medicinale, fitochimie şi fitoterapie,volumul 1, Editura Medicală, Bucureşti, 1993
[5] H. Kenker, B.G. Balder, M.P. Berkel, H.M. Hamstra-Spikkers, J.A. Olthof, "*Proceeding of the Int. Symp. on Instr. TLC*", Brighton, Sussex, U.K., p.105 ,1989

STUDIES ON KINETIC PARAMETERS OF A SECOND-ORDER REACTION OF HYDROLYSIS

Oana Delia STĂNĂŞEL[1], Mioara SEBEŞAN[1], Camelia Daniela ŢICĂRAT (IONAŞ)[2], Mirela ARDELEAN[3]

[1]University of Oradea, Faculty of Informatics and Sciences, Chemistry Department, ostanasel@uoradea.ro

[2]University of Oradea, Faculty of Informatics and Sciences, CSA Master Specialization,

[3]„Onisifor Ghibu" National College from Oradea

Abstract: *The studied reaction is the alkaline hydrolysis of ethyl acetate. The overall order of the reaction is the sum of the orders of the two reagents. The kinetics of the reaction was followed by applying the conductometric method. They worked starting by different initial concentrations of the reactants. Another parameter that has been changed was the temperature. Based on the experimental data, the half-life of the reaction was determined for each individual case. There were established the optimal working conditions for the studied parameters.*

Keywords: conductometric method, hydrolysis, second-order reaction*.*

INTRODUCTION

Reaction of an acid with an alcohol in presence of traces of a mineral or Lewis acid to give an ester as product is called esterification. The reverse reaction, i.e., the splitting of an ester into the component acid and alcohol is known as ester hydrolysis.

In principle, these reactions are reversible, and both reactions can be catalysed either by acids or bases. The acid catalysed hydrolysis reactions are also symmetric, meaning that it is only necessary to reverse the steps to get the mechanism for esterification. But hydrolysis is usually favoured by base catalysis, because the acid formed is removed as the salt, thus driving the reaction forward to completion [1], [2], [3].

The process does not correspond to catalysis in the strict sense of the word, because the hydroxyl ions are consumed in the reaction [4]. The equilibrium is totally shifted to the right due to the stability of the resulting carboxylate ion. A useful indication of the rate of a reaction is the half-life of a substance, which represents the time when its concentration falls to half the initial value. As a result, a reduced half-life indicates a faster reaction rate. When we start by equal initial concentrations of the two reactants, ethyl acetate and sodium hydroxide, we can calculate the half-life regarding sodium hydroxide by applying the conductometric method [5].

The integrated rate law is:

$$\frac{1}{c_R} = \frac{1}{c_{0R}} + kt \qquad (1)$$

where:

c_R - concentration of sodium hydroxide at time t;

c_{0R} - concentration of sodium hydroxide at initial time (at t=0);

k = rate constant of the reaction.

The calculated half-life $t_{1/2}$ is:

$$t_{1/2} = \frac{1}{k \cdot c_{0R}} \qquad (2)$$

The conductance dependence on the concentration of sodium

hydroxide in the reactant mixture is given by the relations:

$$c_R = constant \cdot (G_t - G_f) \quad (3)$$

$$c_{0R} = constant \cdot (G_0 - G_f) \quad (4)$$

where:

G_0 - the conductance of the reactant mixture at the initial moment;

G_t - the conductance of the mixture at time t;

G_f - the conductance of the mixture corresponding to the total hydrolysis of the ester.

EXPERIMENTAL PART

Solutions of sodium hydroxide and ethyl acetate of equal concentrations were prepared. Equal volumes of solutions of the same concentration of sodium hydroxide and ethyl acetate were mixed. The moment of mixing corresponds to the initial moment, against which the determinations were made. For each initial mixture, the conductance was measured for 20 minutes. Measurements were done for the reaction mixture maintained at 20°C, 24°C, and 28°C, respectively. To complete the reaction, a sample identical to the one measured at any of the three temperatures was kept in the water bath at 60°C for 30 minutes. Later then it was cooled and it was measured the conductance. The same procedure was followed for all samples.

It was aimed to determine the optimal conditions in the ranges of values studied, so that the half-life is minimal. The optimal conditions were obtained using the method of factorial experiments [6].

ANOVA test was used to analyze the variations between the experimental data.

RESULTS AND DISCUSSIONS

The results of the conductance measurements for the reactant mixtures of different concentrations at different temperatures, for 20 minutes, were processed in order to obtain the half-life time.

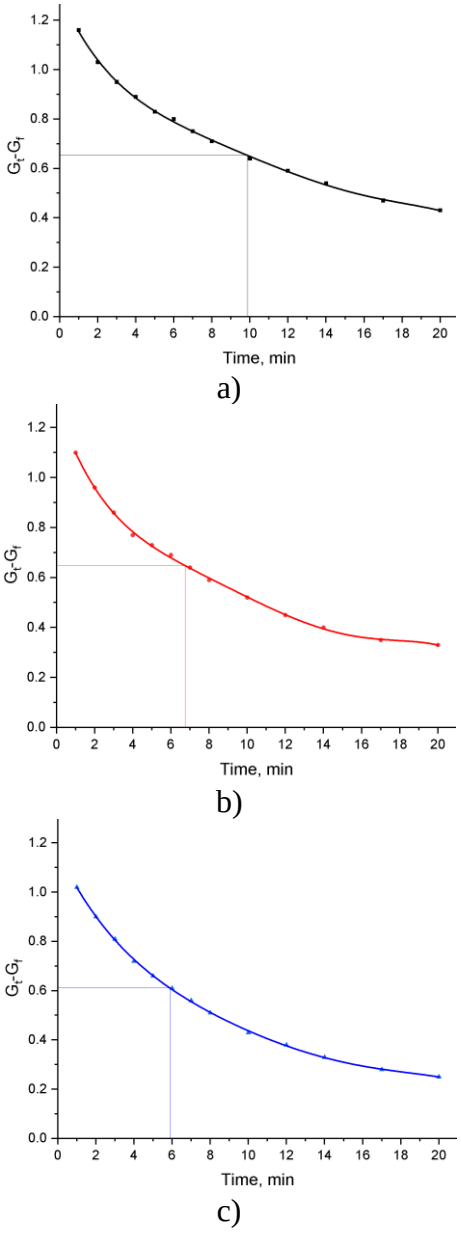

Figure 1. The variation with time of the concentration of sodium hydroxide starting by 0.02M, at working temperatures of 20°C (a), 24°C (b) and 28°C (c).

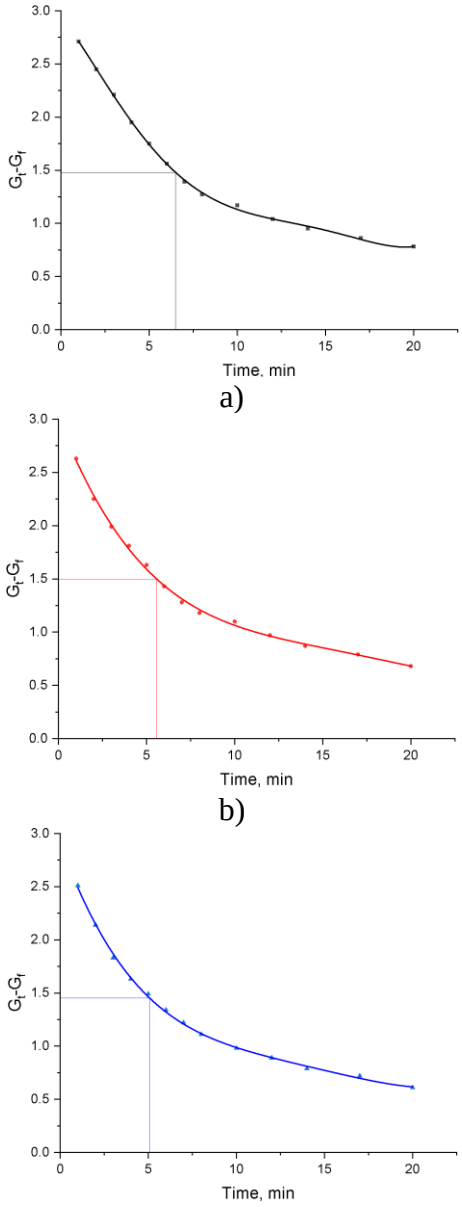

Figure 2. The variation with time of the concentration of sodium hydroxide starting by 0.04M, at working temperatures of 20°C (a), 24°C (b) and 28°C (c).

The variation with time of the concentration of the reactant in this second-order reaction is presented in figures 1-3. You may notice the obtained half-lives in these graphic illustrations, shown in figures 1 for solutions of initial concentrations of 0.02 M, in figures 2 for solutions of initial concentrations 0.04 M, respectively in figures 3 for initial concentrations 0.06M.

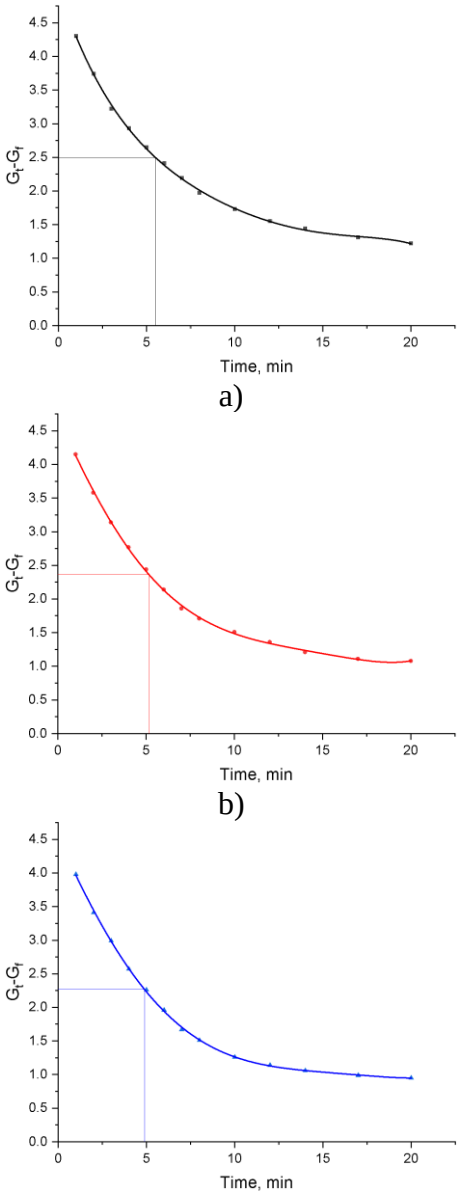

Figure 3. The variation with time of the concentration of sodium hydroxide starting by 0.06M, at working temperatures of 20°C (a), 24°C (b) and 28°C (c).

The temperature and concentration factors at three levels were considered, and the half-life time as a response function. A full factorial

experiment containing 27 experiments was carried out.

The experimental matrix is presented in Table 1.

Table 1. Experimental matrix

		Factor 1	Factor 2	Response 1
Std	Run	A:Conc	B:Temp	Time
7	1	0.02	28	6.43268
6	2	0.06	24	5.1441
12	3	0.06	20	5.48818
17	4	0.04	28	5.08501
10	5	0.02	20	9.85127
2	6	0.04	20	6.49101
18	7	0.06	28	4.8884
4	8	0.02	24	6.7509
21	9	0.06	20	5.65056
11	10	0.04	20	6.69143
13	11	0.02	24	6.98357
25	12	0.02	28	6.56118
22	13	0.02	24	6.52057
14	14	0.04	24	6.49101
24	15	0.06	24	5.30273
23	16	0.04	24	5.82213
1	17	0.02	20	10.1537
5	18	0.04	24	5.29157
27	19	0.06	28	4.97981
3	20	0.06	20	5.3212
9	21	0.06	28	4.79852
19	22	0.02	20	9.55144
20	23	0.04	20	6.35395
8	24	0.04	28	5.19103
15	25	0.06	24	5.05
16	26	0.02	28	6.30628
26	27	0.04	28	4.94525

The ANOVA test allowed the assessment of whether the differences between the experimental data are due to random errors or systematic effects of the experiments. It also allows examining the significance of factors in a multifactorial experiment.

Table 2. ANOVA test results

Source	Model	A-Conc	B-Temp	AB
Sum of Squares	55.39	30.34	16.07	8.98
Mean Square	6.92	15.17	8.04	2.25
F-value	100.93	221.12	117.13	32.73
p-value	< 0.0001	< 0.0001	< 0.0001	< 0.0001
	significant			

The statistical test for ANOVA is the Fischer test (F test). Table 2 shows that the value of the F test is 100.93, which means that the model is significant.

The *p*-value is widely used in statistical hypothesis testing. P values less than 0.0500 indicate that the model terms are significant. In this case, A, B, AB are significant model terms.

The regression model is given by the following relationship:

$$\begin{aligned} y = {} & 6.23 + 1.45 \cdot A1 - 0.4078 \cdot A2 + \\ & + 1.06 \cdot B1 - 0.2973 \cdot B2 + \\ & + 1.12 \cdot A1 \cdot B1 + 0.3637 \cdot A2 \cdot B1 - \\ & - 0.6301 \cdot A1 \cdot B2 + 0.3475 \cdot A2 \cdot B2 \end{aligned} \quad (5)$$

The coded terms equation (5) can be used to make predictions about the response for given levels of each factor. The coded equation (5) can determine the relative influence of factors by comparing factor coefficients.

The significance of the factors in relationship (5) is shown in Table 3.

Table 3. Factor semnification

Concentration, %			Temperature, ^oC		
Value	*A1*	*A2*	*Value*	*B1*	*B2*
0.02	1	0	20	1	0
0.04	0	1	24	0	1
0.06	-1	-1	28	-1	-1

The response surface obtained from the graphical representation of the experimental data is presented in figure 4.

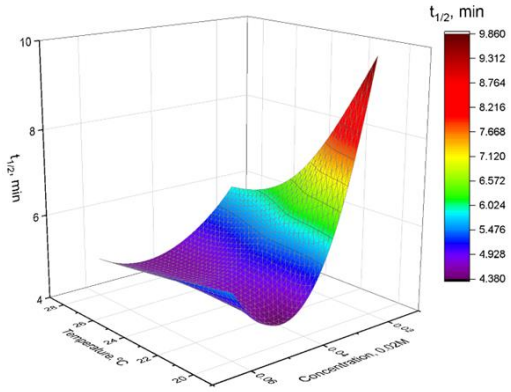

Figure 4. Response surface: half-life depending on concentration and temperature.

From figure 4 you can see the dependence of the half-life according to the process parameters. It is noted that the half-life decreases with increasing concentration and increasing working temperature.

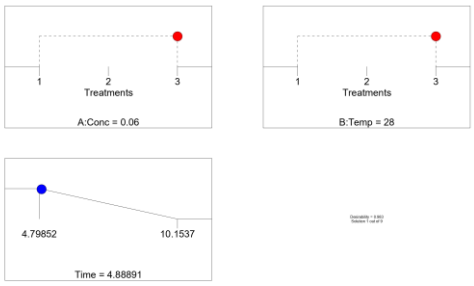

Figure 5. The optimal combination of process parameters that provides the lowest half-life.

Based on the regression model expressed by relationship (1), the optimal combination that provides the lowest half-life in the ranges of values established for concentration and temperature can be determined (figure 5).

Using the "Parallel plot" representation (figure 6) one can identify the optimal combination of parameters for which the minimum half-life is obtained. The highlighted curve represents the optimal combination of parameters which provides the lowest half-life.

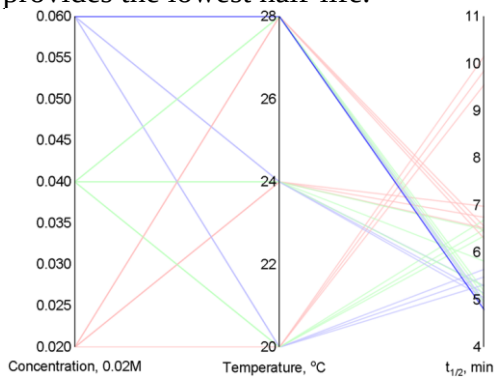

Figure 6. Parallel plot.

CONCLUSIONS

In the alkaline hydrolysis reaction, there is an exchange between ions of different mobilities, namely the more mobile hydroxyl ions are replaced by the less mobile acetate ions, changing the conductance of the reactant mixture.

Gathering the results of the half-lives determined graphically, it can be observed that the values decrease with the increase of the hydrolysis temperature for the reaction mixtures of the three different initial concentrations. This indicates an increase in the rate reaction in the same direction.

If the hydrolysis is maintained at a certain temperature, it was found

experimentally that the rate reaction increases by increasing the initial concentrations of reactants.

The paper presents an experimental method for determining the half-life of the alkaline hydrolysis reaction of ethyl acetate.

The use of factorial experiments presents several advantages such as:

- using the method of factorial experiments, there were possible simultaneous testing of the two factors and the interaction between them;

- the main effects and the interaction between the considered factors were identified and the regression model that mathematically describes the esterification process in the considered interval was determined;

- using the method of factorial experiments, the most favorable combination was identified in order to obtain a very low half-life.

REFERENCES

[1]. ANANTAKRISHNAN, S.V., ANANTARAMAN, A.V., Kinetic studies in ester hydrolysis. Proc. Indian Acad. Sci. 49, p. 174–183, 1959.

[2]. ANCHEYTA, J., Chemical Reaction Kinetics: concepts, methods and case study, John Wiley & Sons Ltd., USA, 2017.

[3]. DRAPPER, N.R., SMITH, H., Applied regression analysis. John Wiley & Sons, Inc., New York, 1981.

[4]. KIRBY, A. J., Hydrolysis and Formation of Esters of Organic Acids. In Comprehensive Chemical Kinetics; Bamford, C. H., Tipper, C. F. H., Eds.; Elsevier, Vol. 10, p. 57207, 1972.

[5]. MARCH, J., Advanced Organic Chemistry: Reactions, Mechanisms, and Structure, 2nd Edn., McGraw-Hill, p. 349-353, 1977.

[6]. PHILLIPS, G.A., HARRISON, D.P., Gross error detection and data reconciliation in experimental kinetics. Ind. Eng. Chem. Res. 32, p. 2530–2536, 1993.

[7]. SHIJA, R., BRUCE SUNDERLAND, V., MCDONALD, C., Alkaline Hydrolysis of Methyl, Ethyl and n-Propyl 4-Hydroxybenzoate Esters in the Liquid and Frozen States. Int. J. Pharm., 80 (1–3), p. 203–211, 1992.

[8]. TURANYI, T., TOMLI, A.S., Analysis of Kinetic Reactions Mechanisms, Springer Edition, 2014.

Trends and Research Directions in Hydrogen Generation

Florin Ciprian DAN[1], Cristina HORA[1] , Horea HORA[2], Petru CREȚ[3]
[1] Faculty of Energy Engineering and Industrial Management,
[2] Faculty of Managerial and Technological Engineering, University of Oradea,
[3]General Administrative Department, University of Oradea
[1]florin.dan@uoradea.ro, [1]chora@uoradea.ro, [2]horahorea@yahoo.com

Abstract: *Hydrogen (H_2), as the most abundant element in the universe, serves as a neutral energy carrier, with environmental implications intricately linked to the methods employed for its production. The viability of hydrogen production depends on the efficiency of its generation, particularly in the field of water electrolysis. As of now, the research field dedicated to H_2 generation has encountered challenges that overcome the efficiency barrier, requiring a critical reassessment of its financial sustainability. Given the complex nature of this technology and its overarching environmental impacts, this study undertakes an up-to-date overview of the trends, achievements, and research directions related to H2 generation by electrolysis of alkaline water.*
Keywords: hydrogen generation and production; hydrogen electrolysis; PEM; AEM; exchange membrane; alkaline water electrolysis.

INTRODUCTION

Considering the environmental ramifications of fossil fuel utilization, particularly in the context of climate change exacerbated by international events such as the 2022 Ukraine war and its repercussions on the energy market, a new of clean energy has emerged in the energy market — hydrogen (H2). Hydrogen production, deriving its primary energy from either fossil fuels or renewables, aligns with the global consensus on decarbonization, favoring the use of renewable energy sources. Although renewable sources present challenges in terms of stability and constancy, hydrogen generation could benefit from renewable overproduction or low-cost renewable outputs.

In contrast to electricity, hydrogen storage presents itself as a simpler, more cost-effective, and easily storable option, often in the form of tanks. As the most abundant element in the universe, boasting the highest energy per weight among common fuels (three times higher than gasoline), and producing only water as a conversion byproduct, hydrogen has become a focal point of energy policies, receiving funding and subsequent research attention.

The acknowledged efficiency of converting power to hydrogen and back, with a round-trip conversion efficiency of 46%, underscores the importance of closely monitoring research developments in this domain[1]. Building on previous reviews conducted in 2018 [2] and 2019[3], this paper presents the results spanning the period of 2020–2022.

Methods of hydrogen generation from fossil fuels include Hydrocarbon Pyrolysis and Hydrocarbon Reforming (Autothermal Reforming, Partial Oxidation, Steam Reforming) [3]. From renewable sources, methods involve Water Splitting and Biomass Processes utilizing Biological (Bio-photolysis, Dark Fermentation, Photo Fermentation) and Thermochemical (Gasification, Pyrolysis, Combustion, Liquefaction) approaches. Water splitting branches into Alkaline, Solid Oxide, and PEM methods, with Solid Oxide operating at higher temperatures (500–800 °C), offering up to 40% of energy supply through heat, thus achieving high electric efficiency. Alkaline (60–90 °C) and PEM (25–80°C) operate at temperatures below 100 °C[2], [3]. Our focus for this review centers on Alkaline and PEM electrolysis due to their greater compatibility with renewable sources and potential deployment at the residential level.

In the field of electrolysis, Alkaline electrolysis exhibits a higher degree of maturity, a slight increase in efficiency (70–80%), and operates at temperatures between 60 °C and 90 °C, using an electrolyte with a pH higher than 7[2]. Conversely, PEM electrolysis operates with an acidic

electrolyte, requiring high-cost Pt catalysts for reactions to occur at working temperatures between 25 °C and 80 °C, yielding efficiencies ranging from 65% to 80%.[4], [5]
Electrolysis is a process in which electrical energy is used to drive a non-spontaneous chemical reaction. In the context of water electrolysis, which is commonly used to produce hydrogen gas (H_2) and oxygen gas (O_2), the chemical reactions occurring at the electrodes, in an alkaline environment. are as follows:
Cathode Reaction:
At the cathode (negative electrode), reduction takes place. In the case of water electrolysis:
$2H_2O + 2e^- \rightarrow H_2 + 2HO^-$
This equation represents the reduction of water molecules (H_2O) and the gain of electrons ($2e^-$) to produce hydrogen gas (H_2) and hydroxyl ions (HO^-).
Anode Reaction:
At the anode (positive electrode), oxidation occurs. In the context of water electrolysis:
$4HO^- \rightarrow O_2 + 2H_2O + 4e^-$
This equation represents the oxidation of hydroxyl ions (HO^-) to produce oxygen gas (O_2), water (H_2O), and the release of electrons ($4e^-$)[5].
Overall Reaction:
The overall reaction for water electrolysis is the combination of the cathode and anode reactions:
$2H_2O \rightarrow 2H_2 + O_2$
This balanced equation represents the electrolysis of water to generate hydrogen gas and oxygen gas[5].

METHODS

Recognizing the complexity and interdisciplinary nature of the investigated field, it becomes imperative to conduct an annual, up-to-date review. Building upon the trajectory set by[2], which provided a more comprehensive overview, and [3], who delved specifically into Proton Exchange Membrane Water Electrolysis (PEMWE), and more recently,[6]—focusing on electrodeposited catalysts for PEMWE in 2020-2022—our objective is to delineate current trends in research and assess the present landscape of published studies.

The highlighted studies offer a spectrum of insights, including the specific area of research, publishing journal, obtained results, financial criteria, and the performance of deployed technologies. These findings serve as valuable guidelines and starting points for researchers, investors, manufacturers, and other stakeholders engaged in the field of hydrogen (H_2) generation.
To achieve a comprehensive understanding, the Systematic Literature Review (SLR) method, following the Preferred Reporting Items for Systematic Reviews and Meta-Analyses (PRISMA) guidelines[7], has been employed. Applying the PRISMA methodology to the referenced papers not only elucidates existing opportunities and niches but also enables researchers and peers to identify gaps, thus facilitating the formulation of a clear research agenda.
Aligned with the PRISMA checklist, the objectives of this review are twofold: to discern prevailing trends and to evaluate the performances highlighted in published research between 2020 and 2022. The focus is on H2 generation from water (H_2O) and alkaline water (H_2O) using both Proton Exchange Membrane (PEM) and Anion Exchange Membrane (AEM) technologies.
In the context of a literature review paper, the substantial disparity between the existing hydrogen (H_2) generation technologies in the market and the imperative to align with environmental commitments such as the Kyoto Protocol [8] and Paris Agreement [9] underscores a critical need for comprehensive understanding. Therefore, the primary objective of this review is to contribute significantly by elucidating the current state of research and providing a panoramic perspective on this domain.
To ensure a rigorous and transparent examination, bias mitigated, and enhance replicability, we adhere to the PRISMA guidelines[7]. This approach not only serves to minimize subjective interpretations in the field but also establishes a foundation for fellow researchers to replicate, build upon, and advance our work.
Our research process is methodically structured across three key stages, as delineated by[10]: (i) *Planning the review*, (ii) *Conducting the review*, and (iii) *Reporting and disseminating the results*.

(i) In the initial *planning stage*, we set the boundaries of our research. Given the status of hydrogen as a next-generation fuel due to

its easy generation and environmentally friendly (H_2O – production), our focus is on evaluating H_2 generation methods [2] that:

- Exhibit zero pollution output.
- Can be perfectly integrated with renewable energies.
- Have low capital expenditures.
- Feature low operational expenditures.
- Integrated technologies with extended lifetimes.
- Produces high purity H_2.
- Have not yet reached technological maturity.

These stringent criteria narrow our research focus to water electrolysis. In alignment with this research domain, we establish a protocol, serving as a comprehensive guide for all steps in this Systematic Literature Review (SLR). The initial step involves defining our input database, which, in this instance, is the EBSCO Discovery Service, chosen for its comprehensive collection of research papers and a commitment to a non-bias and quality policy[4].

(ii) *Formulating* an effective search strategy is pivotal, and we achieve optimal results using the following criteria[7]:

Keywords[4]:

- Hydrogen generation <AND>
- Hydrogen Electrolysis <AND>
- PEM <AND>
- Exchange Membrane

The use of <AND> as a cumulative keyword ensures specificity, while <OR> yielded an excessive number of unrelated results. The inclusion of more keywords to narrow the search resulted in fewer relevant results[4].

Disciplines[4]:

- Applied Sciences
- Chemistry
- Engineering
- Environmental Sciences
- Information Technology
- Life Sciences
- Physics
- Power & Energy
- Science
- Technology

Expanders:

- Also search within the full text of the articles

Search modes:

- Find all my search terms
- Apply related words
- Also search within the full text of the article
- Apply equivalent subjects

Results limits[4]:

- Full text
- Peer-reviewed
- Published date:
- January 2020–February 2022

Language:

- English
-

Following a thorough assessment of the titles in the database, we determine that the results received are pertinent under the specified search criteria[4].

(iii) Progressing to the third stage, *reporting and dissemination*, is included in the research results, where we strive to distill, both textually and graphically, the basic conclusions of our target research. Given the extensive number of research articles analyzed, we outlined a structured exclusion flow, illustrated in figure 1. This flowchart adheres to the PRISMA methodology for reporting systematic reviews [7].

The primary focus centers on electrode materials, with 115 articles distributed across various alloys and compounds such as Ni, Co, Ir, Ru, Cu, Mo, B, Fe, Au, and Pt, addressing anode and cathode material deposition. Secondarily, attention is directed towards electrolysis cells, comprising 46 articles predominantly exploring water electrolysis and alkaline water electrolysis. Additionally, 18 articles concentrate on exchange membranes (PEM and AEM), and eight articles explores electrolyte and electrode shape enhancement methodologies, involving substances like KOH, H2SO4, PO3, chemical deposition, and 3D printing. In figure 2 a pie chart shows the research area distribution.

To discern the Key Performance Indicators (KPIs) trend, we utilize a box and whiskers chart, alongside a separate temporal chart specifically focusing on the primary KPIs described earlier. Figure 3 exemplifies this approach, illustrating the evolution of electrolysis cell efficiency as documented in research papers spanning the 2020–2022 timeframe.

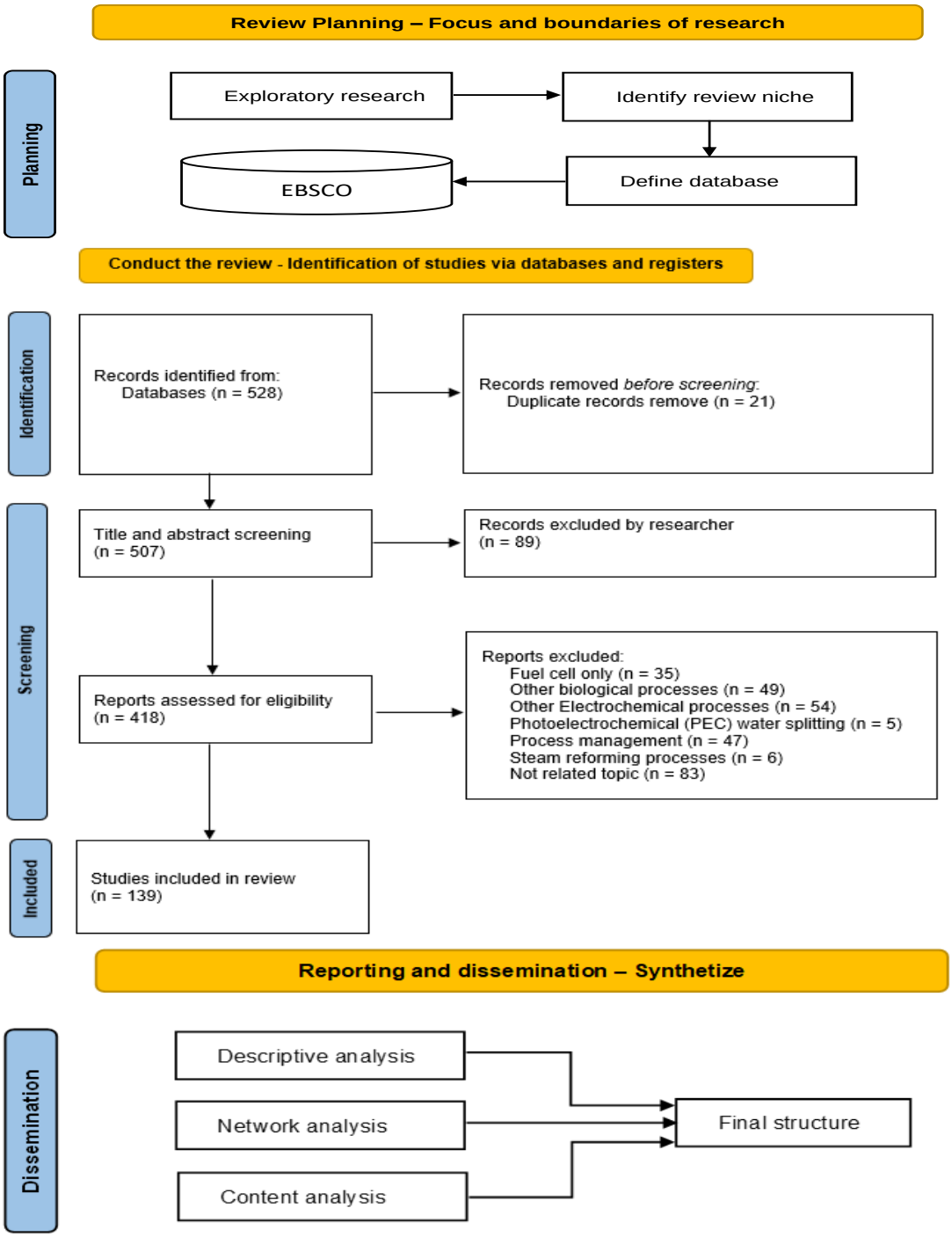

Figure 1. Flow chart of the systematic review procedure applied[7]

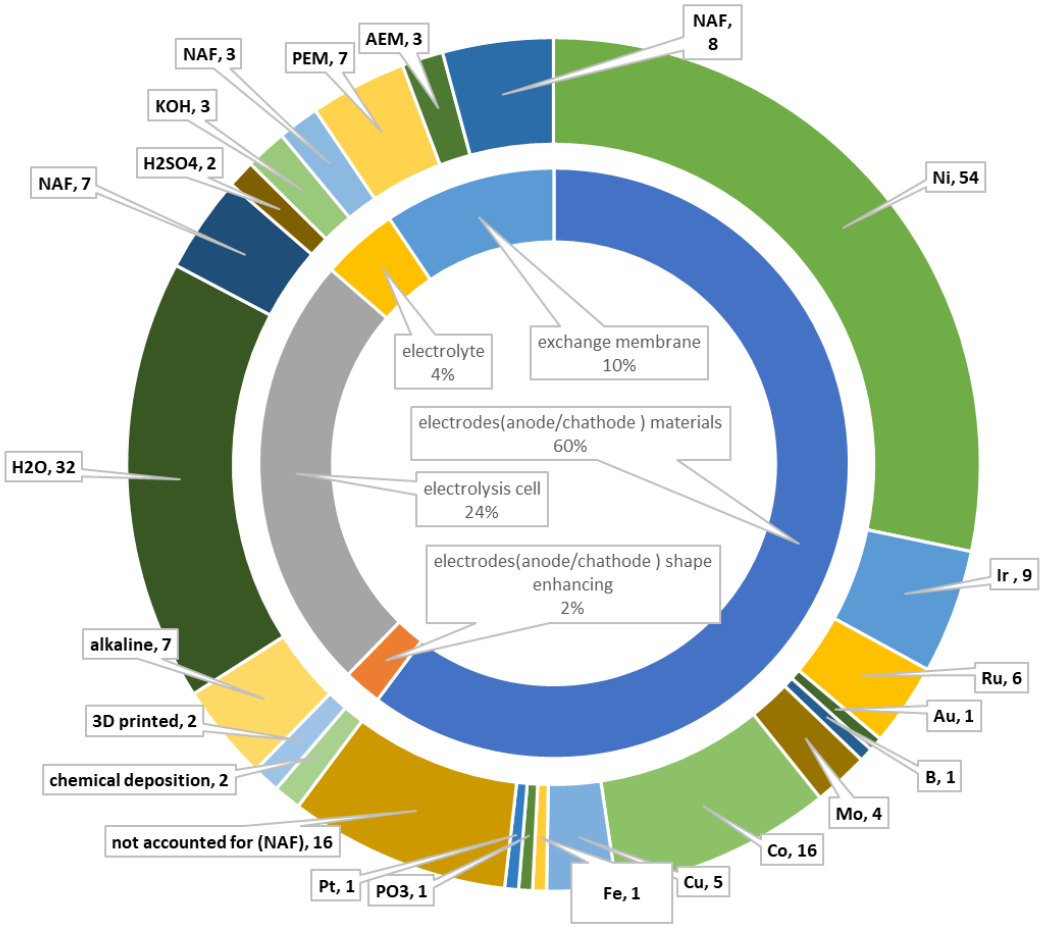

Figure 2. Pie chart showing the research area distribution [4]

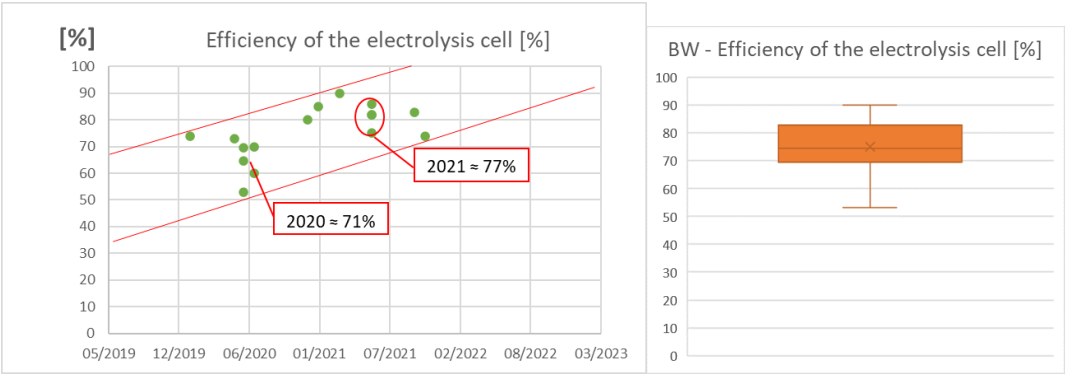

Figure 3. Representation of the electrolysis cell efficiency [11-120]

There is an upward trajectory observed in electrolyte temperature (figure 4) over the past two years, accompanied by a notable correlation between current density and electrolyte temperature. This rise in temperature is attributed to advancements in surface covering materials for electrodes, particularly in Proton Exchange Membrane (PEM) and Anion Exchange Membrane (AEM) technologies. The utilization of new materials for exchange membranes, such as sulfonated poly (phenylene sulfone) [90], is linked to elevated values of electrolyte temperature (median to third quartile).

The graphical representation in figure 5 included not only the Key Performance Indicators (KPIs) associated with hydrogen (H_2) production but also provides insights into the size of the electrolysis system. Specifically, the chart elucidates the correlation between these KPIs and the power consumption for H_2 production. By examining this comprehensive visualization, one can gain a nuanced understanding of how power consumption is intricately linked to both the efficiency of H_2 production and the scale of the electrolysis system. This graphical representation serves as a valuable tool for stakeholders and researchers seeking a holistic view of the interplay between H_2 production, KPIs and the corresponding energy demands within electrolysis systems.

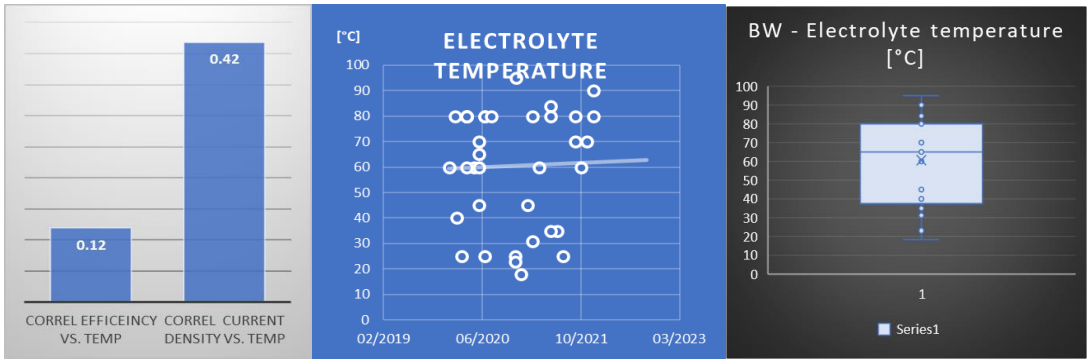

Figure 4. Representation of the electrolyte temperature [12,47,57,59, 62,83,85,89,90,93,98,101,103,105,108,113–115,117,120]

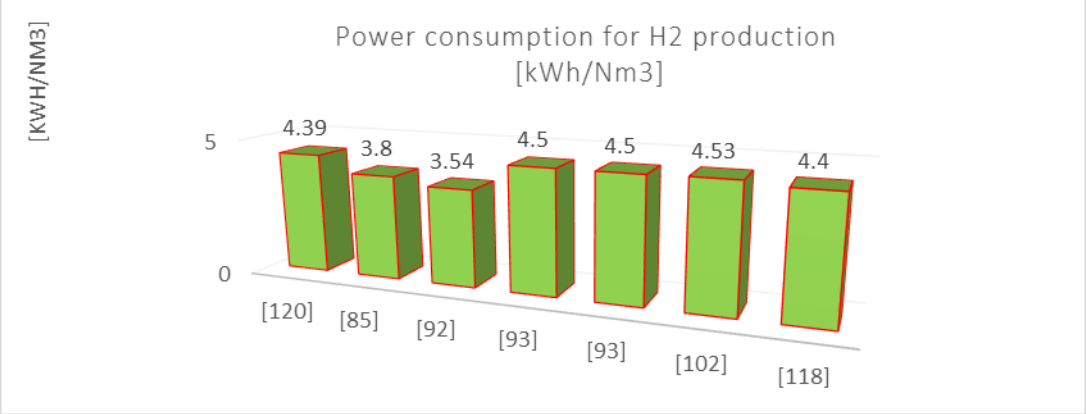

Figure 5. Power consumption for H_2 production [86], [92], [93], [102], 118], [120]

.

CONCLUSIONS

This study introduces a methodology for identifying research focus and trends in water electrolysis, specifically covering the years 2020–2022. A comprehensive review of Key Performance Indicators (KPIs) delineates the state of current research in hydrogen (H_2) generation through alkaline and water electrolysis. Despite notable progress, challenges remain, including low round-trip efficiency, material sustainability in cells, and the impact of electrolyte temperature on cell efficiency. Further research is needed to propel the transition to green hydrogen, recognized globally as an environmentally sound alternative to traditional fossil fuels.

Green Hydrogen, with its high energy density and carbon-free conversion, is gaining global importance. While Alkaline Water Electrolysis (AWE) is favored for large photovoltaic-powered electrolysis projects, Proton Exchange Membrane (PEM) technology is sought after for high-purity H_2 and compatibility with renewable power generation. The declining presence of expensive catalysts for Hydrogen Evolution Reaction (HER) in the research trend signals progress in stability and activity using sustainable materials. However, bridging the market readiness gap remains a challenge.

Observations in OER (Oxygen Evolution Reaction) catalytic processes in PEM highlight the trade-off between stability and production cost. Nickel-based catalysts emerge prominently in the review, addressing vulnerabilities of water-splitting processes through various alloying methods. Copper-based catalysts for OER in AWE show advantages in low toxicity, cost-effectiveness, and excellent electrical conductivity. Cobalt-based catalysts, particularly phosphide-coupled Co, exhibit exceptional HER activity in AWE.

The challenges ahead involve enhancing overall efficiency, particularly in AWE, reducing Capital Expenditure and Operational Expenditure, and extending equipment lifespan. Addressing these challenges is crucial for advancing water electrolysis technologies and optimizing H_2 generation efficiency.

REFERENCES

[1] DiChristopher, “Hydrogen technology faces efficiency disadvantage in power storage race,” S&P Global: New York, NY, USA, NY, 2021. [Online]. Available: www.spglobal.com

[2] J. D. Fonseca, M. Camargo, J.-M. Commenge, L. Falk, and I. D. Gil, “Trends in design of distributed energy systems using hydrogen as energy vector: A systematic literature review,” International Journal of Hydrogen Energy, vol. 44, no. 19, pp. 9486–9504, Apr. 2019, doi: 10.1016/j.ijhydene.2018.09.177.

[3] ShivaKumar, S.; Himabindu, V, “Hydrogen production by PEM water electrolysis—A review,” Sci. Energy Technol, 2019.

[4] C. Hora, F. C. Dan, N. Rancov, G. E. Badea, and C. Secui, “Main Trends and Research Directions in Hydrogen Generation Using Low Temperature Electrolysis: A Systematic Literature Review,” Energies, vol. 15, no. 16, p. 6076, Aug. 2022, doi: 10.3390/en15166076.

[5] G. E. Badea et al., “Sustainable Hydrogen Production from Seawater Electrolysis: Through Fundamental Electrochemical Principles to the Most Recent Development,” Energies, vol. 15, no. 22, p. 8560, Nov. 2022, doi: 10.3390/en15228560.

[6] H. Kim, H. Park, H. Bang, and S.-K. Kim, “Electrodeposition-fabricated catalysts for polymer electrolyte water electrolysis,” Korean J. Chem. Eng., vol. 37, no. 8, pp. 1275–1294, Aug. 2020, doi: 10.1007/s11814-020-0626-y.

[7] M. J. Page et al., “PRISMA 2020 explanation and elaboration: updated guidance and exemplars for reporting systematic reviews,” BMJ, p. n160, Mar. 2021, doi: 10.1136/bmj.n160.

[8] Corporate Author, “Kyoto Protocol.” 2017. [Online]. Available: http://unfccc.int/kyoto_protocol/items/2830.php

[9] “Paris Agreement to the United Nations Framework Convention on Climate Change.” 2015. [Online]. Available: https://unfccc.int/sites/default/files/english_paris_agreement.pdf

[10] A. L. G. Pires, P. Rotella Junior, S. N. Morioka, L. C. S. Rocha, and I. Bolis, "Main Trends and Criteria Adopted in Economic Feasibility Studies of Offshore Wind Energy: A Systematic Literature Review," Energies, vol. 15, no. 1, p. 12, Dec. 2021, doi: 10.3390/en15010012.
[11] Pires, A.L.G.; Rotella Junior, P.; Morioka, S.N.; Rocha, L.C.S.; Bolis, I. Main Trends and Criteria Adopted in Economic Feasi-bility Studies of Offshore Wind Energy: A Systematic Literature Review. Energies 2022, 15, 12. https://doi.org/10.3390/en15010012.
[12] Kovács, K.E.; Dan, B.; Hrabéczy, A.; Bacskai, K.; Pusztai, G. Is Resilience a Trait or a Result of Parental Involvement? The Results of a Systematic Literature Review. Educ. Sci. 2022, 12, 372. https://doi.org/10.3390/educsci12060372.
13. Feng, C.; Wang, F.; Liu, Z.; Nakabayashi, M.; Xiao, Y.; Zeng, Q.; Fu, J.; Wu, Q.; Cui, C.; Han, Y.; et al. A self-healing catalyst for electrocatalytic and photoelectrochemical oxygen evolution in highly alkaline conditions. Nat. Commun. 2021, 12, 5980. https://doi.org/10.1038/s41467-021-26281-0.
14. Kou, T.; Wang, S.; Shi, R.; Zhang, T.; Chiovoloni, S.; Lu, J.Q.; Chen, W.; Worsley, M.A.; Wood, B.C.; Baker, S.E.; et al. Periodic Porous 3D Electrodes Mitigate Gas Bubble Traffic during Alkaline Water Electrolysis at High Current Densities. Adv. Energy Mater. 2020, 10, 2002955. https://doi.org/10.1002/aenm.202002955.
15. Vincent, I.; Lee, E.C.; Kim, H.M. Highly cost-effective platinum-free anion exchange membrane electrolysis for large scale energy storage and hydrogen production. RSC Adv. 2020, 10, 37429–37438. https://doi.org/10.1039/d0ra07190k.
16. Srinivasa, N.; Hughes, J.P.; Adarakatti, P.S.; Manjunatha, C.; Rowley-Neale, S.J.; Ashoka, S.; Banks, C.E. Facile synthesis of Ni/NiO nanocomposites: the effect of Ni content in NiO upon the oxygen evolution reaction within alkaline media. RSC Adv. 2021, 11, 14654–14664. https://doi.org/10.1039/d0ra10597j.
17. Hu, K.; Ohto, T.; Nagata, Y.; Wakisaka, M.; Aoki, Y.; Fujita, J.-I.; Ito, Y. Catalytic activity of graphene-covered non-noble metals governed by proton penetration in electrochemical hydrogen evolution reaction. Nat. Commun. 2021, 12, 203. https://doi.org/10.1038/s41467-020-20503-7.
15. Li, Y.K.; Zhang, G.; Huang, H.; Lu, W.T.; Cao, F.F.; Shao, Z.G. Ni17W3–W Interconnected Hybrid Prepared by Atmosphere- and Thermal-Induced Phase Separation for Efficient Electrocatalysis of Alkaline Hydrogen Evolution. Small 2020, 16, 2005184. https://doi.org/10.1002/smll.202005184.
16. Danilovic, N.; Subbaraman, R.; Chang, K.-C.; Chang, S.H.; Kang, Y.J.; Snyder, J.; Paulikas, A.P.; Strmcnik, D.; Kim, Y.-T.; Myers, D.; et al. Activity-stability trends for the oxygen evolution reaction on monometallic oxides in acidic environments. J. Phys. Chem. Lett. 2014, 5, 2474–2478. https://doi.org/10.1021/jz501061n.
17. Luo, Q.; Peng, M.; Sun, X.; Luo, Y.; Asiri, A.M. Efficient electrochemical water splitting catalyzed by electrodeposited NiFe nanosheets film, Int. J. Hydrogen Energy 2016, 41, 8785–8792. https://doi.org/10.1016/j.ijhydene.2016.04.007.
18. Pu, Z.; Luo, Y.; Asiri, A.B.; Sun, X. Efficient Electrochemical Water Splitting Catalyzed by Electrodeposited Nickel Diselenide Nanoparticles Based Film. ACS Appl. Mater. Interfaces 2016, 8, 4718–4723. https://doi.org/10.1021/acsami.5b12143.
19. Swesi, A.T.; Masud, J.; Nath, M. Nickel selenide as a high-efficiency catalyst for oxygen evolution reaction. Energy Environ. Sci. 2016, 9, 1771–1782. https://doi.org/10.1039/C5EE02463C.
20. Jiang, N.; You, B.; Sheng, M.; Sun, Y. Bifunctionality and Mechanism of Electrodeposited Nickel-Phosphorous Films for Effi-cient Overall Water Splitting. ChemCatChem 2016, 8, 106–112. https://doi.org/10.1002/cctc.201501150.
21. Liu, Q.; Gu, S.; Li, C.M. Electrodeposition of nickel-phosphorus nanoparticles film as a Janus electrocatalyst for electro-splitting of water. Power Sources 2015, 299, 342–346. https://doi.org/10.1016/j.jpowsour.2015.09.027.
22. Kim, B.K.; Kim, S.-K.; Cho, S.K.; Kim, J.J. Enhanced catalytic activity of electrodeposited Ni-Cu-P toward oxygen evolution reaction. Appl. Catal. B-Environ. 2018, 237, 409–415. https://doi.org/10.1016/j.apcatb.2018.05.082.
23. Zang, Z.; Liu, S.; Xiao, J.; Wang, S. Fiber-based multifunctional nickel phosphide electrodes for flexible energy conversion and storage. J. Mater. Chem. A 2016, 4, 9691–9699. https://doi.org/10.1039/C6RA20737E.

24. Yuan, B.; Sun, F.; Li, C.; Huang, W.; Lin, Y. Formation of Prussian blue analog on Ni foam via in-situ electrodeposition method and conversion into Ni-Fe-mixed phosphates as efficient oxygen evolution electrode. Electrochim. Acta 2019, 313, 91. https://doi.org/10.1016/j.electacta.2019.03.089.
25. Chodankar, N.R.; Bagal, I.V.; Ryu, S.-W.; Han, Y.-K.; Kim, D.-H. Nano-Micro-Structured Nickel-Cobalt Hydroxide/Ni2P2O7 Assembly on Nickel Foam: An Outstanding Electrocatalyst for Alkaline Oxygen Evolution Reaction. ChemCatChem 2019, 11 4256–4261. https://doi.org/10.1002/cctc.201900865.
26. Gao, M.Y.; Yang, C.; Zhang, Q.B.; Yu, Y.W.; Hua, Y.X.; Li, Y.; Dong, P. Electrochemical fabrication of porous Ni-Cu alloy nanosheets with high catalytic activity for hydrogen evolution. Dong Electrochim. Acta 2016, 215, 609–616. https://doi.org/10.1016/j.electacta.2016.08.145.
27. Rad, P.J.; Aliofkhazraei, M.; Darband, G.B. Ni-W nanostructure well-marked by Ni selective etching for enhanced hydrogen evolution reaction. Int. J. Hydrogen Energy 2019, 44, 880–894.
28. Sun, T.; Cao, J.; Dong, J.; Du, H.; Zhang, H.; Chen, J.; Xu, L. Ordered mesoporous Ni Co alloys for highly efficient electrocatalytic hydrogen evolution reaction. Int. J. Hydrogen Energy 2017, 42, 6637–6645. https://doi.org/10.1016/j.ijhydene.2017.01.071.
29. Sun, C.; Zeng, J.; Lei, H.; Yang, W.; Zhang, Q. Direct Electrodeposition of Phosphorus-Doped Nickel Superstructures from Choline Chloride–Ethylene Glycol Deep Eutectic Solvent for Enhanced Hydrogen Evolution Catalysis. ACS Sustain. Chem. Eng. 2018, 7, 1529–1537. https://doi.org/10.1021/acssuschemeng.8b05302.
30. Navarro-Flores, E.; Chong, Z.; Omanovic, S. Characterization of Ni, NiMo, NiW and NiFe electroactive coatings as electro-catalysts for hydrogen evolution in an acidic medium. J. Mol. Catal. A Chem. 2005, 226, 179–197. https://doi.org/10.1016/j.molcata.2004.10.029.
31. Damian, A.; Omanovic, S. Ni and NiMo hydrogen evolution electrocatalysts electrodeposited in a polyaniline matrix. J. Power Sources 2006, 158, 464–476. https://doi.org/10.1016/j.jpowsour.2005.09.007.
32. Martinez, S.; Metikoš-Huković, M.; Valek, L. Electrocatalytic properties of electrodeposited Ni–15Mo cathodes for the HER in acid solutions: Synergistic electronic effect. J. Mol. Catal. A Chem. 2006, 245, 114–121. https://doi.org/10.1016/j.molcata.2005.09.040.
33. Kim, J.H.; Kim, J.; Kim, H.; Kim, J.; Ahn, S.H. Facile fabrication of nanostructured NiMo cathode for high-performance proton exchange membrane water electrolyzer. J. Ind. Eng. Chem. 2019, 79, 255–260. https://doi.org/10.1016/j.jiec.2019.06.049.
34. Badawy, W.; Nady, H.; Negem, M. Cathodic hydrogen evolution in acidic solutions using electrodeposited nano-crystalline Ni–Co cathodes. Int. J. Hydrogen Energy 2014, 39, 10824–10832. https://doi.org/10.1016/j.ijhydene.2014.05.049.
35. Nady, H.; Negem, M. Ni–Cu nano-crystalline alloys for efficient electrochemical hydrogen production in acid water. RSC Adv. 2016, 6, 51111–51119. https://doi.org/10.1039/C6RA08348J.
36. Nady, H.; Negem, M. Electroplated Zn–Ni nanocrystalline alloys as an efficient electrocatalyst cathode for the generation of hydrogen fuel in acid medium. Int. J. Hydrogen Energy 2018, 43, 4942–4950. https://doi.org/10.1016/j.ijhydene.2018.01.119.
37. Mollamahale, Y.B.; Jafari, N.; Hosseini, D. Electrodeposited Ni-W nanoparticles: Enhanced catalytic activity toward hydrogen evolution reaction in acidic media. Mater. Lett. 2018, 213, 15–18. https://doi.org/10.1016/j.matlet.2017.11.003.
38. Kim, H.; Park, H.; Kim, D.-K.; Oh, S.; Choi, I.; Kim, S.-K. Electrochemically Fabricated NiW on a Cu Nanowire as a Highly Porous Non-Precious-Metal Cathode Catalyst for a Proton Exchange Membrane Water Electrolyzer. ACS Sustain. Chem. Eng. 2019, 7, 8265–8273. https://doi.org/10.1021/acssuschemeng.8b06643.
39. Wang, X.; Su, R.; Aslan, H.; Kibsgaard, J.; Wendt, S.; Meng, L.; Dong, M.; Huang, Y.; Besenbacher, F. Tweaking the composition of NiMoZn alloy electrocatalyst for enhanced hydrogen evolution reaction performance. Nano Energy 2015, 12, 9–18. https://doi.org/10.1016/j.nanoen.2014.12.007.
40. Kim, H.; Park, H.; Kim, D.-K.; Choi, I.; Kim, S.-K. Pulse-electrodeposited nickel phosphide for high-performance proton exchange membrane water electrolysis. J. Alloy. Compd. 2019, 785, 296–304. https://doi.org/10.1016/j.jallcom.2019.01.192.
41. Walter, C.; Menezes, P.W.; Driess, M. Perspective on intermetallics towards efficient electrocatalytic water-splitting. Chem. Sci. 2021, 12, 8603–8631. https://doi.org/10.1039/d1sc01901e.

42. Yu, C.; Lu, J.; Luo, L.; Xu, F.; Shen, P.K.; Tsiakaras, P.; Yin, S. Bifunctional catalysts for overall water splitting: CoNi oxyhy-droxide nanosheets electrodeposited on titanium sheets. Electrochimica Acta 2019, 301, 449–457. https://doi.org/10.1016/j.electacta.2019.01.149.
43. Nan, K.; Du, H.; Su, L.; Li, C.M. Directly Electrodeposited Cobalt Sulfide Nanosheets as Advanced Catalyst for Oxygen Evo-lution Reaction. ChemistrySelect 2018, 3, 7081–7088. https://doi.org/10.1002/slct.201801482.
44. Liu, T.; Liang, Y.; Liu, Q.; Sun, X.; He, Y.; Asiri, A.M. Electrodeposition of cobalt-sulfide nanosheets film as an efficient elec-trocatalyst for oxygen evolution reaction. Electrochem. Commun. 2015, 60, 92–96. https://doi.org/10.1016/j.elecom.2015.08.011.
45. Jiang, N.; You, B.; Sheng, M.; Sun, Y. Electrodeposited Cobalt-Phosphorous-Derived Films as Competent Bifunctional Catalysts for Overall Water Splitting. Angew. Chem. Int. Ed. 2015, 54, 6251–6254. https://doi.org/10.1002/anie.201501616.
46. Zhu, Y.-P.; Liu, Y.-P.; Ren, T.-Z.; Yuan, Z.-Y. Self-Supported Cobalt Phosphide Mesoporous Nanorod Arrays: A Flexible and Bifunctional Electrode for Highly Active Electrocatalytic Water Reduction and Oxidation. Adv. Funct. Mater. 2015, 25, 7337–7347. https://doi.org/10.1002/adfm.201503666.
47. Rapson, T.D.; Ju, H.; Marshall, P.; Devilla, R.; Jackson, C.J.; Giddey, S.; Sutherland, T.D. Engineering a solid-state metalloprotein hydrogen evolution catalyst. Sci. Rep. 2020, 10, 3774. https://doi.org/10.1038/s41598-020-60730-y.
48. Kumar, B.; Rao, G.K.; Saha, S.; Ganguli, A.K. Cu-Based Nanocomposites as Multifunctional Catalysts. ChemPhysChem 2015, 17, 155–161. https://doi.org/10.1002/cphc.201500944.
49. You, B.; Jiang, N.; Liu, X.; Sun, Y. Simultaneous H2 Generation and Biomass Upgrading in Water by an Efficient No-ble-Metal-Free Bifunctional Electrocatalyst. Angew. Chem. Int. Ed. 2016, 55, 9913–9917. https://doi.org/10.1002/ange.201603798.
50. Zhu, Y.P.; Yin, J.; Abou-Hamad, E.; Liu, X.; Chen, W.; Yao, T.; Mohammed, O.F.; Alshareef, H.N. Highly Stable Phospho-nate-Based MOFs with Engineered Bandgaps for Efficient Photocatalytic Hydrogen Production. Adv. Mater. 2020, 32, 1906368. https://doi.org/10.1002/adma.201906368.
51. Themuwara, A.C.; Dheer, L.; Attanayake, N.H.; Yan, Q.; Waghmare, U.V.; Strongin, D.R. Co-Mo-P Based Electrocatalyst for Superior Reactivity in the Alkaline Hydrogen Evolution Reaction. ChemCatChem 2018, 10, 4832. https://doi.org/10.1002/cctc.201801389.
52. Bai, N.; Li, Q.; Mao, D.; Li, D.; Dong, H. One-Step Electrodeposition of Co/CoP Film on Ni Foam for Efficient Hydrogen Evolution in Alkaline Solution. ACS Appl. Mater. Interfaces 2016, 8, 29400–29407. https://doi.org/10.1021/acsami.6b07785.
53. Chen, X.; Li, Q.; Che, Q.; Chen, Y.; Xu, X. Interface Engineering of Crystalline/Amorphous Co2P/CoMoPx Nanostructure as Efficient Electrocatalysts for Hydrogen Evolution Reaction. ACS Sustain. Chem. Eng. 2018, 7, 2437–2445. https://doi.org/10.1021/acssuschemeng.8b05315.
54. Wu, H.; Zuo, X.; Wang, S.-P.; Yin, J.-W.; Zhang, Y.-N.; Chen, J. Theoretical and experimental design of Pt-Co(OH)2 electro-catalyst for efficient HER performance in alkaline solution. Prog. Nat. Sci. Mater. Int. 2019, 29, 356–361. https://doi.org/10.1016/j.pnsc.2019.05.009.
55. Zhang, N.; Ma, W.; Jia, F.; Wu, T.; Han, D.; Niu, L. Controlled electrodeposition of CoMoSx on carbon cloth: A 3D cathode for highly-efficient electrocatalytic hydrogen evolution. Int. J. Hydrogen Energy 2016, 41, 3811–3819. https://doi.org/10.1016/j.ijhydene.2015.12.173.
56. Saadi, F.H.; Carim, A.I.; Verlage, E.; Hemminger, J.C.; Lewis, N.S.; Soriaga, M.P. CoP as an Acid-Stable Active Electrocatalyst for the Hydrogen-Evolution Reaction: Electrochemical Synthesis, Interfacial Characterization and Performance Evaluation. J. Phys. Chem. C 2014, 118, 29294–29300. https://doi.org/10.1021/jp5054452.
57. Djara, R.; Lacour, M.-A.; Merzouki, A.; Cambedouzou, J.; Cornu, D.; Tingry, S.; Holade, Y. Iridium and Ruthenium Modified Polyaniline Polymer Leads to Nanostructured Electrocatalysts with High Performance Regarding Water Splitting. Polymers 2021, 13, 190. https://doi.org/10.3390/polym13020190.
58. Dang, Q.; Lin, H.; Fan, Z.; Ma, L.; Shao, Q.; Ji, Y.; Zheng, F.; Geng, S.; Yang, S.-Z.; Kong, N.; et al. Iridium metallene oxide for acidic oxygen evolution catalysis. Nat. Commun. 2021, 12, 6007. https://doi.org/10.1038/s41467-021-26336-2.
59. Su, H.; Zhou, W.; Zhou, W.; Li, Y.; Zheng, L.; Zhang, H.; Liu, M.; Zhang, X.; Sun, X.; Xu, Y.; et al. In-situ spectroscopic observation of dynamic-coupling oxygen on atomically dispersed iridium

electrocatalyst for acidic water oxidation. Nat. Commun. 2021, 12, 6118. https://doi.org/10.1038/s41467-021-26416-3.
60. Kim, Y.J.; Lim, A.; Kim, J.M.; Lim, D.; Chae, K.H.; Cho, E.N.; Han, H.J.; Jeon, K.U.; Kim, M.; Lee, G.H.; et al. Highly efficient oxygen evolution reaction via facile bubble transport realized by three-dimensionally stack-printed catalysts. Nat. Commun. 2020, 11, 4921. https://doi.org/10.1038/s41467-020-18686-0.
61. Elezović, N.R.; Zabinski, P.; Lačnjevac, U..; Pajić, M.N.K.; Jović, V.D. Electrochemical deposition and characterization of iridium oxide films on Ti2AlC support for oxygen evolution reaction. J. Solid State Electrochem. 2020, 25, 351–363. https://doi.org/10.1007/s10008-020-04816-7.
62. Knöppel, J.; Möckl, M.; Escalera-López, D.; Stojanovski, K.; Bierling, M.; Böhm, T.; Thiele, S.; Rzepka, M.; Cherevko, S. On the limitations in assessing stability of oxygen evolution catalysts using aqueous model electrochemical cells. Nat. Commun. 2021, 12, 2231. https://doi.org/10.1038/s41467-021-22296-9.
63. Li, R.; Wang, H.; Hu, F.; Chan, K.C.; Liu, X.; Lu, Z.; Wang, J.; Li, Z.; Zeng, L.; Li, Y.; et al. IrW nanochannel support enabling ultrastable electrocatalytic oxygen evolution at 2 A cm−2 in acidic media. Nat. Commun. 2021, 12, 3540. https://doi.org/10.1038/s41467-021-23907-1.
64. Lee, B.-S.; Ahn, S.H.; Park, H.-Y.; Choi, I.; Yoo, S.J.; Kim, H.-J.; Henkensmeier, D.; Kim, J.Y.; Park, S.; Nam, S.W.; et al. De-velopment of electrodeposited IrO2 electrodes as anodes in polymer electrolyte membrane water electrolysis. Appl. Catal. B: Environ. 2015, 179, 285–291. https://doi.org/10.1016/j.apcatb.2015.05.027.
65. Din, M.A.U.; Irfan, S.; Dar, S.U.; Rizwan, S. Synthesis of 3D IrRuMn Sphere as a Superior Oxygen Evolution Electrocatalyst in Acidic Environment. Chem.–A Eur. J. 2020, 26, 5662–5666. https://doi.org/10.1002/chem.201905063.
66. Kim, J.Y.; Choi, J.; Kim, H.Y.; Hwang, E.; Ahn, S.H.; Kim, S.-K. Activity and stability of the oxygen evolution reaction on electrodeposited Ru and its thermal oxides. Appl. Surf. Sci. 2015, 359, 227–235. https://doi.org/10.1016/j.apsusc.2015.10.082.
67. Kim, J.Y.; Park, H.; Kim, H.; Hwang, E.; Ahn, S.H.; Kim, S.-K. Electrochemical Preparation of Ru/Co Bi-layered Catalysts on Ti Substrates for the Oxygen Evolution Reaction. Bull. Korean Chem. Soc. 2016, 37, 1270–1277. https://doi.org/10.1002/bkcs.10853.
68. Cross, M.W.; Smith, R.P.; Varhue, W.J. RuO2 Nanorods as an Electrocatalyst for Proton Exchange Membrane Water Electrolysis. Micromachines 2021, 12, 1412. https://doi.org/10.3390/mi12111412.
69. Zhang, Z.; Jiang, C.; Li, P.; Yao, K.; Zhao, Z.; Fan, J.; Li, H.; Wang, H. Benchmarking Phases of Ruthenium Dichalcogenides for Electrocatalysis of Hydrogen Evolution: Theoretical and Experimental Insights. Small 2021, 17, 2007333. https://doi.org/10.1002/smll.202007333.
70. Ehsan, M.A.; Suliman, M.H.; Rehman, A.; Hakeem, A.S.; Al Ghanim, A.; Qamar, M. Fabrication of platinum thin films for ultra-high electrocatalytic hydrogen evolution reaction. Int. J. Hydrogen Energy 2020, 45, 15076–15085. https://doi.org/10.1016/j.ijhydene.2020.03.218.
71. Huan, T.N.; Rousse, G.; Zanna, S.; Lucas, I.T.; Xu, X.; Menguy, N.; Mougel, V.; Fontecave, M. A Dendritic Nanostructured Copper Oxide Electrocatalyst for the Oxygen Evolution Reaction. Angew. Chem. Int. Ed. 2017, 56, 4792–4796. https://doi.org/10.1002/anie.201700388.
72. Xu, H.; Feng, J.-X.; Tong, Y.-X.; Li, G.-R. Cu2O–Cu Hybrid Foams as High-Performance Electrocatalysts for Oxygen Evolution Reaction in Alkaline Media. ACS Catal. 2016, 7, 986–991. https://doi.org/10.1021/acscatal.6b02911.
73. Deng, S.; Shen, Y.; Xie, D.; Lu, Y.; Yu, X.; Yang, L.; Wang, X.; Xia, X.; Tu, J. Directional construction of Cu2S branch arrays for advanced oxygen evolution reaction. J. Energy Chem. 2019, 39, 61–67.
74. Merki, D.; Fierro, S.; Vrubel, H.; Hu, X. Amorphous molybdenum sulfide films as catalysts for electrochemical hydrogen production in water. Chem. Sci. 2011, 2, 1262–1267. https://doi.org/10.1039/C1SC00117E.
75. Li, C.; Bo, X.; Li, M.; Guo, L. Facile electrodeposition fabrication of molybdenum-tungsten sulfide on carbon cloth for elec-trocatalytic hydrogen evolution. Int. J. Hydrogen Energy 2017, 42, 15479–15488. https://doi.org/10.1016/j.ijhydene.2017.05.046.

76. Sun, J.; Zhang, X.; Jin, M.; Xiong, Q.; Wang, G.; Zhang, H.; Zhao, H. Robust enhanced hydrogen production at acidic conditions over molybdenum oxides-stabilized ultrafine palladium electrocatalysts. Nano Res. 2020, 14, 268–274. https://doi.org/10.1007/s12274-020-3083-3.
77. Blackstone, C.; Ignaszak, A. Van der Waals Heterostructures—Recent Progress in Electrode Materials for Clean Energy Ap-plications. Materials 2021, 14, 3754. https://doi.org/10.3390/ma14133754.
78. Gupta, S.; Patel, M.K.; Miotello, A.; Patel, N. Metal Boride-Based Catalysts for Electrochemical Water-Splitting: A Review. Adv. Funct. Mater. 2019, 30, 1906481. https://doi.org/10.1002/adfm.201906481.
79. Hughes, J.P.; Rowley-Neale, S.; Banks, C. Enhancing the efficiency of the hydrogen evolution reaction utilising Fe3P bulk modified screen-printed electrodes via the application of a magnetic field. RSC Adv. 2021, 11, 8073–8079. https://doi.org/10.1039/d0ra10150h.
80. Yu, J.; Le, T.A.; Tran, N.Q.; Lee, H. Earth-Abundant Transition-Metal-Based Bifunctional Electrocatalysts for Overall Water Splitting in Alkaline Media. Chem.–A Eur. J. 2020, 26, 6423–6436. https://doi.org/10.1002/chem.202000209.
81. Antonyshyn, I.; Jimenez, A.M.B.; Sichevych, O.; Burkhardt, U.; Veremchuk, I.; Schmidt, M.; Ormeci, A.; Spanos, I.; Tarasov, A.; Teschner, D.; et al. Al 2 Pt for Oxygen Evolution in Water Splitting: A Strategy for Creating Multifunctionality in Electroca-talysis. Angew. Chem. Int. Ed. 2020, 59, 16770–16776. https://doi.org/10.1002/anie.202005445.
82. Le Bideau, D.; Chocron, O.; Mandin, P.; Kiener, P.; Benbouzid, M.; Sellier, M.; Kim, M.; Ganci, F.; Inguanta, R. Evolutionary Design Optimization of an Alkaline Water Electrolysis Cell for Hydrogen Production. Appl. Sci. 2020, 10, 8425. https://doi.org/10.3390/app10238425.
83. Hu, Q.; Lin, J.; Zeng, Q.; Fu, C.; Li, J. Optimal control of a hydrogen microgrid based on an experiment validated P2HH model. IET Renew. Power Gener. 2019, 14, 364–371. https://doi.org/10.1049/iet-rpg.2019.0544.
84. Xue, F.; Su, J.; Li, P.; Zhang, Y. Application of Proton Exchange Membrane Electrolysis of Water Hydrogen Production Technology in Power Plant. IOP Conf. Ser. Earth Environ. Sci. 2021, 631, 012079. https://doi.org/10.1088/1755-1315/631/1/012079.
85. Jianghao, N. Research on the Hydrogen Production Technology. IOP Conf. Series Earth Environ. Sci. 2021, 813, 012004. https://doi.org/10.1088/1755-1315/813/1/012004.
86. An, L.; Wei, C.; Lu, M.; Liu, H.; Chen, Y.; Scherer, G.G.; Fisher, A.C.; Xi, P.; Xu, Z.J.; Yan, C.H. Recent Development of Oxygen Evolution Electrocatalysts in Acidic Environment. Adv. Mater. 2021, 33, 2006328. https://doi.org/10.1002/adma.202006328.
87. Trinh, N.V.; Nguyen, X.L.; Kim, Y.; Yu, S. Characteristics of Water Transport of Membrane Electrolyte over Selected Tem-perature for Proton Exchange Membrane Fuel Cell. Polymers 2022, 14, 2972. https://doi.org/10.3390/polym14152972.
88. Arminio-Ravelo, J.A.; Quinson, J.; Pedersen, M.A.; Kirkensgaard, J.J.K.; Arenz, M.; Escudero-Escribano, M. Synthesis of Iridium Nanocatalysts for Water Oxidation in Acid: Effect of the Surfactant. ChemCatChem 2019, 12, 1282–1287. https://doi.org/10.1002/cctc.201902190.
89. Klose, C.; Saatkamp, T.; Münchinger, A.; Bohn, L.; Titvinidze, G.; Breitwieser, M.; Kreuer, K.; Vierrath, S. All-Hydrocarbon MEA for PEM Water Electrolysis Combining Low Hydrogen Crossover and High Efficiency. Adv. Energy Mater. 2020, 10, 1903995. https://doi.org/10.1002/aenm.201903995.
90. Matienzo, D.; Settipani, D.; Instuli, E.; Kallio, T. Active IrO2 and NiO Thin Films Prepared by Atomic Layer Deposition for Oxygen Evolution Reaction Catalysts 2020, 10, 92; doi:10.3390/catal10010092.
91. Takatsu, N.; Farzaneh, H. Techno-Economic Analysis of a Novel Hydrogen-Based Hybrid Renewable Energy System for Both Grid-Tied and Off-Grid Power Supply in Japan: The Case of Fukushima Prefecture. Appl. Sci. 2020, 10, 4061. https://doi.org/10.3390/app10124061.
92. Kalbasi, R.; Jahangiri, M.; Tahmasebi, A. Comprehensive Investigation of Solar-Based Hydrogen and Electricity Production in Iran. Int. J. Photoenergy 2021, 2021, 6627491. https://doi.org/10.1155/2021/6627491.
93. Li, S.; Kang, Q.; Baeyens, J.; Zhang, H.L.; Deng, Y.M. Hydrogen Production: State of Technology. IOP Conf. Ser. Earth Environ. Sci. 2020, 544, 012011. https://doi.org/10.1088/1755-1315/544/1/012011.

94. Holzapfel, P.K.R.; Bühler, M.; Escalera-López, D.; Bierling, M.; Speck, F.D.; Mayrhofer, K.J.J.; Cherevko, S.; Pham, C.V.; Thiele, S. Fabrication of a Robust PEM Water Electrolyzer Based on Non-Noble Metal Cathode Catalyst: [Mo 3 S 13]2− Clusters Anchored to N-Doped Carbon Nanotubes. Small 2020, 16, 2003161. https://doi.org/10.1002/smll.202003161.
95. Xue, F.; Su, J.; Li, P. Technical Research on Hydrogen Supply Chain Industry. IOP Conf. Ser. Earth Environ. Sci. 2020, 558, 022040. https://doi.org/10.1088/1755-1315/558/2/022040.
96. Gunawan, T.A.; Singlitico, A.; Blount, P.; Burchill, J.; Carton, J.G.; Monaghan, R.F.D. At What Cost Can Renewable Hydrogen Offset Fossil Fuel Use in Ireland's Gas Network? Energies 2020, 13, 1798. https://doi.org/10.3390/en13071798.
97. Peksen, M. Hydrogen Technology towards the Solution of Environment-Friendly New Energy Vehicles. Energies 2021, 14, 4892. https://doi.org/10.3390/en14164892.
98. Aubras, F.; Damour, C.; Benne, M.; Boulevard, S.; Bessafi, M.; Grondin-Perez, B.; Kadjo, A.; Deseure, J. A Non-Intrusive Sig-nal-Based Fault Diagnosis Method for Proton Exchange Membrane Water Electrolyzer Using Empirical Mode Decomposition. Energies 2021, 14, 4458. https://doi.org/10.3390/en14154458.
99. Niaz, H.; Lakouraj, M.M.; Liu, J. Techno-economic feasibility evaluation of a standalone solar-powered alkaline water elec-trolyzer considering the influence of battery energy storage system: A Korean case study. Korean J. Chem. Eng. 2021, 38, 1617–1630. https://doi.org/10.1007/s11814-021-0819-z.
100. Phoumin, H.; Kimura, F.; Arima, J. Potential Renewable Hydrogen from Curtailed Electricity to Decarbonize ASEAN's Emissions: Policy Implications. Sustainability 2020, 12, 10560. https://doi.org/10.3390/su122410560.
101. Samani, A.E.; D'Amicis, A.; De Kooning, J.D.; Bozalakov, D.; Silva, P.; Vandevelde, L. Grid balancing with a large-scale elec-trolyser providing primary reserve. IET Renew. Power Gener. 2020, 14, 3070–3078. https://doi.org/10.1049/iet-rpg.2020.0453.
102. Kopteva, A.; Kalimullin, L.; Tcvetkov, P.; Soares, A. Prospects and Obstacles for Green Hydrogen Production in Russia. Energies 2021, 14, 718. https://doi.org/10.3390/en14030718.
103. Marzi, E.; Morini, M.; Gambarotta, A. Analysis of the Status of Research and Innovation Actions on Electrofuels under Horizon 2020. Energies 2022, 15, 618. https://doi.org/10.3390/en15020618.
104. Nguyen, H.; Han, J.; Nguyen, X.; Yu, S.; Goo, Y.-M.; Le, D. Review of the Durability of Polymer Electrolyte Membrane Fuel Cell in Long-Term Operation: Main Influencing Parameters and Testing Protocols. Energies 2021, 14, 4048. https://doi.org/10.3390/en14134048.
105. Boulmrharj, S.; Khaidar, M.; Bakhouya, M.; Ouladsine, R.; Siniti, M.; Zine-Dine, K. Performance Assessment of a Hybrid System with Hydrogen Storage and Fuel Cell for Cogeneration in Buildings. Sustainability 2020, 12, 4832. https://doi.org/10.3390/su12124832.
106. Wilberforce, T.; Olabi, A.G. Performance Prediction of Proton Exchange Membrane Fuel Cells (PEMFC) Using Adaptive Neuro Inference System (ANFIS). Sustainability 2020, 12, 4952. https://doi.org/10.3390/su12124952.
107. D'Ovidio, G.; Ometto, A.; Villante, C. A Novel Optimal Power Control for a City Transit Hybrid Bus Equipped with a Parti-tioned Hydrogen Fuel Cell Stack. Energies 2020, 13, 2682. https://doi.org/10.3390/en13112682.
108. Gül, M.; Akyüz, E. Hydrogen Generation from a Small-Scale Solar Photovoltaic Thermal (PV/T) Electrolyzer System: Nu-merical Model and Experimental Verification. Energies 2020, 13, 2997. https://doi.org/10.3390/en13112997.
109. Li, K.; Fan, Q.; Chuai, H.; Liu, H.; Zhang, S.; Ma, X. Revisiting Chlor-Alkali Electrolyzers: from Materials to Devices. Trans. Tianjin Univ. 2021, 27, 202–216. https://doi.org/10.1007/s12209-021-00285-9.
110. Lee, H.I.; Dung, D.T.; Kim, J.; Pak, J.H.; Kim, S.K.; Cho, H.S.; Cho, W.C.; Kim, C.H. The synthesis of a Zirfon-type porous separator with reduced gas crossover for alkaline electrolyzer. Int. J. Energy Res. 2019, 44, 1875–1885. https://doi.org/10.1002/er.5038.
111. Dawood, F.; Shafiullah, G.; Anda, M. Stand-Alone Microgrid with 100% Renewable Energy: A Case Study with Hybrid Solar PV-Battery-Hydrogen. Sustainability 2020, 12, 2047. https://doi.org/10.3390/su12052047.

112. Mori, M.; Stropnik, R.; Sekavčnik, M.; Lotrič, A. Criticality and Life-Cycle Assessment of Materials Used in Fuel-Cell and Hydrogen Technologies. Sustainability 2021, 13, 3565. https://doi.org/10.3390/su13063565.
113. Londono, J.V.; Mazza, A.; Pons, E.; Lok, H.; Bompard, E. Modelling and Control of a Grid-Connected RES-Hydrogen Hybrid Microgrid. Energies 2021, 14, 1540. https://doi.org/10.3390/en14061540.
114. Ying, Z.; Wang, Y.; Zheng, X.; Geng, Z.; Dou, B.; Cui, G. Modeling and experimental assessment of the novel HI-I2-H2O elec-trolysis for hydrogen generation in the sulfur-iodine cycle. Int. J. Energy Res. 2020, 44, 6285–6296. https://doi.org/10.1002/er.5334.
115. Yan, X.; Biemolt, J.; Zhao, K.; Zhao, Y.; Cao, X.; Yang, Y.; Wu, X.; Rothenberg, G.; Yan, N. A membrane-free flow electrolyzer operating at high current density using earth-abundant catalysts for water splitting. Nat. Commun. 2021, 12, 4143. https://doi.org/10.1038/s41467-021-24284-5.
116. Yang, F.; Kim, M.J.; Brown, M.; Wiley, B.J. Alkaline Water Electrolysis at 25 A cm−2 with a Microfibrous Flow-through Elec-trode. Adv. Energy Mater. 2020, 10, 2001174. https://doi.org/10.1002/aenm.202001174.
117. Li, X.; Zhao, L.; Yu, J.; Liu, X.; Zhang, X.; Liu, H.; Zhou, W. Water Splitting: From Electrode to Green Energy System. Nano-Micro Lett. 2020, 12, 131. https://doi.org/10.1007/s40820-020-00469-3.
118. Iqbal, W. et al; Assessment of Wind Energy Potential for the Production of Renewable Hydrogen in Sindh Province of Pakistan, Processes 2019, 7, 196; doi:10.3390/pr7040196.
119. Tachikawa, T.; Beniya, A.; Shigetoh, K.; Higashi, S. Relationship Between OER Activity and Annealing Temperature of Sputter-Deposited Flat IrO2 Thin Films. Catal. Lett. 2020, 150, 1976–1984. https://doi.org/10.1007/s10562-020-03105-2.
120. Zhang, X.; Zhang, W.; Yang, W.; Liu, W.; Min, F.; Mao, S.S.; Xie, J. Catalyst-coated proton exchange membrane for hydrogen production with high pressure water electrolysis. Appl. Phys. Lett. 2021, 119, 123903. https://doi.org/10.1063/5.0060150.

COMPARATIVE STUDY OF ENZYME ACTIVITY AND FAT CONCENTRATION FROM DIFERENT TYPES OF DEHYDRATED OILSEEDS

Anda Ioana Grațiela PETREHELE[1], Alexandrina FODOR[1], Gabriela Elena BADEA[1], Lenuța Iuliana LUKACS[2], Camelia IONAS[1]

[1]University of Oradea, Faculty of Informatics and Sciences, 1 University St., 410048, Oradea, Romania, e-mail: andapetrehele@yahoo.com
[2]Masterand CSA I, University of Oradea, Faculty of Informatics and Sciences, 1 University St., 410048, Oradea, Romania

Abstract. *In this paper, a comparative study was carried out between samples of raw grains rich in fats that are frequently used as food. The samples taken in the study were dehydrated organic soybean powder and also hazelnut, walnut, sunflower and pumpkin grains. In the first experiment they were used to obtain an enzyme extract in ether, and the enzyme activity was followed in the hydrolysis reaction of fats from an olive oil sample. Following this experiment, the enzyme activity decreased in the order: walnuts > pumpkin > soybean > peanut > sunflower. In the case of determining the total fats content by the extracts in ethyl ether using Soxhelt method, for this was founded to decrease in the next sequence: walnuts > sunflower > peanut > pumpkin > soybean. The last determined parameter was the saponification index, which varied in the same way as total fats.*

Keywords: lipase, fats, saponification index, peanut, sunflower, pumpkin, soybean, walnut

INTRODUCTION

In this paper we aimed to make a comparative study between the properties of seeds from different plants, used as food with an increased content of unsaturated and saturated fats. In parallel, we followed how certain parameters characterization of the content of the enzyme responsible for the dissociation of lipids, but also the content of saturated and unsaturated fats in them, vary and we compared the results obtained [1-3].

Lipase activity was determined by measuring the increase in the acidity of some lipids as a result of the action of an enzyme preparation obtained from oleaginous plant tissues, such as the samples of raw seeds chosen by us, dehydrated soybeans, raw sunflower seeds, pumpkin seeds, walnut kernels and peanuts. The ideal substrate for the study of lipase activity are lipids from the same biological material [4, 5].

Lipids (fats) under the action of the enzyme lipase are dissociated by hydrolysis into glycerol and fatty acids, according to the reaction below [6, 7]:

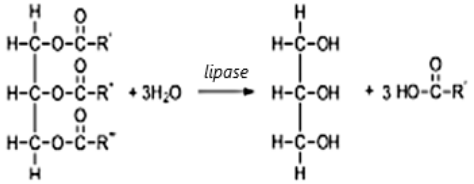

The measurement of lipase activity is done by determining the number of moles of fatty acids produced, reported as oleic acid molecules [8-10]. The determination of the number of moles of oleic acid is done by titrating them with NaOH in the presence of

phenolphthalein, according to the neutralization reaction below:

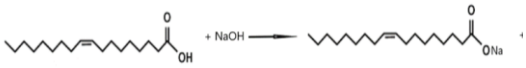

The dosage of fats is based on the property of this to be soluble in organic solvents such as ethyl ether, petroleum ether, unlike the other main constituents in tissues [11]. Extraction of fats with solvents is done either in the Soxhlet extractor or by distribution in the separatory funnel. In the extract, fats and other substances soluble in ether, such as pigments, essential oils, resins pass. The global product, which remains after removing the solvent, is called crude fat [12].

The constants that characterize a fat both physically and chemically are the following: density, solidification point, saponification index, iodine index, acidity index, refractive index and others [13]. The saponification index expresses the number of milligrams of potassium hydroxide required to completely saponify one gram of fat. The higher the molecular mass of the glyceride, respectively of the fatty acids, the lower the amount of potassium hydroxide required for saponification. So, the value of the saponification index gives us indications on the chemical constitution of the analysed lipids [14]. The method is based on the hot saponification reaction of fats with alcoholic KOH solution, as can be seen in the image below. The chemical reaction used to determine the saponification index is:

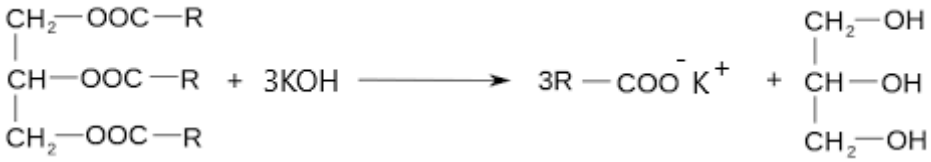

The above reaction is carried out in an excess of KOH, and the resulting excess is titrated with hydrochloric acid of the same concentration, in the presence of phenolphthalein indicator. By the difference between the acid consumed when titrating the same volume of KOH in the presence and absence of the biological sample, the saponification index can be determined, which is expressed in mg KOH/g lipids [12-14]:

$$KOH + HCl \rightarrow KCl + H_2O$$

MATERIALS AND METHODS

All samples were products marketed in our country. Soy was an organic product in the form of a dehydrated powder. The rest of the samples were in the form of raw, dehydrated, unheated grains. The olive oil used was a fresh product. All reagents used were high analytical purity. 99.5% ethyl alcohol and double distilled water were used to prepare the solutions required in all analytical methods used in this study.

The samples chosen for this study were dehydrated raw grains or powder of the following varieties, known for their high fat content and frequently used as food (Fig. 1): peanut, sunflower, pumpkin, soybean and walnut.

Fig. 1. Samples of whole and crushed raw grains samples taken in study (peanut, sunflower, pumpkin, soybean and walnut)

For the samples, the enzymatic activity and the total amount of lipids were determined by extraction with ethyl ether, including both saturated and unsaturated lipids, specific to plant products. For the oils obtained from them by extraction in ethyl ether, the saponification index was determined.

Preparation of samples

An enzyme extract was obtained for each analysed sample. In a first phase, all the samples of grains, soybeans, walnut kernels and peanuts were crushed in a pestle mortar. About 1.0 g of each mortared sample was weighed on the analytical balance. The crushed and weighed samples were transferred into 100 mL Berzelius beakers and 10 mL of ethyl ether was added over each sample. The samples were covered with aluminium foil and left to extract for 2 hours, shaking periodically. The ether extract was separated by decantation and recovered in other stoppered Erlenmeyer beakers. 5 mL of ethyl ether was added to the samples in the Berzelius glasses and left to extract for one hour. After that, the amount of ethyl ether is decanted again with the oil extract in Erlenmeyer beakers with stoppers. Erlenmeyer beakers with the ether extract will be used in subsequent experiments. The Berzelius glasses with the defatted plant material were dried for one hour in an oven at 30 °C. The defatted seeds contain lipase. The dried plant material samples in the Berzelius beakers are reweighed on the analytical balance. The obtained result will be used to determine the amount of lipids separated by extraction in cold ethyl ether.

Determination of enzyme (lipase) activity

0.2 g of defatted grains were introduced into an Erlenmeyer beaker and mixed with 3 ml of olive oil. 2ml of pH 4.7 buffer solution was added and the glass was placed in a water bath at 30 °C for 30 minutes. 15 mL of ethyl alcohol was dropped to the glass and was stirred to homogenize. The mouth of the glass was covered with an aluminium foil. Then, the fatty acids in the sample were titrated with 0.1N NaOH in the presence of phenolphthalein as an indicator. Blank sample was a mixture consisting of 0.2 g of defatted grains, 3 mL of olive oil, 2 mL of pH 4.7 buffer solution and 15 mL of ethyl. The mixture thus obtained was

stirred, two drops of phenolphthalein were added in it and it was immediately titrated with NaOH 0.1N. For each sample, the experiment was repeated two more times.

:

Lipase activity was expressed in micromoles of oleic acid that are formed as a result of lipase action, per minute and gram of enzyme preparation. The mathematical relationship which express the results in this case was

$$Enzimatic\ (lipase)\ activity\ (\mu moli\ \ min^{-1}\ g^{-1}) = \frac{(V_B - V_S)\cdot F_{NaOH}\cdot 100}{t\cdot V_{oil}\cdot m_{extract}}$$

where

- V_B is the volume of 0.1N NaOH consumed during the titration of the control sample (mL);
- V_S is the volume of 0.1N NaOH consumed when titrating the sample after 30 minutes of thermostating at 30 °C (mL);
- F_{NaOH} is the factor of the NaOH solution used in the titration of fatty acids resulting from the hydrolysis reaction carried out by lipase
- t is the time expressed in minutes, how long the enzymatic hydrolysis lasted (30 minutes)
- V_{oil} represents the volume of oil, sample hydrolysed by lipase (mL)
- $m_{extract}$ is the mass of dehydrated seeds containing the lipase whose action was determined in the hydrolysis reaction of the fats in the oil (g).

Quantitative determinations of fats by solvent extraction

10 g mortared of the dried grains samples were kept for two hours before use at 95°C in an oven to remove moisture. To be sure that the moisture removal was done correctly, the samples were weighed after the first hour and reweighed after the second hour of oven drying. There should be no differences between the two successive determinations. About 5 g of sample was introduced into a filter paper cartridge. A minimum of 4 successive refluxes were performed during three hours for each biological sample analysed [9]. After 3 hours of extraction, the cartridge was removed, dried again in the oven at 95°C for two hours and weighed again.

The mathematical formula used to express the concentration of total fats in 100 g of dry grains sample was:

$$Total\ fats\ (g\%) = \frac{(m_i - m_f)\cdot 100}{m_{sample}}$$

Where

- m_i is the initial mass of the cartridge with the sample from which the lipids were extracted (g);
- m_f is the final mass of the sample cartridge after the lipids (g) have been extracted and dried in an oven for two hours;
- m_{sample} is the mass of biological material from which the lipids were hot extracted in ethyl ether (g)

Determination of the saponification index

In a 150 - 200 cm^3 flask equipped with an ascending refrigerant, the fat samples resulting from the determination of total lipids, 1 - 2 g of fat (G) was placed and over, 25 mL of alcoholic solution of 0,5 N potassium hydroxide was added. The flask with the lipid mixture and the 0.5 N KOH alcoholic solution was heated to boiling on a water bath for 30 minutes. After 30 minutes, the heating was stopped, the flask with the reaction mixture was cooled under running water and 1-2 drops of 1% phenolphthalein indicator were added. Since only part of the KOH solution was involved in the saponification reaction, the colour of the solution should have been red. Otherwise, an additional 25 mL of 0.5 N KOH should have been added to the sample and refluxed for an additional 30 min. The red sample solution was titrated until colourless with the 0.5 N HCl solution. In another Erlenmeyer beaker, a blank sample was prepared in parallel, adding 25 mL of 0.5 N KOH alcoholic solution and 1-2 drops of phenolphthalein While stirring, KOH excess was titrated with 0.5 N HCl until colourless.

The volume of 0.5 N KOH used in the saponification reaction was determined from the difference between the volumes of 0.5 N HCl used in the titration of the blank and the sample. The calculation of the mass of KOH (mg) used in the titration of 1 g of lipids from the samples, which represents the saponification index, is determined with the equation:

$$Saponification\ index\ (mg\ KOH\ g^{-1}) = \frac{(V_B - V_S) \cdot F_{KOH} \cdot c_{KOH} \cdot M_{KOH}}{m_{fats}}$$

where

- V_B is the volume of 0.5 N HCl used in the titration of the control sample (mL);
- V_S is the volume of 0.5 N HCl used for sample titration (mL);
- FKOH is the KOH solution factor
- C_{KOH} is the normal concentration of the alcoholic KOH solution used in the saponification of lipids (0.5 N);
- M_{KOH} is the molecular mass of KOH (M=56.0153 g/mol)
- m_{fats} is the sample mass and represents in this case the mass of fats extracted by the Soxhelt method (g)

RESULTS INTERPRETATION

In figure 2 it can be seen that high values of lipase activity were found especially in walnut kernels and pumpkin grains, followed by dehydrated soybeans, peanuts and finally sunflower seeds. Through the ethyl ether extraction method, the richest in lipase was found to be walnut kernels, and the poorest in lipase were sunflower seeds.

For total fats, the results obtained are represented in Figure 3. As can be seen, the highest concentration of total lipids was recorded in the walnut core, and the lowest in the dehydrated soybean sample. Otherwise, the concentration of total lipids between sunflower seeds and peanuts were very closed, over 49 g%, and were somewhat higher than in pumpkin seeds for which a concentration of 45 g% was obtained. All lipid concentrations were expressed per 100 g biological material dried in oven at 95°C.

In Fig 4 it can be seen that the highest value of the saponification index was obtained for the walnut kernel. This is, in conclusion, among the analysed species the richest in fatty acids, or in other words it presents the most carboxylic groups in one gram of fatty material separated by extraction in ethyl ether. At the opposite pole is the

dehydrated soybean, which possibly, due to the processing method, no longer has specific properties of soybeans, being partially defatted, part of the amount of lipids was lost in the product preparation process. Saponification indices intermediate and quite close in value were found for pumpkin seeds, sunflower seeds and peanuts. The evolution of the saponification index from the fatty material extracted with ethyl ether from the analysed plant samples, or in other words the quantity of fatty acids in the samples, is better suggested in figure 4:

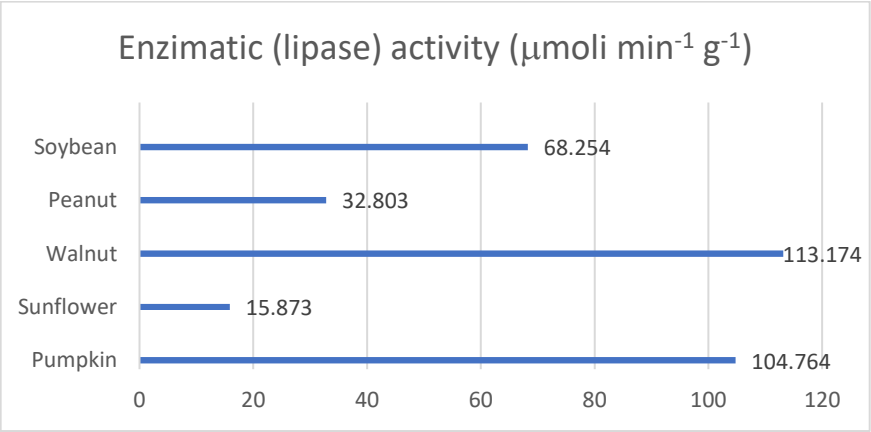

Fig. 2. Lipase activity for the ether extracts (peanut, sunflower, pumpkin, soybean and walnut seeds)

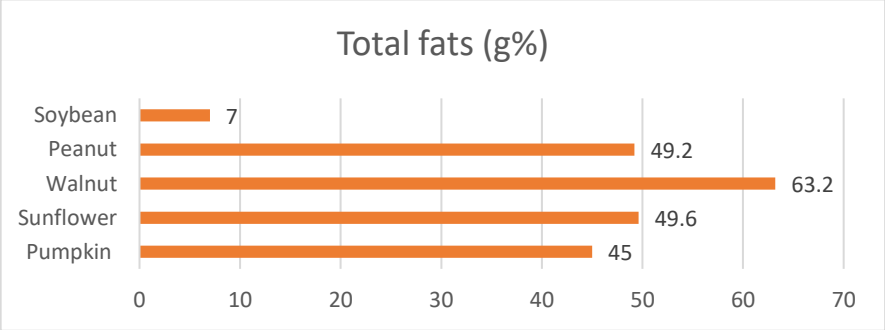

Fig. 3. Determination of total fats in ether from the analysed samples (peanut, sunflower, pumpkin, soybean and walnut grains)

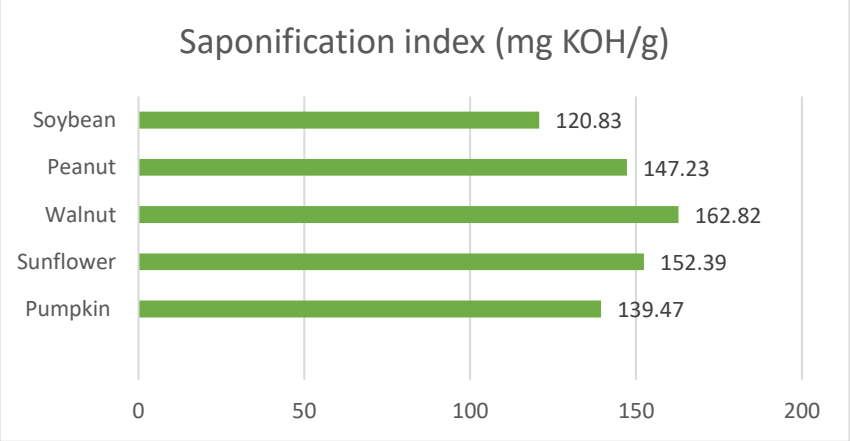

Fig. 4. Determination of the saponification index for the studied biological materials (peanut, sunflower, pumpkin, soybean and walnut grains)

If all the parameters analysed in this paper are combined, a diagram represented in Fig. 5. From which the following observations can be made:

- total lipids and the saponification index vary very similarly, both parameters increase in the studied biological materials in the order: Dehydrated soybean > pumpkin > peanut > sunflower > walnut
- the evolution of enzymatic (lipase) activity is instead more different, but the highest value was also recorded here for the walnut kernel. A very high value was also obtained for dehydrated soybeans, which shows that despite the fact that fats have been lost in the preparation of the respective product, the enzyme concentration is high.
- although the analysis methods for lipase and for the saponification index are very similar, the fact that different parts of the plant material used were taken into consideration led to very different results:
- the similar results from the determination of total lipids and the saponification index considered the same part of the plant material and therefore their evolution is very similar.

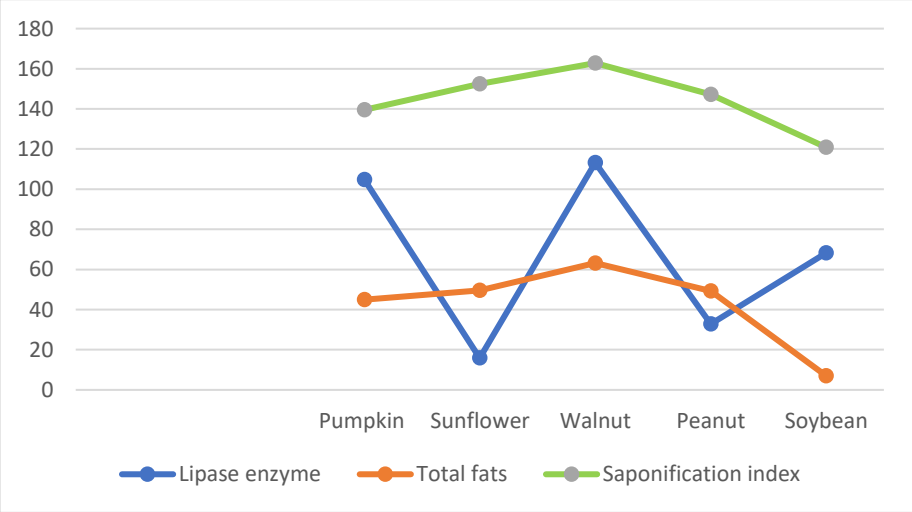

Fig. 5. Comparative variation of fat characterization parameters from the studied biological samples (peanut, sunflower, pumpkin, soybean and walnut grains)

CONCLUSION

Following this experiment, the enzyme activity decreased in the order: walnut > pumpkin > soybean > peanut > sunflower. In the case of determining the total fat content by the Soxhelt extraction method in ethyl ether, the fat content decreased in the sequence: nuts > sunflower > peanut > pumpkin > soybean. The last parameter determined was the saponification index, which varied as total fats did. The results obtained showed that among the analysed samples, walnuts had the highest enzyme activity, but also the highest fats content, which proved that they would be a very good source of food and energy for the body. The situation of the organic soy powder found to be very interesting, which presented a high enzymatic activity, although a high efficiency in breaking down fats into fatty acids and glycerol, but a lower fat content, which recommends them for a hypocaloric diet, with a lower fat intake, but metabolically efficient.

REFERENCES

1. Drăgănescu, C. (1993), *Biochimie,* Ed. Did. și Ped., București
2. Banu, C. et. al. (2007), *Suveranitate, Securitate și siguranță alimentară,* Ed.ASAB, București
3. Sueishi, Y. Nii, R. (2020), A comparative study of the antioxidant profiles of olive fruit and leaf extracts against five reactive oxygen species as measured with a multiple free-radical scavenging method. *J. Food Sci*., Vol. 85, pp. 2737–2744
4. Liu, X., Wang, S.,Tamogami, S., Chen, J.;, Zhang, H. (2021), Volatile profile and flavor characteristics of ten edible oils. *Anal. Lett.* Vol. 54, pp. 1423–1438.
5. Da S. Pereira A. et al (2022), Lipases as effective green biocatalysts for phytosterol esters' production: A Review, *Catalysts*, Vol. 12(88), pp 1-28. https://doi.org/10.3390/catal12010088
6. Kotogán A. et al. (2022), Hydrolysis of edible oils by fungal lipases: an effective tool to produce bioactive extracts with antioxidant and antimicrobial potential, *Foods*, Vol.11(1711), pp 1-19. https://doi.org/10.3390/foods11121711
7. Mossoba M.M. et al. (2009), Nutrition Labeling: Rapid Determination of Total transFats by Using Internal Reflection Infrared Spectroscopyand a Second Derivative Procedure, *J. Am Oil Chem Soc*, Vol. 86, pp. 1037–1045
8. Naudet M., Hautfenne A. (1985), Determination of total sterols in fats and oils, *J. Pure & App!. Chem*., Vol. 57(6), pp. 899—904
9. Hautfenne A. (1982), Standard methods for the analysis of oils, fats and derivatives, *J. Pure & Appl.Chem.,* Vol.54(6), pp. 1257—1295
10. Gonçalves, B. et al., (2023.), Composition of nuts and their potential health benefits—an overview, *Foods*, Vo. 12(5), pp. 942-948. https://doi.org/10.3390/foods12050942
11. Ivanova M. et al. (2022), Saponification value of fats and oils as determined from 1h-nmr data: the case of dairy fats., *Foods*, Vol. 11, pp. 1466-1472. https://doi.org/10.3390/foods11101466
12. Muhammad A., Muhammad A., Zeb A., (2013), Physicochemical analysis and fatty acid composition of oil extracted from olive fruit, *Food Science and Quality Management*, Vol 19, pp 1-5, ISSN 2225-0557
13. Chira N., Todaşcă C., Nicolescu A., Păunescu G., Roşca S. (2009), Determination of the technical quality indices of vegetable oils by modern physical techniques, *U.P.B. Sci. Bull., Series B,* Vol. 71(4), pp. 3-12;
14. Proaño F. et al. (2015), Evaluation of three saponification methods on two types of fat as protection against bovine ruminal degradation, *Cuban Journal of Agricultural Science,* Vol. 49(1), pp. 1-5

DETERMINATION OF COPPER AND IRON IN WASTE WATER FROM COPPER MINING

Codrin BALEA[1], Anda Ioana Grațiela PETREHELE[2], Alexandrina FODOR[2], Claudia Mona MORGOVAN[2]

[1] Master CSA student, , Faculty of Informatics and Sciences, University of Oradea

[2] Department of Chemistry, Faculty of Informatics and Sciences, University of Oradea

Abstract: *In this paper we studied wastewater from the mining industry Cupru Min S.A Roşia Poieni Plant, respectively the sterile deposit from Geamăna, Alba, carrying out a study in order to determine the concentrations of copper and iron in the wastewater covering the sterile deposit. Because the sterile deposit of the Geamana copper mine is covered by waters, which have orange, green and yellow colors, it can be easily seen that they are toxic, polluted waters, and copper and iron concentrations are high. The purpose of this work was to analyze three wastewater samples taken from three different points in the sterile pond and determine copper and iron concentrations by atomic absorption spectroscopy method. Prior to the analysis of the two metals, the pH of the samples and the total suspensions were determined. Since the waste water samples show advanced turbidity and deposits if left to settle, 10 ml of HCl of different concentrations: 10%, 20%, 30% and concentrated acid were added to each of the samples in order to dissolve the metals in the deposits. After analysis, it was observed that for both Cu and Fe, concentrations significantly exceed the regulated MACs for waste water (respectively 0,2 mg/l for Cu and total dissolved metals 2 mg/l).*

Keywords: waste water, sterile deposit, copper and iron concentration.

INTRODUCTION

The existence of heavy metals in water, arising as a result of mining operations in Romania, is a major problem both for human health and for the entire food chain. Due to their high toxicity, capacity for accumulation and contamination, these potentially harmful elements for all ecosystems pose a real danger to humans and animals in the contaminated area. Pollution caused by mining activity and the presence of large amounts of heavy metals in the environment induced by human activity is one of the most important tasks of current environmental problems. In Romania, contamination with these elements, in areas where there have been ore holdings, represents a real challenge for research. In the mining area of Roșia Poieni under study, waste dumps and sterile ponds remained, which represent a real danger to the health of the food chain. Excessive amounts of heavy metals such as iron, copper, zinc, lead, cadmium have been detected both in and around the dumps. The excessive increase in the quantities of these elements in soil and water, mainly due to pollution, leads to metabolic disorders in plants and also affects the quality of food, which could be harmful to human health [1-7].

EXPERIMENTAL PART

1. Determination of pH

The evaluation of the acidity of a solution is made by pH, which represents the negative decimal logarithm of the concentration of hydrogen ions (hydronium), expressed in moles per liter. The pH of natural waters varies little from neutral pH due to the presence of CO_2, carbonates and bicarbonates. Hard waters have a higher pH than soft waters (due to the higher concentration of salts that give basic hydrolysis - carbonates and metal bicarbonates, mainly). The pH of wastewater can be acidic or alkaline and is a cause of disturbance of the biological balance of the receiving tank, preventing the normal self-purification process. Colorimetric methods (approximate measurement and electrometric (accurate measurement) are used to determine the pH of water [8].

The exact pH measurement is done using a device called the pH meter, which is essentially an electric cell whose electromotive force depends on the concentration of protons (H+) in solution. The galvanic cell consists of a reference electrode (silver or calomel) and a pH-sensor electrode (glass electrode).

pH = - lg [H+]

Principle of the method: the potential difference between a glass electrode and a reference electrode (usually calomel electrode - saturated KCl solution), introduced into the water sample to be analysed, varies linearly with the pH of the sample. The presence of competing species can cause distortion of measurement, so the operational definition of pH has been introduced. It is based on the concept that pH is measured with a hydrogen electrode combined with a reference electrode (to form the appropriate galvanic cell). The reference electrode solution is brought into contact with the hydrogen electrode solution through a KCl bridge with a minimum concentration of 3.5 mol/1000 g solvent.

2. Determination of suspended matter (total suspensions)

The total suspended solids content is the amount of suspended substances present in a measured volume of water, filtered and dried at 105 °C. Any water-insoluble substance can persist for more or less time depending on the weight: very light particles or colloidal particles remain practically indefinitely in suspension, being found in continuous motion in water. Suspended solids present in wastewater can be solid organic or inorganic compounds, or liquids immiscible with water such as oils and fats. The suspended matter parameter is a monitoring parameter, included as a conventional pollutant. The wastewater has variable content of suspended solids, depending on where it comes from [8].

The principle of the method: separation of suspended particles by filtration or centrifugation. The solids in the filter are dried at a standard temperature of 105 °C and then weighed.

Procedure (filter paper method) The installation is prepared for vacuum filtration; Shake the sample vigorously and measure 100 mL into a measuring cylinder, pour this portion of the sample into the filter funnel. Rinse the cylinder with a small portion of distilled water, then pour the contents into the filter funnel. If the content of suspensions is low, a larger sample volume may be used; When filtration is complete, remove the filter carefully with tweezers and place in the oven. Dry for at least 1 hour at 103 to 105 °C. Cool in a desiccator and weigh; Repeat the drying, exication and weighing cycle until the loss in mass is less than 0,5 mg; Note the weighed final mass (g).

Calculation: the total suspensions (expressed in mg/L) present in the test water shall be determined with the following relationship:

Total suspensions = 1000, where: $\frac{m1-m}{V}$

m=filter mass, mg;

m1= mass of filter and mass of solids in the water sample remaining on the filter after filtration, mg; V= filtered sample volume, mL

Table 1. pH and total suspensions

Sample No	Ph	Total suspension
1.	3,34	2921 mg/l
2.	4,22	3002 mg/l
3.	4,69	3323 mg/l

3. Spectrophotometric determination of iron from mining wastewater

The work aims to determine iron concentrations in water samples taken from different areas, which end up on the tailings mining deposit. The identification will be achieved by atomic absorption spectrometry, by suction of samples, with atomization in flame [8].

Reagents and apparatus

- Standard solution Iron, manufacturer Merck, c(Fe) = 1000mg/L;
- Ultrapure nitric acid, HNO_3 density 1,37 g/cm^3;
- Ultra pure water
- Automatic pipettes with adjustable volume;
- Volumetric flasks, 25, 50 and 100 ml;
- Ultrapure water generator;
- Atomic absorption spectrometer model PinAAcle 900T.

Procedure

.

After verifying the working method, the standard sols are prepared, dilutions of highly concentrated samples are prepared as needed in our work, expecting excessive concentrations of the analyte in question, then entering the stage of performing the determinations themselves with the spectrometer.

Preparation of standard (calibration) solutions - The standard solution starts from a concentration of 1000 mgFe^{3+}/L It is proposed the preparation variant by repeated dilutions obtaining standard solutions of concentrations: 0.5; 1; 1.5; 2; 2.5; and mg Fe^{3+} /L, solutions following which the calibration curve is drawn.

The calibration curve shall be plotted according to the instrument manufacturer's recommendations in order to respect linearity as well as linearity. At least one calibration at least four points is indicated and absorbance readings should be traced at wavelength 248,33 nm

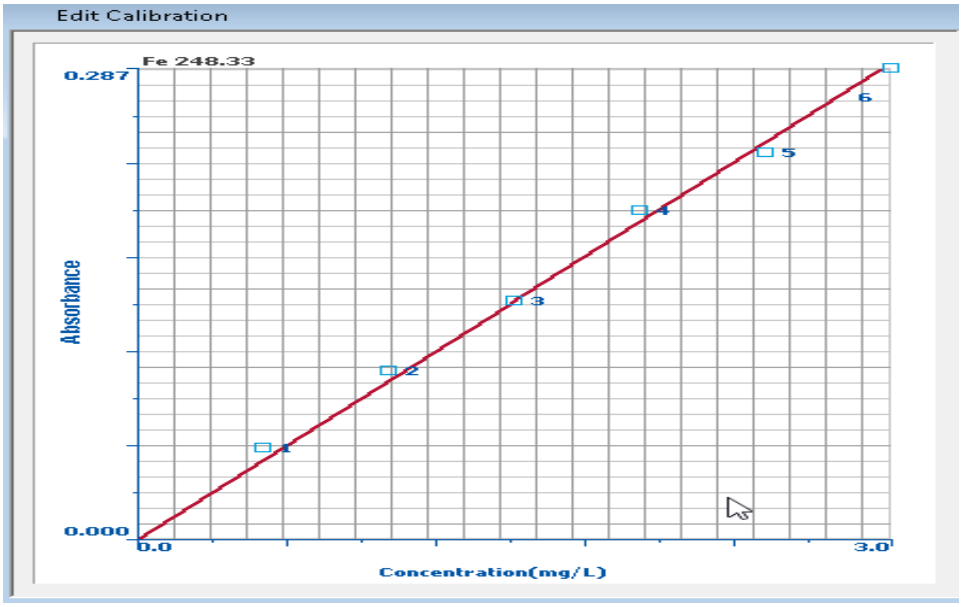

Analyte	Fe 248.33
Slope	0.09672
Intercept	0.00000
Correlation coefficient	0.997642

Figure 2. Calibration curve for Fe^{3+} determination

The three initial samples noted P1, P2, P3 treated with HCl concentrations of 10%, 20%, 30% and concentrated HCl were analysed for Fe^{3+} concentrations, denoted as follows:

P1C10; P1C20; P1C30; P1CNC
P2C10; P2C20; P2C30; P2CNC
P3C10; P3C20; P3C30; P3CNC
The results of the analyses carried out are shown in figure 3:

From the analysis of the samples, it is found that the concentration levels for iron vary within very wide limits, from tens of mg/l to several g/l.
In the following figures, iron concentrations were plotted for each of the three samples, P1, P2 and P3, depending on the concentration of added hydrochloric acid (10 ml per 100 ml sample).

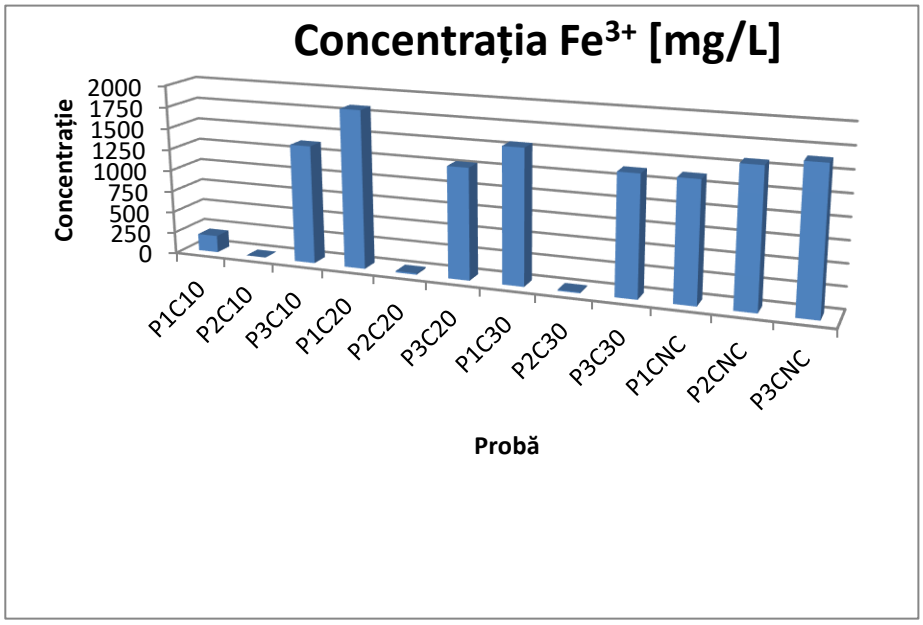

Figure 3. Fe^{3+} concentrations in test samples [mg/L]

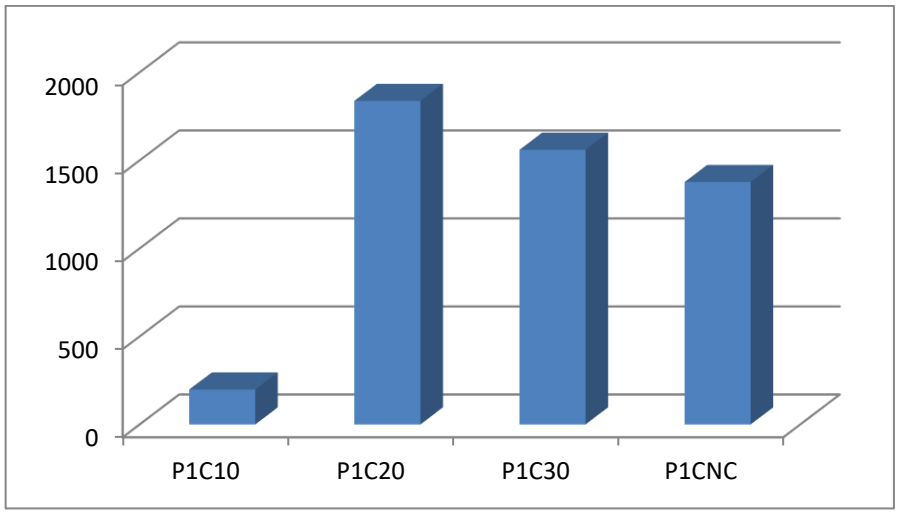

Figure 4. Fe^{3+} concentrations [mg/L] in sample P1 as a function of added HCl concentration

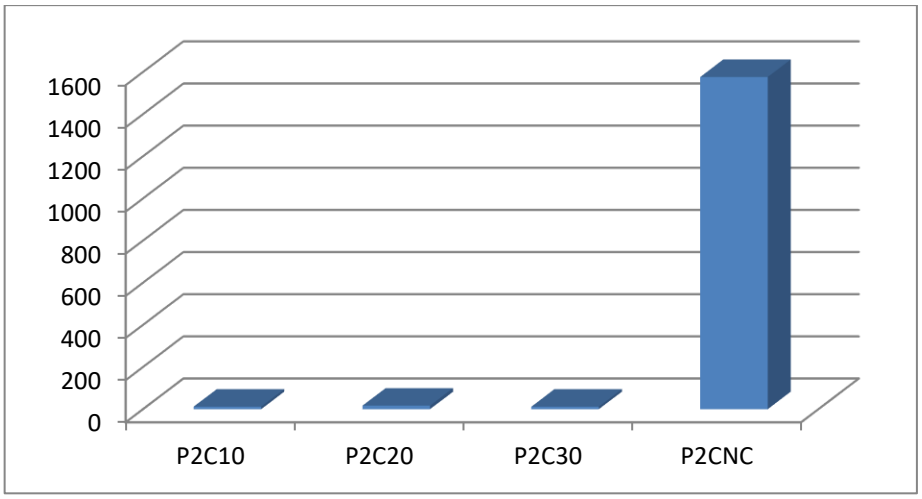

Figure 5. Fe^{3+} concentrations [mg/L] in sample P2 as a function of added HCl concentration

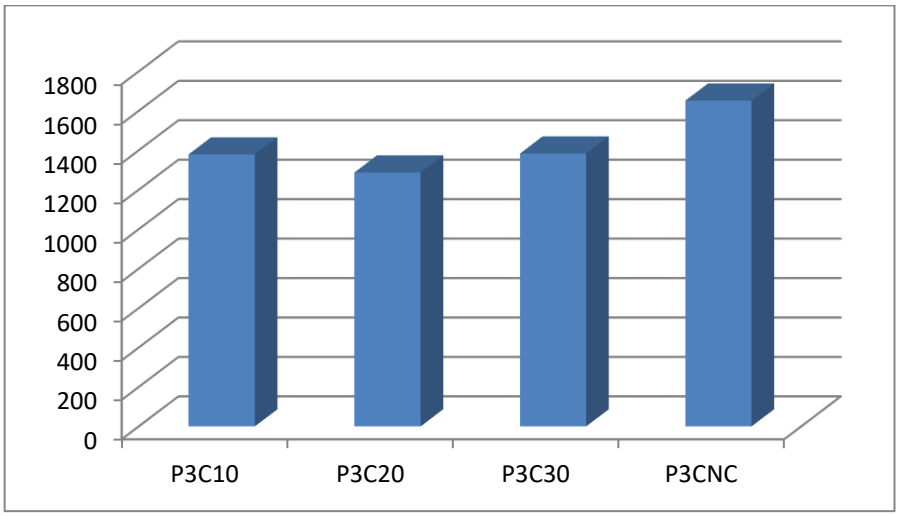

Figure 6. Fe^{3+} concentrations [mg/L] in sample P3 as a function of added HCl concentration

From the analysis of the data obtained, it can be seen that different values of Fe concentrations were obtained for the three wastewater samples, depending on the HCl concentration added. HCl of various concentrations (10%, 20%, 30% and concentrate) of 10 ml per 100 ml sample was added to dissolve copper and iron from the sediment in solution. After shaking the samples for 20 minutes, they were filtered. From the filtrate obtained, Fe and Cu were then analyzed by atomic absorption spectroscopy. Since the atomic absorption spectrophotometer does not allow analysis of samples with very high concentrations, the samples were diluted accordingly.

From the graphs above, it can be seen that for sample P1, the highest amount of Fe was determined in the sample in which HCl was added 20%, and the smallest in the sample with HCl 10%.

In sample P2, it is observed that Fe dissolved best in concentrated HCl. However, since there is a very large difference between the other HCl concentrations, it can be assumed that an error has occurred, either in dilution of samples or in data processing.

For sample P3, the highest degree of dissolution of Fe was in concentrated HCl, but the other values are also close.

In general, higher Fe3+ concentration values were obtained by addition of concentrated HCl, except for P1, where the highest value was obtained when adding 20% HCl, however comparable values were obtained.

4. Determination of copper in mining wastewater by atomic absorption spectrometry

The analysis of the concentration of copper ions in the acidic wastewater of the mining deposit is pursued, the method applied being atomic absorption spectrometry, by suction of samples with flame atomization [8].

With this method, absobance = f (concentration), copper concentrations up to 1.6 mg/l at a wavelength of 324.75 nm can be measured optimally, but respecting linearity. Work is carried out with air flame and acetylene.

Making determinations goes through the following steps:

- preparation of reagents;
- preparation of samples for measuring the analytical signal;
- the preparatory operation of the system and its start-up;
- editing the sample information file;
- plotting the calibration curve;
- analysis of samples;
- displaying results;
- shutting down the system;

We have as standard solution with a concentration of 1000 mg Cu^{2+} /l from this prepare in a volumetric flask 100 ml intermediate solution of concentration 10 mg Cu^{2+} /l. In these 50 ml and 25 ml volumetric flasks, dilutions necessary to obtain the concentration standard solutions. Next, plot a calibration curve for the determination of Cu^{2+}:

The results of the analyses carried out are shown in Figure 8.

From analysis of samples, it is found that concentration levels for copper range from less than 1 mg/l to a maximum value of around 25 mg/l.

In the following figures, copper concentrations were plotted for each of the three samples, P1, P2 and P3, depending on the concentration of added hydrochloric acid (10 ml per 100 ml sample).

From the analysis of the data obtained, it can be seen that different values of Cu concentrations were obtained for the three wastewater samples, depending on the HCl concentration added. HCl of various concentrations (10%, 20%, 30% and concentrate) of 10 ml per 100 ml sample was added to dissolve copper and iron from the sediment in solution. After shaking the samples for 20 minutes, they were filtered. From the filtrate obtained, Fe and Cu were then analyzed by atomic absorption spectroscopy. Since the atomic absorption spectrophotometer does not allow analysis of highly concentrated samples, the samples were diluted accordingly.

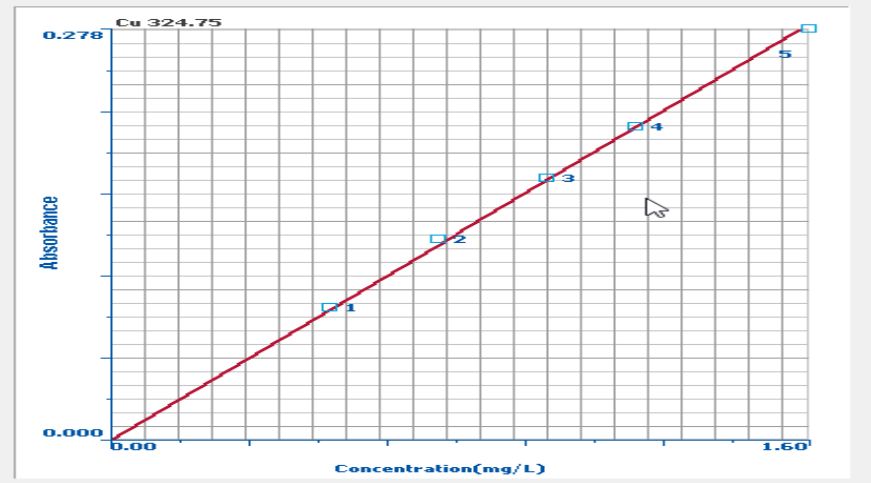

Figure 7. Calibration curve for Cu^{2+} determination.

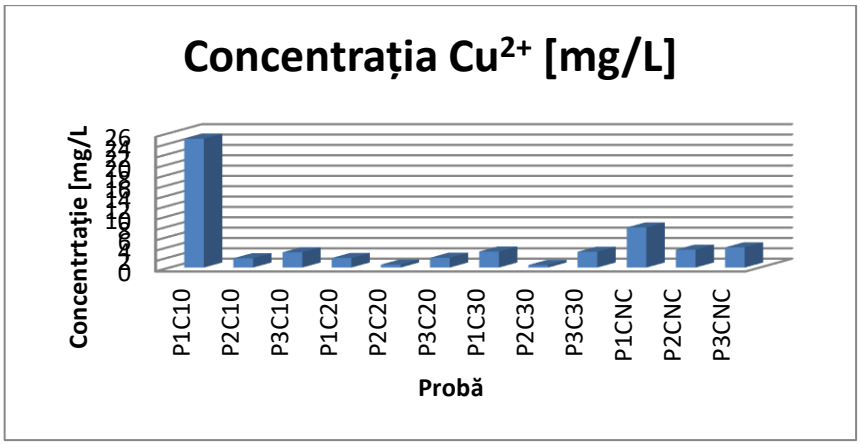

Figure 8. Cu^{2+} concentration in test samples

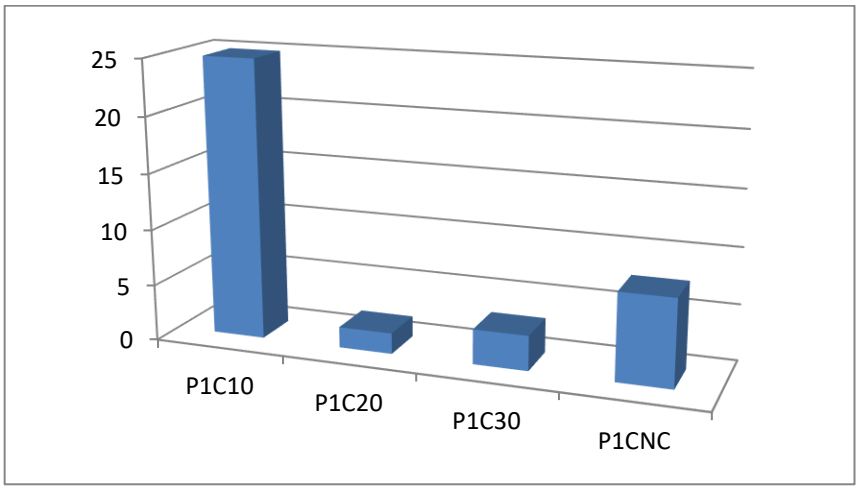

Figure 9. Cu^{2+} concentrations [mg/L] in sample P1, depending on the added HCl concentration

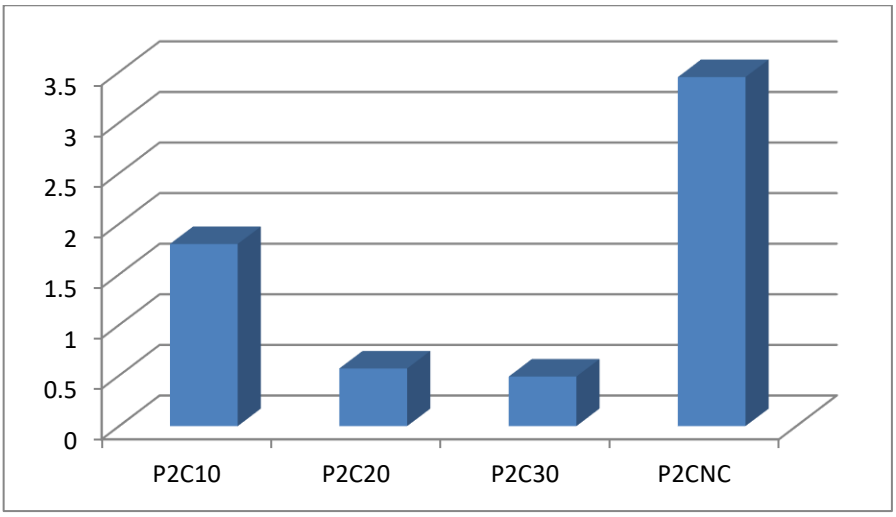

Figure 10. Cu^{2+} concentrations [mg/L] in sample P2 as a function of added HCl concentration

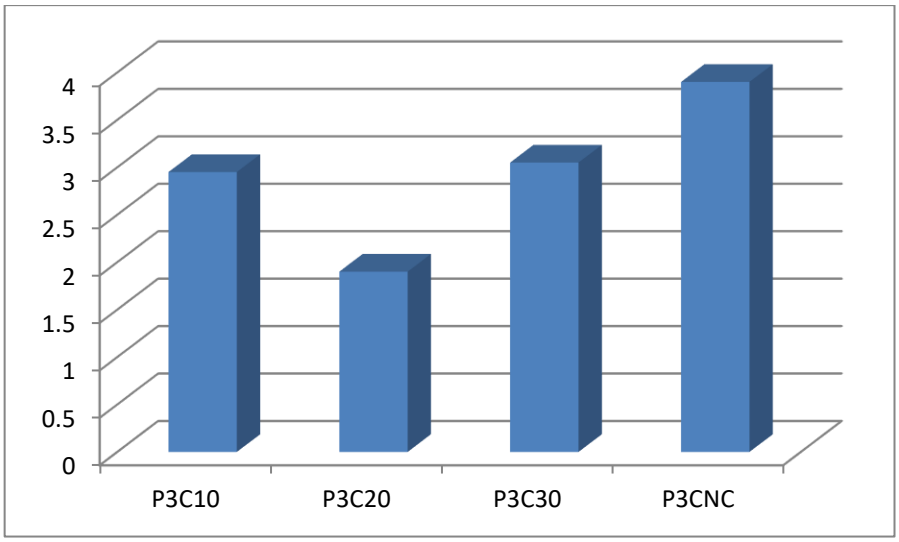

Figure 11. Cu^{2+} concentrations [mg/L] in sample P3 as a function of added HCl concentration

From the graphs above, it can be seen that for sample P1, the largest amount of Cu was determined in the sample in which HCl 10% was added, and the smallest in the sample with HCl 20%. In sample P2, it is observed that Cu dissolved best in concentrated HCl, but the value is comparable to that obtained for 10% HCl. For sample P3, the highest degree of dissolution of Cu was in concentrated HCl, but also in 10% HCl the value is close. Apart from P1, where the situation is reversed, it is observed that the highest Cu^{2+} concentration values were obtained with the addition of concentrated HCl, but the value is comparable to that obtained by adding 10% HCl.

CONCLUSIONS

Based on the study carried out on the pollution of waters from the mining residue in the above cases, we find that these acidified waters that eventually reach the surface of the sterile deposit have various colors from orange, green, purple to yellow. First of all, these shades of color were the first reports of considerable concentrations of metals in wastewater samples as well as other chemicals harmful to the environment and implicitly to vegetation, living things and humans. The wastewater resulting from the mining process is polluted with acidic solutions, used to extract metals.

.

The purpose of this work was to analyze three wastewater samples taken from three different points in the sterile pond and determine copper and iron concentrations by atomic absorption spectroscopy method. Prior to the analysis of the two metals, the pH of the samples and the total suspensions were determined. Since the waste water samples show advanced turbidity and deposits if left to settle, 10 ml of HCl of different concentrations: 10%, 20%, 30% and concentrated acid were added to each of the samples in order to dissolve the metals in the deposits. After analysis, it was observed that for both Cu and Fe, concentrations significantly exceed the regulated MACs for waste water (respectively 0,2 mg/l for Cu and total dissolved metals 2 mg/l).

As expected, Cu concentrations remaining after exploitation are not very high, on the mg/l order, however, by comparison, Fe concentrations are very high, on the order of g/l. This could be explained by the fact that the ore is rich in iron, or, due to the fact that acids are used in the process of extracting copper, they corrode the machinery used in the technological process, or they can also be abandoned machines even in the sterile deposit. Following the analyzes carried out, it was found that the wastewater covering the sterile deposit resulting from copper mining undoubtedly contains a high concentration of metals forming a polluted environment around the deposit, which affects life in that area

REFERENCES:

[1] Ardelean, Florinela, Iordache, Vlad, Ecologie și protecția mediului, Matrix Rom, București, 2007
[2] Bica, Ion, Elemente de impact asupra mediului, Matrix Rom, București, 2000
[3. Mănescu Sergiu, Cucu Manole, Chimia sanitară a mediului București, 1994
[4] Filipoiu, Mircea, Burlacu, Gabriel, Frumosu, Ladislau, Ecologia-dicționar enciclopedic, Editura Tehnică, București, 2006
[5] Popescu, Maria, Popescu, Miron, Ecologie aplicată, Matrix Rom, București, 2000
[6] Jerry A Nathanson, Polution Environment, 2023, The Enciclopedia Britanica, 4-5
[7] Louise Voller, Anna Glent Overgard, Impacts of copper mining on people and nature, 2016, Jesper Nymar, 18-23
[8] Bîzocu, Codruța, Ivan, Camelia, Monitorizarea calității mediului-analize de laborator, Târgu Jiu, 2020

STUDIES ON THE COMPOSITION OF SURFACE WATER AND SPRING WATERS FROM THE VICINITY OF A COPPER MINING OPERATION

Andrei RÎȘTEIU[1], Anda Ioana Grațiela PETREHELE[2], Oana Delia STĂNĂȘEL[2]
Claudia Mona MORGOVAN[2], Camelia PORUMB[3]
[1] Master CSA student, Faculty of Informatics and Sciences, University of Oradea
[2] Department of Chemistry, Faculty of Informatics and Sciences, University of Oradea
[3]Faculty of Arts, University of Oradea

Abstract: *Due to the fact that water pollution with metals is one of the most serious pollutions, perhaps also from the perspective of action on organisms, the purpose of this paper was to analyze four water samples, two samples being groundwater (spring) and the other two being surface water, near a copper mining operation. The samples were organoleptically analyzed, their pH and alkalinity were determined, then copper and iron concentrations were determined using atomic absorption spectrometry. Surface waters, which come from the immediate vicinity of the plant, are richer in copper and iron, the concentration of metals being above the MAC (maximum admitted concentration). Samples that have been taken from groundwater have a concentration close to the MAC for each metal. It is thus observed that spring waters have not been contaminated with heavy metals from mining, whereas surface waters have higher concentrations of the two metals analyzed, exceeding the MACs.*
Keywords: ***surface and spring water, copper and iron concentration, copper mining.***

INTRODUCTION

Water is an essential resource for human survival. With increasing water consumption, its quality faces serious challenges. Industrialisation, agricultural production and urban life have led to environmental degradation and pollution, negatively affecting the watercourses (rivers/oceans) necessary for life, thus ultimately affecting human health and sustainable social development.

Water is an important factor in ecological balances, and its pollution is a current problem with more or less serious consequences for the population. Water pollution shall mean alteration of the physical, chemical and biological characteristics of water caused directly or indirectly by human activities and rendering water unfit for normal use for the purposes for which such use was possible before such alteration occurred

Suspended or dissolved inorganic substances are more commonly found in industrial wastewater. These include, first of all, heavy metals (Pb, Cu, Zn, Cr), chlorides, sulfates, etc.; inorganic salts (Ca, Mg) lead to increased salinity of waters, and some of them can cause increased hardness; Chlorides in large quantities make water unsuitable for drinking and industrial water supply, irrigation, etc. Through bioaccumulation, heavy metals have toxic effects on aquatic organisms, while inhibiting self-treatment processes.

The industrial development of recent decades, worldwide, has led to an increase in the load of wastewater with pollutants difficult to retain by classical technologies. This paper aims to treat a topical and implicitly increasingly present topic in the society we live in: water pollution. Due to the fact that water pollution with metals is one of the most serious pollutions, perhaps also from the perspective of action on organisms, the purpose of this work was to analyze four water samples, two samples being groundwater (spring) and the other two being surface water, near a copper mining operation [1-9].

EXPERIMENTAL PART

1. Determination of organoleptic properties

The most important organoleptic parameters are: smell, temperature, taste, color.

1.1.Smell.

In general, the smell of natural water is caused by the presence of organic and inorganic substances.

Smell can be measured with sensory methods, and specific concentrations can be

measured with instrumental methods – "olfactometers" – with accurate reading.
In the sensory method, human subjects are exposed to odors that have been diluted with odorless air.
1.2. Temperature.
Water temperature is a very important parameter due to its effects on the potential of chemical reactions, aquatic life, etc.
1.3. Colour. Drinking water must be colourless, free from suspended particles.
1.4. Taste. Drinking water should not have a specific taste.
1.5. Electrical conductivity

Electrical conductivity is a physical property that refers to the property of water to allow electric current to pass through. The conductivity of water increases with its content in solutes. Water, in general, regardless of source, contains besides H2O molecules (pure water) and a lot of other substances. As we purify water, conductivity decreases. The conductivity of water gives us information about its chemical composition and represents the concentration of ions and their movement. For electrical conductivity, law no. 458/2002 on drinking water quality, provides: MAC 2500 μS/cm [10-11].

Table 1. Representation of organoleptic/physical parameters

No.crt.	**Parameter**	**Exhibit 1**	**Exhibit 2**	**Exhibit 3**	**Exhibit 4**
1.	Temperature	15°C	17°C	18°C	17°C
2.	Color	Colourless + fluidified colloidal suspensions	Colourless	Colourless	colourless + fluidified colloidal suspensions
3.	Conductivity	924 μS/cm	513 μS/cm	628 μS/cm	823 μS/cm

2. Determination of the fixed residue

The determination of the fixed residue shall be carried out according to method standard SR ISO 9963-1.
Fixed residue means all inorganic and organic substances dissolved in water which are not volatile at 105 °C. It is usually expressed in mg/l.
To carry out the determination, take as a sample about 1 l of water. Before the actual determination, the turbid waters are filtered.
2.1. Shaken fixed residue

Procedure
Pour into a petri dish of at least 100 ml volume, pour 100 ml of test sample after having previously homogenized the sample vial to homogenize suspensions or sediment.
Place the Petri dish in a thermoregulatory oven (with ventilation) at a constant temperature of 105 °C. Keep until dry evaporation; weigh the petri dish.

Repeat drying in the oven to constant weight.

The difference between the mass of the plate after evaporation (with the residue of the water sample) and the tare of the Petri dish is the fixed shaken residue.
Fixed residue = $G/V \cdot 1000$ [mg/l]
where: G - is the weight of the fixed residue, in mg, V - volume of water taken for determination, in ml

Note: If the amount of fixed residue weighed is less than 50 mg, repeat the determination using a larger quantity of water.
2.2. Filtered fixed residue

Procedure
Filter part of the water sample through a blue tape filter. 100 ml is taken from the filtrate, first measure the tare of the Petri dish; Add 100 ml filtrate, place in the ventilated oven at 105 °C. Keep until evaporative to dryness, weigh the plate.
Repeat drying in the oven to constant weight.

Table 2. Fixed residue

Sample No	Stung fixed residue	Filtered fixed residue
1.	3341 mg/l	3323 mg/l + suspensions 18 mg/l
2.	3012 mg/l	3002 mg/l + suspensions 10 mg/l
3.	2933 mg/l	2921 mg/l + suspensions 12 mg/l
4.	3742 mg/l	3722 mg/l + suspensions 20 mg/l

3. Determination of alkalinity

The alkalinity of water is given by the presence of bicarbonates, alkaline, alkaline - earth carbonates and hydroxides. The determination is made according to STAS 6364/78.

The alkalinity of surface waters is not standardized as a quality index, but its determination is especially important for assessing temporary hardness (carbonate). The method is based on neutralization of a quantity of test water with a dilute acid in the presence of indicator.

Reagents:

• 0.1 N hydrochloric acid;
• Phenolphthalein, 1% solution in alcohol;
• Methloranj 0.1 % in water;

Procedure

Determination of permanent alkalinity

Se take 100 ml of analytical water and place it in an Erlenmayer vial and add 2 drops of phenolphthalein. If pink staining does not occur, permanent alkalinity is zero (water pH below 8.2). If pink colouration occurs, titrate the sample with HCl 0,1 N until the sample becomes colourless.

The calculation formula is as follows:

P (mval/l) = ml HCl 0,1 N = $f \cdot V \cdot$

V = ml HCl 0,1 N used for titration in the presence of phenolphthalein;

f = hydrochloric acid factor 0,1 N.

Determination of total alkalinity

Measure 100 ml of test water in an Erlenmayer flask, add 2 to 3 drops of methloranj and titrate with 0,1 N HCl until the colour changes from yellow to orange.

The calculation formula is as follows:

T (mval/l) = ml HCl 0,1 N = $f \cdot V \cdot$

V = ml HCl 0,1 N used for titration in the presence of methloranj;

f = hydrochloric acid factor 0,1 N.

4. Determination of pH

The pH tells us the concentration of hydrogen ions in the water and depends on the chemical composition of the water. To determine the pH, the Multi 720 Inolab multimeter was used, to which a combined electrode was attached and the pH function of the device was used. The multimeter has been previously calibrated using the standard solutions recommended by the manufacturer of the device. According to O. 161/2006, for surface waters it was recommended that the pH value be in the range of 6.5-8.5 [11].

Table 3. pH and alkalinity of the water samples analysed

Determined parameter	Exhibit 1	Exhibit 2	Exhibit 3	Exhibit 4
Ph	9,31	7,91	7.52	4.25
Alkalinity: permanent	1,5	0.4	0.8	1.4
total (mval/l)	4,2	0.8	1,7	1.9

5. Determination of copper and iron concentrations by atomic absorption spectroscopy

Atomic absorption spectroscopy (AA or AAS spectroscopy) is one of the oldest elemental analysis techniques that has been developed commercially. Flame atomic absorption spectroscopy (Flame AA or AAS) was developed in 1952 and first commercially launched as an analytical technique in the 1960s. Since then, the technique has remained popular for its reliability as well as its simplicity. It uses the principle that atoms (and ions) can absorb light at a specific, unique wavelength when this specific wavelength of light is supplied with energy, which is subsequently absorbed by the atom. The electrons in the atom move from the ground state to the excited state, so by measuring the amount of light absorbed, the concentration of the element in the sample can be measured. Basically in AAS, a solution containing the analyte is introduced into a flame, that flame converts the samples into ground-state free atoms that can be excited; A lamp emitting at a wavelength specific to atoms is passed through the flame, and as light energy is absorbed, electrons in atoms are brought into an excited state.

Lambert–Beer Law describes the relationship between light absorption and element concentration; Thus, according to the law, the amount of light absorbed is proportional to the number of atoms excited in the ground state in the flame.

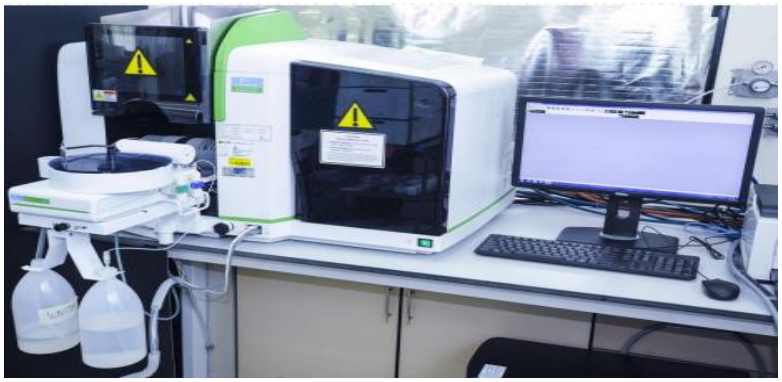

Figure 1. Atomic absorption spectrophotometer

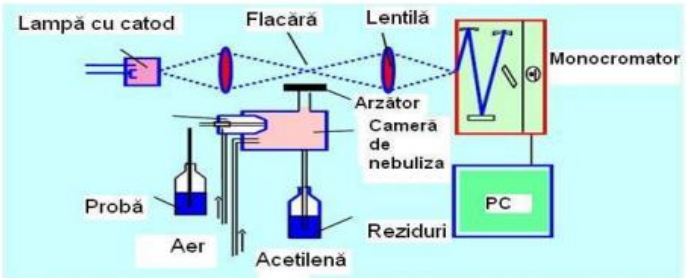

Figure 2. Diagram of the atomic absorption spectrophotometer
http://www.repository.utm.md/bitstream/handle/5014/3825/Conf_UTM_2010_I_pg303-306.pdf?sequence=1&isAllowed=y

Procedure

After sampling, they are subjected to double filtration; A first filtration in which filter paper with larger pores is used to remove larger impurities, the filtered water is exposed to a second filtration, filtration which is carried out with filter paper with small pores, in order to remove the finest suspensions to avoid problems of clogging the suction pipes and circuit of the apparatus. When the filtration step is ready, the samples are stored in suitable containers and, if analysis is not carried out immediately, the samples are acidified according to the standards. The next step is to start the atomic absorption spectrometer, due to the fact that it needs a heating time of at least 15 minutes; While the apparatus is heating up, five

solutions of known concentration are developed to serve the calibration curve. For this purpose, account shall be taken of the maximum permitted concentration recommended by the manufacturer of the apparatus so that the calibration curve is correctly drawn, and then, taking account of that maximum concentration, appropriate dilutions shall be made. When the apparatus has reached a suitable temperature for analysis, samples of known concentration are introduced to plot the calibration curve; A properly executed calibration curve must have a correlation coefficient above 0,995. Therefore, the next step is the actual analysis of the evidence. Water samples may have a higher concentration of metal than the maximum contained in the standard, in this case dilutions of 10, 20, 50, etc. are made to bring the concentration of the metal within the permissible limit [10]..

5.1.Copper

In the first phase, the calibration curve was established by preparing the 5 solutions of known concentration. Figure 4. After the calibration curve was successfully performed, the actual analysis of the samples was carried out.

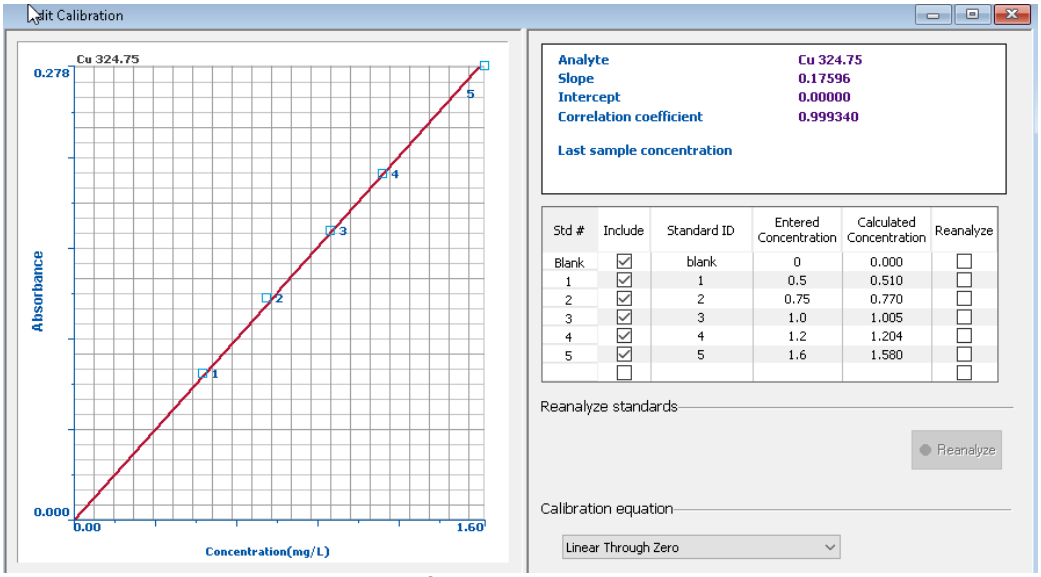

Figure 4. Cu^{2+} calibration curve

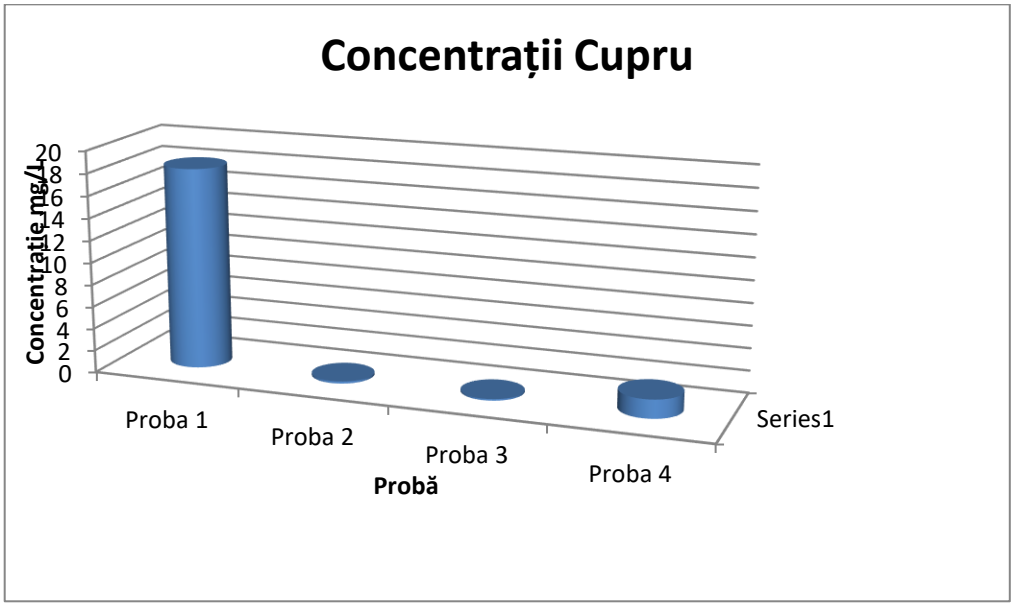

Figure 5. Copper concentration in samples analysed

It is noticed that Sample 2 and Sample 3 have similar concentrations, which is somewhat expected, given that both samples come from spring waters, the springs not being very far from each other. Sample 1 is shown to have a very high concentration of copper, which is also not surprising; Sample 4 surprises due to the fact that both Sample 1 and 4 are taken from surface waters, the discrepancy between them being quite pronounced. According to Law 458/2002 with subsequent amendments and completions, Law no. 311/2004, Government Ordinance no. 11/2010, Law no. 124/2010 and Government Ordinance no. 1/2011, the maximum permissible concentration of copper is 0.1mg/L. From Figure 6, it can be seen that samples two and three, originating from spring waters, contain a copper concentration close to the MAC. Samples 1 and 4 respectively come from surface water near copper mining, and Cu2+ concentrations exceed the MAC.

.

5.2. Iron

And in the case of iron determination, it is necessary to perform a calibration curve. Calibration curve shown in Figure 7

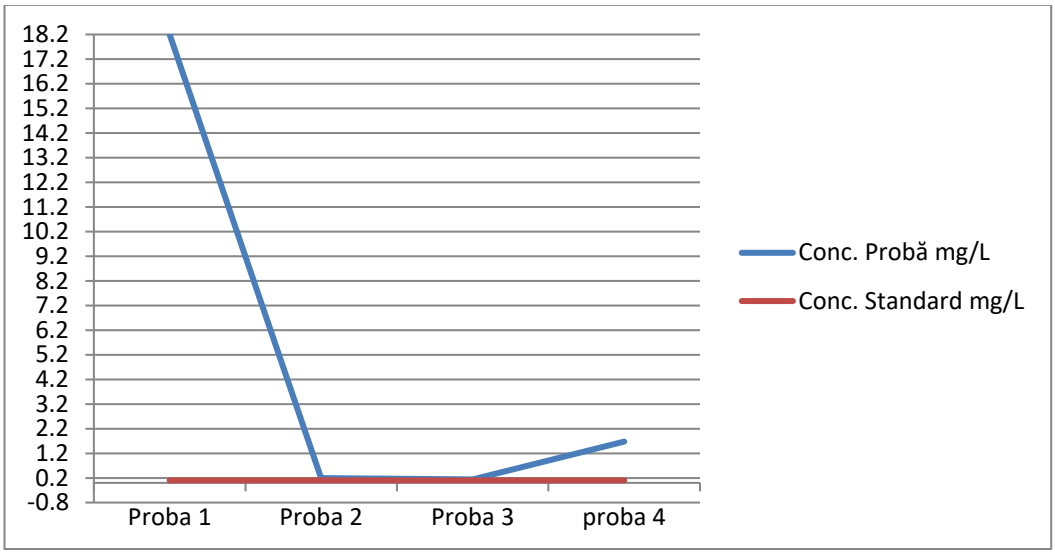

Figure 6. Copper concentration in samples relative to maximum admitted concentration

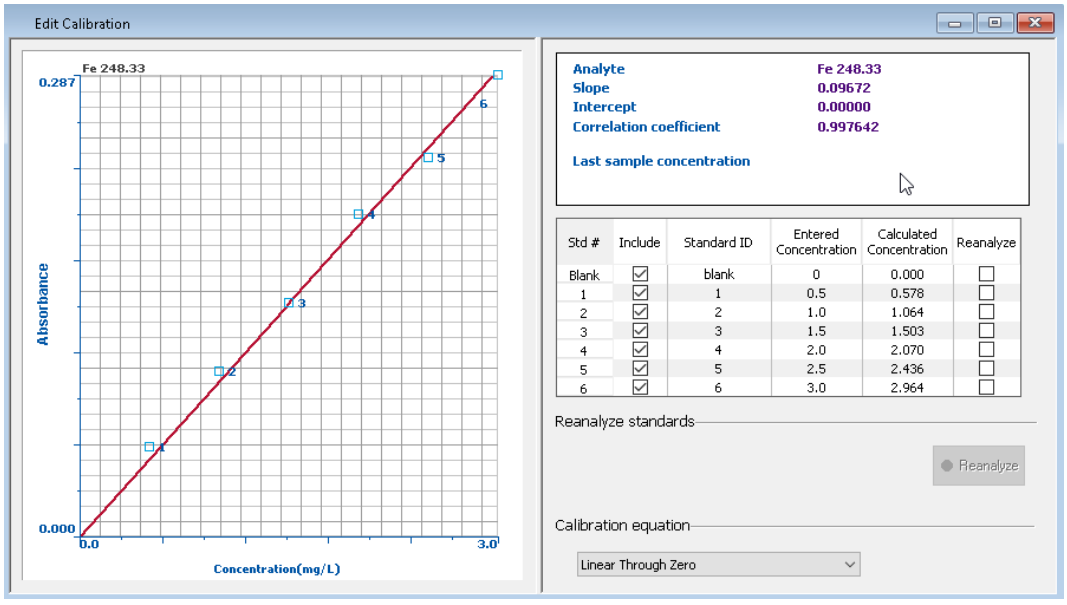

Figure 7. Calibration curve for Fe^{3+} determination

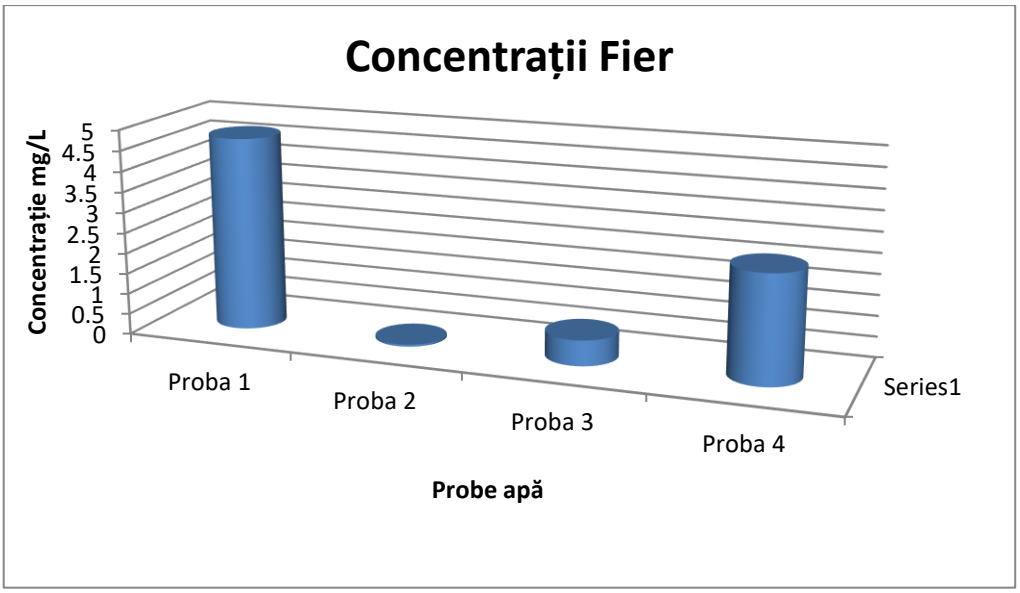

Figure 8. Iron concentration in test samples

Note that Sample 2 has the lowest concentration, with Sample 1 again being highly concentrated, followed by Sample 4 and Sample 3 respectively. Law 458/2002 with subsequent amendments and completions Law no. 311/2004, Government Order no. 11/2010, Law no. 124/2010 and Government Order no. 1/2010 state that the MAC for iron is 200µg/L or 0.2 mg/l.

From the graph, it appears that only water from sample 2 could be consumed without problems, not exceeding the MAC. All other samples exceed the maximum permitted concentration threshold.

It can be seen that in sample 1 copper is in a much higher concentration compared to that of iron. In samples 2 and 3 respectively the concentrations of the metals to be analyzed are close, and in the last sample, a slight discrepancy between the concentrations of the 2 metals is observed.

CONCLUSIONS

Analysis of water samples taken from an area near a copper mining undertaking reveals the influence of soil nature associated with human activities on water quality.

Thus, four water samples were taken from four different locations, two of which were taken from surface water and two from groundwater (spring) near a copper mining operation. The samples were organoleptically analyzed, their pH and alkalinity were determined, then copper and iron concentrations were determined using atomic absorption spectrometry.

Surface waters coming from the immediate vicinity of the plant, as expected, are richer in copper and iron, with metal concentrations above the CMA. Samples that have been taken from groundwater have a concentration close to the MLA for each metal.

Thus, it is observed that spring waters have not been contaminated with heavy metals from mining, while surface waters have higher concentrations of the two analyzed metals, which exceed CMA, so they are unfit for consumption and indicate that they are polluted due to mining activity in the vicinity.

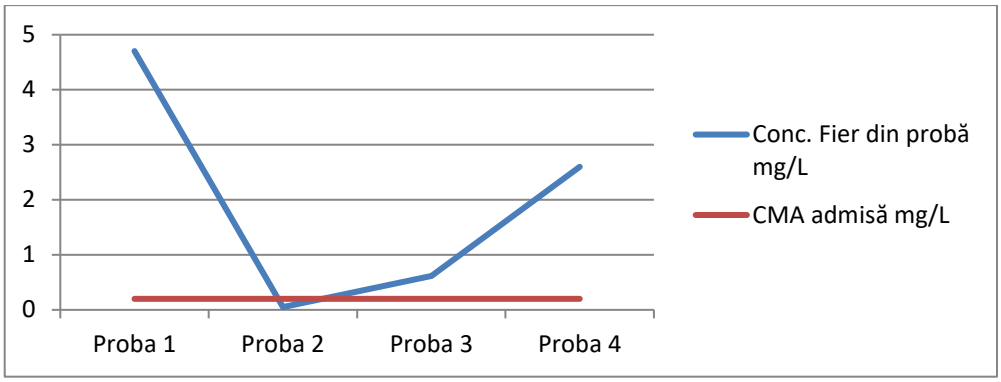

Figure 9. Iron concentration in samples in relation to maximum admitted concentration

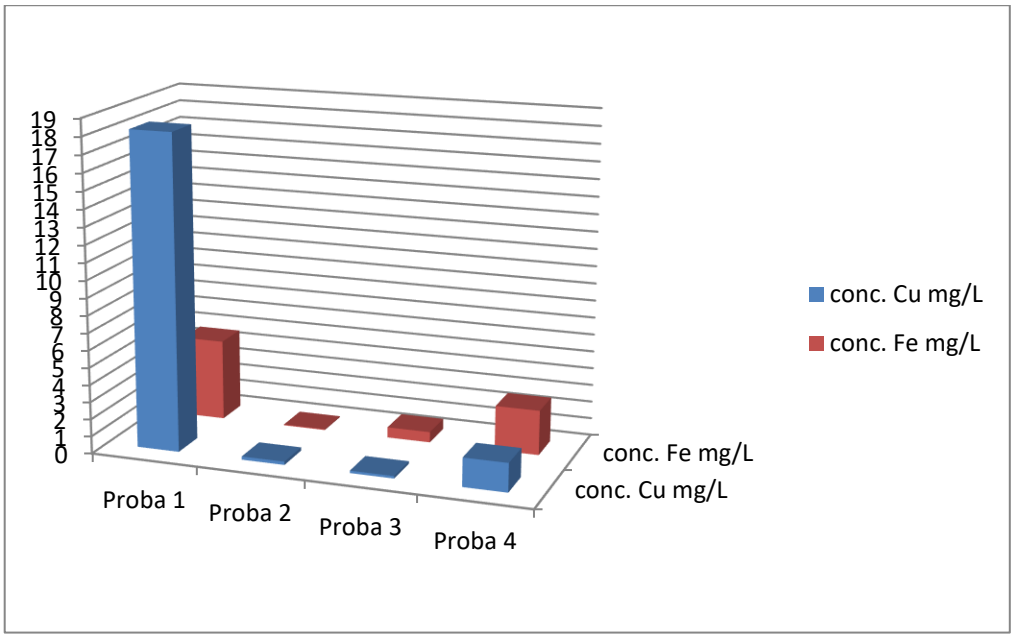

Figure 10. Concentration of copper and iron in samples to be analysed

REFERENCES:

1. Nathonson, J.A revizuit 11 iunie 2023, Environmental pollution
2. Cipilea, L.I (1978), *Poluarea mediului ambiant*, Ed. Tehnică, Bucureşti.
3. Mănescu, S. (1978). *Chimia sanitară a mediului*, Editura Medicală, București
4. Manescu S., Dumitrescu,, H., Barduta, Z., Diaconescu, M.L. (1982), *Chimia sanitara a mediului*, II, Ed. Medicala, Bucuresti.
5. East Central University, 9 septembrie 2019, Causes of environmental pollution.
6. Chaudhry FN, 31 martie 2017, Factors affecting water pollution.
7. Anubhav Singh, Anuj Sharma, Rohit K. Verma, Rushikesh L. Chopade, Pritam P. Pandit, Varad Nagar, Vinay Aseri, Sumit K. Choudhary, Garima Awasthi, Kumud K. Awasthi și Mahipal S. Sankhla, 15 iunie 2022, Heavy Metal Contamination of Water and Their Toxic Effect on Living Organisms.
8. Ghimecesu, G, Hîcu, I. (1974), *Chimia şi controlul poluării apei*, Ed. Tehnică, Bucureşti.
9. Li Lin, Haoran Yang, Xiaocang Xu, revizuit de Behzad Shamoradi, Atlik Kulakli, Effects of Water Pollution on Human Health and Disease Heterogeneity
10. Andronic, Luminița, Duță, Anca, (2013) *Analize fizico-chimice și metode avansate de epurare a apelor uzate* , Universitatea Transilvania, Brașov
11. Bîrzocu, Codruța, Ivan, Camelia, (2020) *Monitorizarea calității mediului-analize de laborator*, Universitatea Târgu Jiu.

(12pt)

INSTRUCTIONS FOR AUTHORS (TIMES 14 PT BOLD, CAPITAL LETTERS, CENTRED)

(12pt)

First name SURNAME[1], First name SURNAME[2] (12 pt bold)

[1]Affiliations and addresses (12 pt)

(12pt)

Abstract: *Abstract of 50-120 words (12 pt italic). It contains concise information about: objectives of the work, the results obtained, conclusions*

Key words: List 2-6 keywords. (l0 pt, italic).

(12pt)

INTRODUCTION (l2PT. CAPITAL, BOLD)

The paper has to be written in English. Each paper should be concise including text, figures and tables. Authors are kindly requested to submit in electronic format, Microsoft Word file form, 2003, 2007, 2010. The suggested structure of the main text: Introduction; Methods and Materials, Results and Discussions; Conclusions; References. (12pt)

INFORMATION (12 PT CAPITAL, BOLD)

Page layout:Use A4 format (210 x 297 mm), Margins: Top – 2,5cm, Bottom - 3 cm, Left- 4 cm and Right - 3 cm Paragraphs: alignment - justified, line spacing – 1,

Font style: Times New Roman.Text: l2pt.: regular, text in tables: 10 pt, 1 line space and centred, 2 columns, Equations: Equation editor, 12 pt, centred,References (12pt)

c*aption of tables and figures: 12 pt, italic*

Tables, together with figures should be placed in their order of appearance in the text and numbered consecutively. Table captions containing the number of the table, and should be placed above the table. Tables should be clearly captioned and all symbols should be properly explained in either the table or its caption.

Figures (min. 300 dpi) can be in colour, but must also be clear enough for black and white reproduction. They should be centred and numbered consecutively and so referred to in the text. Each must be clearly captioned (after the Figure number) below the figure. Equations will be centred and numbered consecutively (right aligned).

All references would be cited in brakets [1*]

All papers cited should be listed under the **REFERENCES** (1 column), in order of appearance (Journal Article)

[1] Abbott, M. B., Petersen, M. M., and Skovgaard, O. (1978). On the numerical modelling of short waves in shallow water, Jnl Hydraulic Res; Vol 16 (3), pp. 23-44.
(Report)
[2] Carter, B., and Connell, C. (1980). Moa Point Wastewater Treatment Plant and Outfall Study, Report for the Wellington City Council, Wellington, pp. 31.
(Book)
[3] Grady, C.P.L., and Lim, H.(1980). Biological Wastewater Treatment Theory and Application, Marcel Dekker, New York, pp. 375.